Quaternary alkaline and calc-alkaline basalts in southern British Columbia: mixed signals from mantle sources above the southern edge of the Juan de Fuca–Pacific slab window

by

Christa Lynn Sluggett
B.Sc. (Honours) University of British Columbia, 2003

THESIS SUBMITTED IN PARTIAL FULFILMENT OF
THE REQUIREMENTS FOR THE DEGREE OF

MASTER OF SCIENCE

In the
Department of Earth Sciences

SIMON FRASER UNIVERSITY

Summer 2008

APPROVAL

Name: **Christa Sluggett**

Degree: **Master of Science**

Title of Thesis: **Quaternary alkaline and calc-alkaline basalts in southern British Columbia: mixed signals from mantle sources above the southern edge of the Juan de Fuca–Pacific slab window**

Examining Committee:

Chair: **Dr. Andrew Calvert**
Professor, Department of Earth Sciences

_____

Dr. Derek Thorkelson
Senior Supervisor
Professor, Department of Earth Sciences

_____

Dr. Dan Marshall
Supervisor
Associate Professor, Department of Earth Sciences

_____

Dr. Kelly Russell
Supervisor
Professor, EOS, University of British Columbia

_____

Dr. James Scoates
Supervisor
Associate Professor, EOS, University of British Columbia

_____

Dr. Laurence Coogan
External Examiner
Assistant Professor, EOS, University of Victoria

Date Defended/Approved: August 18th, 2008

ABSTRACT

Subaerial lava flows of the Quaternary valley lavas mark the end of Chilcotin Group intraplate volcanism in southern British Columbia. Two geographically defined units are recognized: the Quilchena and Lambly Creek lavas. Erupting intermittently from discrete centres, lava flowed into existing paleodrainages from 1.5 Ma (Lambly Creek) to 780–100 ka (Quilchena). Erosion removed most of the estimated 8.8–21.1 km^3 of lava. Internal features are well preserved, some indicative of flow inflation and transport direction. The lavas are alkaline to calc-alkaline basalts, trachy-basalts, basaltic andesites and trachy-basaltic andesites, with trace element characteristics similar to ocean island basalt and εNd values from +8.0 to +8.4. The magmas resulted from partial melting of garnetiferous asthenosphere that upwelled through the subducted Nootka Fault and thermally eroded Explorer and northern Juan de Fuca plates south of a slab window. Geochemical modelling indicates that the mantle source was heterogeneous, composed of variably enriched peridotite.

Keywords: Cordilleran geology; Quaternary volcanism; Chilcotin Group; Ar–Ar geochronology; mantle chemistry

DEDICATION

For Tawni and Sandy,
and Grandma, who loved rocks.

ACKNOWLEDGEMENTS

It's been a long time from start to finish, but I finished, largely due to the support of so many people. First, a huge thank-you to my supervisor, Derek Thorkelson, who never quit supporting and encouraging me, especially through the dark days of my writing process. I couldn't have done this without all your help.

Jason Pellett was instrumental in the completion of this thesis. Thank-you for making me sit down and write, listening to me rant (both about how the thesis was driving me crazy and geology in general), editing, and all the general support (feeding me!) as life became crazy. Also thank-you to my parents and sister and the Pellett family for encouraging me for the last four years.

I would also like to acknowledge Ryan Ickert and Dejan Milidragovic, who provided unequalled field support and entertainment (Bon Jovi and bears anyone?), and made the Cordlab a highly amusing and enlightening place to work each day. And thank you to Sarah M., Jessica, Tricia, Nathan, Sarah B., Mike, Scott, Gabe, Richard, and Megan – whether it was coffee or drinks at the pub, having you there made school fun.

This thesis was made considerably better through the support and input of Dan Marshall, Kelly Russell and James Scoates. Dan is also thanked for his words of encouragement as my deadline drew near. Laurence Coogan's comments and queries at my defense greatly improved the final version of this thesis, and Tom Ullrich was a great help with my Ar–Ar analyses. Charles Fitton, who started this project in 2000, is thanked

for having created a wonderful sketch of the Missezula Lake East section, and leaving behind a very organized suite of samples. And thank you to Dave Chutter and the Westbank First Nation for allowing me access to the valley lavas on their respective properties.

My time at SFU was greatly enhanced by my participation in the Graduate Issues Committee and helping organize our department graduate talks, so a big thank-you to all the graduate and undergraduate students who came and supported the events. And thank-you to Glyn and Guillaume for their help with the graduate talk series. Rodney, Matt, Glenda and Tarja are thanked for their behind-the-scene support that kept me up and running.

And finally, thank you to the team at Geoscience BC ('Lyn, Rhonda, Angel, Lauren and others). Your support, in the form of time off and encouragement, directly contributed to the completion of this thesis.

TABLE OF CONTENTS

LIST OF FIGURES

LIST OF TABLES

CHAPTER 1:
RECENT INTRAPLATE VOLCANIC ACTIVITY IN SOUTHERN BRITISH COLUMBIA

1.1 Summary

Late Cenozoic intraplate volcanoes are widespread in British Columbia and range from small monogenetic cones to stratovolcanoes and extensive lava fields (Souther, 1991; Souther and Yorath, 1991). Included in this swath of recent intraplate volcanism are the Quaternary "valley lavas" of south-central British Columbia (although more commonly known as the "valley basalts," the lavas are not all basalts, and so the term "valley lavas" is used in this thesis) (Lambert, 1963; Preto, 1979). These lavas are herein included in the Chilcotin Group (Tipper, 1978), although not all previous workers have done so, as outlined below.

This thesis examines the physical volcanology, geochemistry and timing of the "valley lavas," describes their relationship with other lavas of the Chilcotin Group, and provides a regional synthesis of Late Cenozoic volcanic activity. Chapter 1 examines the previous work on the Chilcotin Group, including the valley lavas. Chapter 2, which is written in the style of a journal article, describes the new research on the valley lavas carried out for this thesis. The appendices provide tables of data and a description of analytical methods and modelling procedures.

1.2 The Chilcotin Group

Reinecke (1920) was the first to separate what would be later known as the Chilcotin Group from other Paleogene rocks in south-central British Columbia, referring to them as the "Upper Volcanics." Rice (1947) later subdivided the lavas into the plateau basalts and valley basalts, recognizing their respective relationships to topography at the time of eruption. The name "Chilcotin Group" was first proposed by Tipper (1978), encompassing the Upper Miocene and/or Pliocene plateau basalts and the associated sediments of the southern Chilcotin Plateau (Bevier 1982; 1983a; 1983b).

Bevier (1982; 1983a; 1983b) conducted the first comprehensive study of the Chilcotin Group plateau lavas (and associated volcanic plugs), examining their stratigraphy, chemistry and eruptive history. The lavas were found to be Miocene to Pliocene transitional basalts, aerially extensive, yet thin (Bevier, 1983a, b; see Figure 1). The outpouring of Chilcotin Group lavas originated from a series of vents aligned parallel to the trend of the coeval Pemberton Belt arc-related volcanics. The Chilcotin eruptions were interpreted as a result of asthenospheric upwelling in the back-arc to the Pemberton centres related to the subduction of the Farallon / Juan de Fuca plate to the west (Bevier, 1983a).

A type section of the Chilcotin Basalts was not introduced until Mathews (1989) recommended Bevier's (1983b) "amphitheatre" site on the northern rim of the Chilcotin River valley below Beaumont Lake. Mathews (1989) further confined the definition of the Chilcotin Group to include the Early Miocene to Early Pliocene basaltic lavas and the associated sedimentary and pyroclastic rocks from the Okanagan Highland to the Nechako Plateau, but not the later Pleistocene to Holocene valley lavas (lavas that

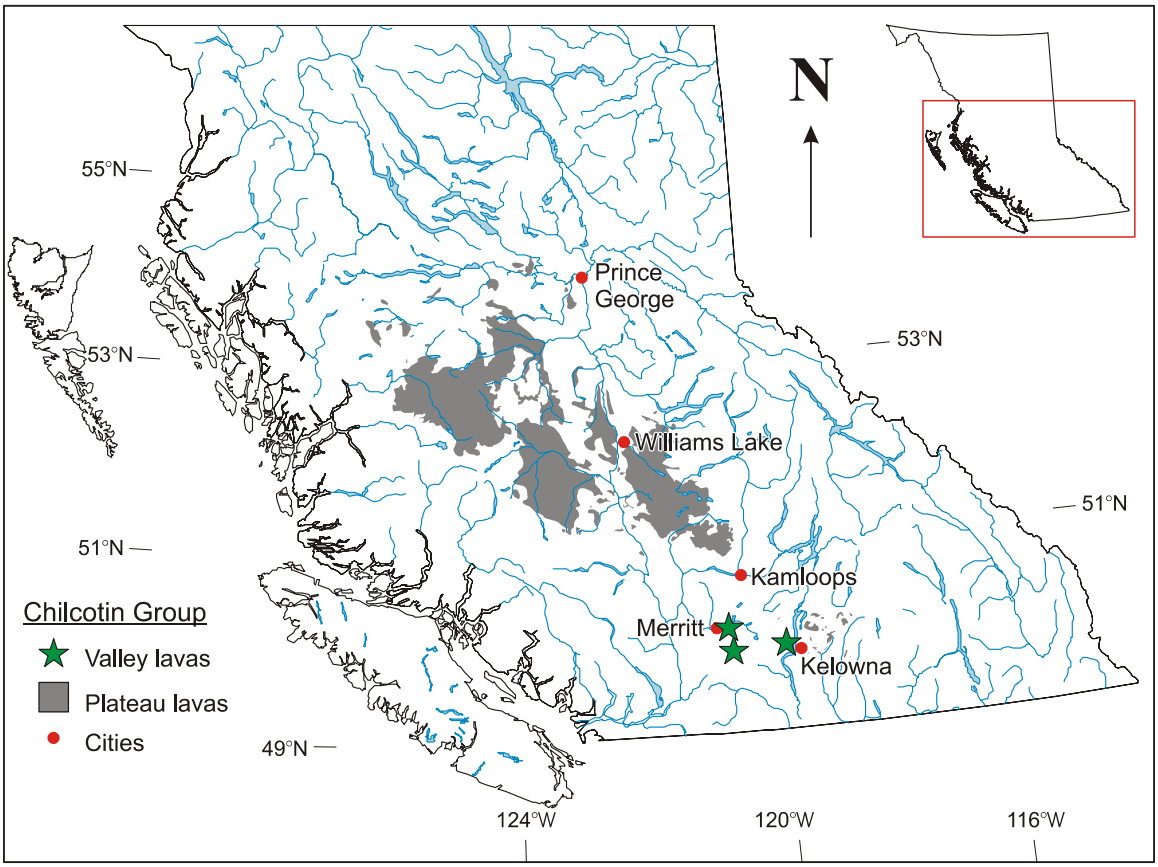

Figure 1. Distribution of Chilcotin Group volcanism in southern British Columbia
Map prepared using MapPlace (BC Geological Survey, May 2008).

postdate Quaternary plateau incision). Mathews (1988, 1989) also dated the Chilcotin Group using K–Ar methodology, noting that eruption appeared to be particularly focused in three intervals: 14–16 Ma, 6–9 Ma, and 1–3 Ma. Church (1980) employed paleomagnetic analyses to aid in the determination of eruptive ages.

Although the Chilcotin Group is extensively dated (mainly by the K–Ar method), it is not comprehensively characterized for its geochemical composition. Major element compositions exist for flows throughout the lava field, but comprehensive trace and rare earth element (REE) data is limited, and typically focused on specific areas (Bevier, 1983a; Smith, 1986; Dostal et al., 1996; Coish et al., 1998; Anderson et al., 2001). The lavas are generally classified as transitional basalts, straddling the alkaline–subalkaline subdivision, and range from nepheline to quartz normative (Bevier, 1983a; Smith, 1986). Limited trace element concentrations show slight to moderate LREE enrichment, with LREE enrichment increasing from the subalkaline tholeiites to the alkaline basalts (Smith, 1986; Dostal et al., 1996). The trace element patterns are very similar to that of a typical Ocean Island Basalt (OIB) (Smith, 1986; Dostal et al., 1996). Where available, the HREE patterns suggest melting of a garnet source (Dostal et al., 1996). Limited Pb, Sr and Nd isotopic compositions demonstrate that the Chilcotin group is moderately depleted ($^{87}Sr/^{86}Sr = 0.7028 – 0.7039$ and $^{143}Nd/^{144}Nd = 0.51310 – 0.51284$), that crustal contamination of the magmas was insignificant, and that small variations in isotopic composition could be attributed to mantle heterogeneity (Bevier, 1983a; Smith, 1986).

Overall, the Chilcotin Basalts have been attributed to a depleted mantle source, with some degree of mixing with an enriched mantle component (OIB), and with no assimilation of continental crust (as suggested by their isotopic ratios and xenoliths being

solely mantle-derived) (Bevier, 1983a; Smith, 1986; Dostal et al., 1996; Coish et al., 1998). Mantle upwelling is most commonly suggested to have triggered the partial melting which caused the eruption of the lavas; mantle plume and back-arc spreading hypotheses of Chilcotin Group origins have been discussed and disregarded (see Dostal et al., 1996). An alternative proposal by Rohr and Currie (1997) suggests that the transfer from subduction to strike–slip motion along the Queen Charlotte fault triggered the destabilization of the over-thickened continental crust along an east-dipping low angle normal fault, resulting in deformation of the lithosphere and asthenospheric upwelling behind the Coast Mountains.

The most recent work on the Chilcotin Group is focused on redefining the areal extent of the lavas and their thicknesses, and characterizing the lithofacies contained within the Group (Andrews and Russell, 2007; Gordee et al., 2007; Farrell et al., 2007; Andrews and Russell, 2008). Previous workers interpreted the lavas as an extensive (25,000–50,000 km^2 and 3300 km^3), thick (~100 m) lava plateau extending across much of British Columbia's interior (e.g. Bevier, 1983b; Mathews, 1989). However, the current understanding of the Chilcotin Group suggests that it is thinner (~25 m thick) and less extensive than previously thought, with the thickest sections (>50 m) confined to paleodrainages. Outside of the paleodrainages, the Chilcotin Group is a thin cover, and may not exist at all in areas where it is currently mapped (Andrews and Russell, 2007; 2008).

1.3 "Valley basalts" or "Valley lavas"

In comparison to the Chilcotin plateau lavas to which they are most often compared, the "valley basalts" or "valley lavas" have received considerably less study.

Lambert (1963) completed the most detailed work on the valley basalts with a physical and petrographic study of basaltic flows exposed west of Quilchena Creek, just south of the Nicola valley. He described the lavas as thin, flat-lying flows, with exposed sections being up to 50 m thick and composed of five to six flows. The age of the lavas was determined to be Pleistocene, as the lavas overlie unconsolidated sand and gravel (Lambert, 1963).

The regional extent of the lavas around Merritt were mapped by Preto (1979) between Missezula Lake (along Highway 5A, south of Apsen Grove), to Courtenay Lake (east of Merritt). The lavas are also included on Monger's (1989a, b) 1:250,000 Hope and Ashcroft map sheets as the "valley basalts" and Tempelman-Kluit's (1989) 1:250,000 Penticton map sheet as the "Lambly Creek Basalt". Figure 1 shows the location of the valley lavas compared to the plateau lavas of the Chilcotin Group.

The geochemistry of the valley lavas has only been evaluated as part of the Chilcotin Group. A thesis by Smith (1986) includes analyses of four valley lava samples (near Quilchena Creek), and Nd and Sr isotopic analyses of two samples as part of a larger study of the Chilcotin Group. Geochronological results for the valley lavas are slightly more abundant, with two published K-Ar dates and paleomagnetic analyses on the Lambly Creek lavas near Kelowna (Church, 1980; Mathews, 1988), and three unpublished K-Ar ages for valley lavas near Merritt (Breitsprecher and Mortensen, 2004). Paleomagnetic analyses for the valley lavas near Merritt and along Quilchena Creek are published in Fulton et al. (1992).

Prior to this study, preliminary fieldwork in the Merritt area was completed in 2000 by Richard Fitton, a former student of Dr. Thorkelson. Tasks included collection of

geochemical samples and preliminary sketches of many of the exposed sections, most notably at Missezula Lake. These samples and sketches were evaluated as part of this study, with some of the Missezula Lake samples ultimately being analyzed, and the Missezula Lake sketch being modified and included in Chapter 2.

CHAPTER 2:
QUATERNARY ALKALINE AND CALC-ALKALINE LAVAS IN SOUTHERN BRITISH COLUMBIA: MIXED SIGNALS FROM MANTLE SOURCES ABOVE THE SOUTHERN EDGE OF THE JUAN DE FUCA–PACIFIC SLAB WINDOW

2.1 Abstract

Subaerial lava flows of the Quaternary valley lavas mark the end of Chilcotin Group intraplate volcanism in southern British Columbia. The valley lavas are herein divided into two geographical units: the Quilchena lavas near Merritt and the Lambly Creek lavas near Kelowna. Erupting intermittently from discrete centres, lava flowed into existing paleodrainages. Subsequent erosion removed most of the estimated 8.8–21.1 km^3 of lava, and discontinuous lava terraces are preserved along valley walls today. Internal features are well-preserved, some indicative of flow inflation and transport direction. New whole-rock $^{40}Ar/^{39}Ar$ ages indicate that the Lambly Creek lavas (1.5 Ma) erupted before the Quilchena lavas (780–100 ka).

The valley lavas are basalts, trachybasalts, basaltic andesites and trachybasaltic andesites, with εNd from +8.0 to +8.4 and trace element characteristics similar to ocean island basalt and other northern Cordilleran intraplate volcanic belts. The Quilchena lavas consist of distinct alkaline and calc-alkaline types that are not related by fractional crystallization or degree of partial melting. Instead, the lavas were derived from heterogeneous, garnet-bearing asthenospheric mantle composed of enriched peridotite with pods or streaks of less enriched material, with no input from old, enriched

subcontinental lithospheric mantle. The enriched asthenosphere appears to have gained access to the overriding North American plate via upwelling around and through the thin, cracked and thermally eroded subducted slab of the Explorer and Juan de Fuca plates. The upwelling is part of a larger system of mantle upflow that has occurred through the northern Juan de Fuca / Pacific slab window in the Late Cenozoic.

2.2 Introduction

The nature and timing of volcanism in continental margins is related to the configuration of subducting plates and intervening slab windows. Arc volcanism above the subducting plates is typically calc-alkaline, whereas volcanism above the slab windows is commonly alkaline to tholeiitic with intraplate signatures (Hole et al., 1991; Thorkelson, 1996). Volcanic fields located at the transition from subducting-plate to slab window environments commonly have unusual petrologic associations, including rocks of calc-alkaline, alkaline, tholeiitic and adakitic affinity (Thorkelson, 1996). For example, Patagonian lavas attributed to the intersection of Chile Ridge segments with the Chile Trench range from tholeiitic lavas derived from an OIB-like asthenospheric melt interacting with crustal and slab-melt components, to alkaline lavas derived from a pristine asthenospheric source (Gorring et al., 1997; Gorring and Kay, 2001; D'Orazio et al., 2005).

The Chilcotin Group of southern British Columbia is a succession of Miocene to Pleistocene mafic lavas that erupted above the transition between subduction and slab window environments. This transition occurs where the northern edge of the Farallon plate (presently the Juan de Fuca and Explorer plates) flanks the slab window beneath central British Columbia (Figure 2) (Madsen et al., 2006).

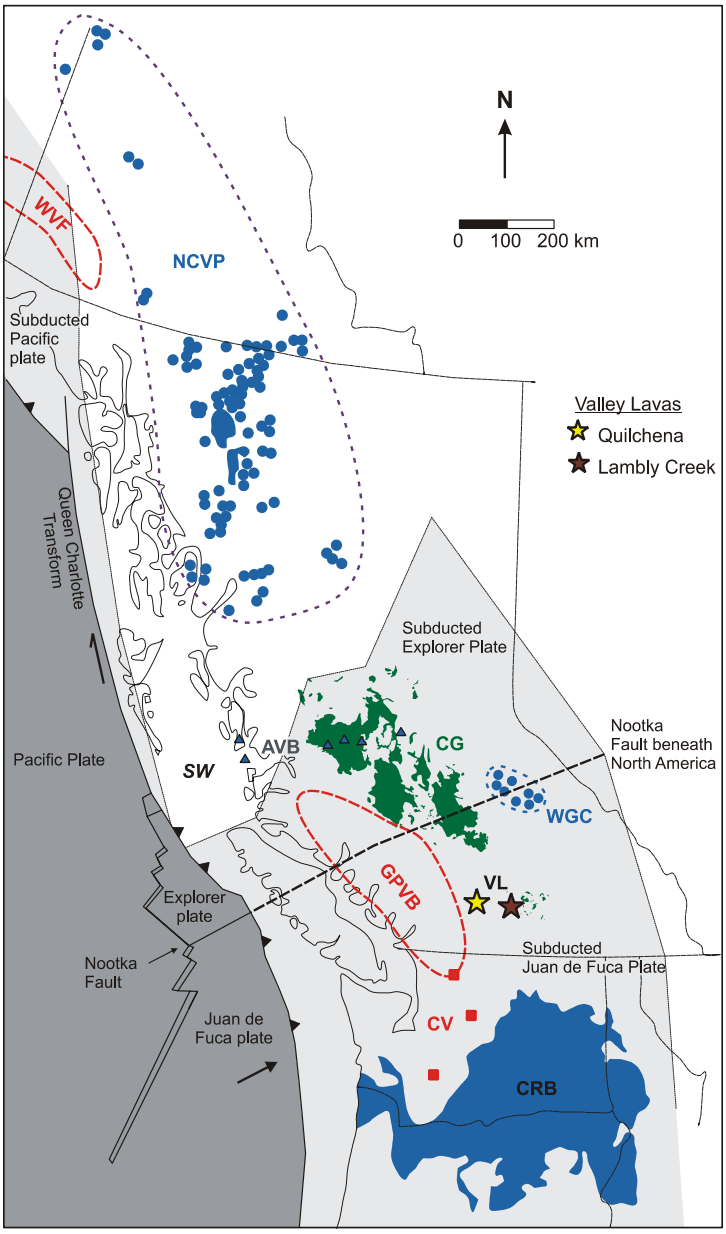

Figure 2. **The location of Cenozoic arc and intraplate volcanic features in Alaska, Yukon Territory, British Columbia, Washington and Oregon with respect to the present-day tectonic setting**

Arc volcanism is shown with a red dashed line (GPVB, Garibaldi and Pemberton volcanic belts; WVF, Wrangell Volcanic Field) or square (CV, Cascade Range volcanoes). Non-arc volcanism other than the Chilcotin Group is shown in blue (AVB, Anahim Volcanic Belt; CRB, Columbia River Basalts; NCVP, Northern Cordilleran Volcanic Province; WGC, Wells Gray–Clearwater volcanics). The Chilcotin Group plateau lavas (CG) are shown in green, and the valley lavas are indicated with stars. Grey shading beneath North America indicates the subducted portions of the Pacific, Juan de Fuca and Explorer Plates, and the slab window related to the subducting Juan de Fuca ridge is shown in white (labelled SW). Tectonic setting after Madsen et al. (2006). Distribution of volcanic features after Tolan et al. (1989), Russell and Edwards (2000), Madsen et al. (2006), and MapPlace (BC Geological Survey, May 2008).

In this paper, the youngest (Quaternary) lavas of the Chilcotin Group, which lie above the northern edge of the Juan de Fuca plate, are examined. These lavas were erupted approximately 170–240 km east of the Cascade–Garibaldi arc and 500–600 km from the Cascadia trench. The lavas are well exposed as discontinuous terraces along several valleys between the cities of Merritt and Kelowna. New information on lava stratigraphy, morphology, petrology and age show that the lavas have a mixed geochemical signature consistent with petrogenesis above a thin and broken plate edge.

2.3 Late Cenozoic Tectonics and Volcanism

Over the past 200 Ma, subduction, arc magmatism and terrane accretion dominated the evolution of western North America. By the Cenozoic, the Farallon, Kula and possibly Resurrection plates were subducting beneath North America, forming a complex system of subducting slabs and slab windows (Atwater, 1970; Engebretson et al., 1985; Haeussler et al., 2003; Madsen et al, 2006). By the Oligocene, all of these plates except for small remnants of the Farallon had subducted or fused to the Pacific plate (Madsen et al., 2006). Consequently, in Miocene to Recent time the Juan de Fuca (Farallon), Cocos (Farallon) and Pacific plates were subducting beneath North America. Subduction of the intervening spreading ridges led to the development of slab windows beneath much of British Columbia and Yukon and the southwestern United States (Thorkelson and Taylor, 1989; Madsen et al., 2006).

The northern part of the Juan de Fuca plate broke away along the Nootka Fault at 4 Ma to become the Explorer plate (Riddihough, 1984). The Nootka fault is thought to continue beneath the North American plate, separating the subducted parts of the Juan de

Fuca and Explorer plates possibly as far east as the Wells Gray–Clearwater volcanic field (Madsen et al., 2006). After separating from the Juan de Fuca plate, the Explorer plate stopped subducting and now is essentially fixed relative to North America, (Riddihough, 1977; Rohr and Furlong, 1995; Dziak, 2006). The subducted slab apparently remains beneath southern British Columbia with its northern edge extending from the northern end of Vancouver Island northeastward beneath central British Columbia. The Juan de Fuca plate continues to subduct at 4 to 4.5 cm/yr at an angle of ~11° near the trench, and is gently folded into two arch structures beneath Puget Sound and Georgia Strait (Riddihough, 1984; Bostock and VanDecar, 1995; Ramachandran et al., 2005). However, recent work suggests that the northern end of the Juan de Fuca plate may no longer be subducting beneath North America, and therefore the active Juan de Fuca – North America subduction zone may be smaller than previously thought (Dziak, 2006).

2.3.1 Arc Volcanism: The Cascade–Garabaldi Belt

The combination of plates and spreading ridges subducting beneath North America from the northwestern United States to Alaska resulted in widespread and variable volcanism through the Miocene and onwards. Subduction of the Juan de Fuca (Farallon) plate beneath southern British Columbia and the northwestern United States produced arc volcanism of the Cascade–Garabaldi belt, including Mount St. Helens, Mount Baker and Mount Garibaldi (Souther, 1991). Cascade volcanism in southern British Columbia began around 29 Ma and progressively moved northward, tracking the migration of the northern edge of the Juan de Fuca (Farallon) plate from northern Washington to northern Vancouver Island (Souther and Yorath, 1991; Madsen et al, 2006). Westward migration of the Cascade–Garibaldi arc over the past several Ma

suggests progressive steepening of subduction angles of the Juan de Fuca and Explorer slabs (Green et al., 1988; Madsen et al., 2006).

2.3.2 Late Cenozoic Plate Edge and Intraplate Volcanism

The Pacific plate has been moving north-northwest, parallel to the British Columbian coastline and subducting beneath Alaska, for most of the Late Cenozoic (Madsen et al., 2006), giving rise to the Aleutian volcanic arcs (Jicha et al., 2006). Currently, the eastern edge of the Pacific slab extends beneath the southwestern Yukon and easternmost Alaska, near the Wrangell volcanic belt (Frederiksen and Bostock, 1998; Madsen et al., 2006). This edge and the northwestern edge of the Explorer slab define a slab window that extends from central British Columbia to the Yukon (Thorkelson and Taylor, 1989; Madsen et al., 2006). Widespread volcanism of intraplate affinity occurred above the slab window from Miocene to Recent time, including the Northern Cordilleran volcanic province and the Edgecumbe volcanic field (Madsen et al., 2006). The Anahim volcanic belt extends east across the slab window to above the Explorer slab, and has been interpreted as a hot-spot track from an underlying mantle plume (Bevier et al, 1979). The Chilcotin Group extends south from the current slab window to above the Explorer and Juan de Fuca slabs (Madsen et al, 2006). East of the Chilcotin Group, the Wells Gray–Clearwater field lies over the projected subsurface continuation of the Nootka fault (Madsen et al., 2006). South of the Chilcotin Group, flood basalts of the broadly coeval Columbia River Group erupted east of the Cascade arc in the northwestern United States.

2.3.3 Chilcotin Group Volcanism

The Chilcotin Group is composed of basaltic flows (trachybasalt to basaltic andesite) and minor associated pyroclastics and sediments, which erupted behind the coeval Cascade arc to form a flat-lying lava plateau in southern British Columbia (Bevier, 1983a, 1983b; Andrews and Russell, 2007). The basalts cover 36,500 km^2 of mainly Mesozoic and Cenozoic rocks of the Intermontane belt (Andrews and Russell, 2007). At the onset of volcanism, the slab window lay beneath this region, with the edge of the Juan de Fuca plate migrating northward as eruption of the Chilcotin Group continued (Madsen et al., 2006). Chilcotin volcanism began at ca. 32 Ma and continued into the Quaternary, with an apparent peak at ca. 9 Ma (Bevier, 1983b; Mathews, 1989; Dostal et al., 1996; Breitsprecher and Mortensen, 2004). The entire field appears to have been active for this duration, with the exception of the last 3 Ma when volcanism was more focused in the southern half of the field (Anderson et al., 2001; Breitsprecher and Mortensen, 2004).

2.3.4 Late Chilcotin Group Volcanism: The Valley Lavas

Chilcotin Group volcanism progressed from plateau-forming lavas in the Oligocene–Pliocene to valley-filling lavas in the Quaternary. The older "plateau basalts" formed broad, overlapping shield volcanoes, mantling the low local relief (<100 m) of the Neogene interior plateau and its paleodrainages (Figure 3a) (Bevier, 1983b; Mathews, 1989; Tribe, 2005; Andrews and Russell, 2007). Uplift followed by glacial and fluvial activity incised deep valleys through the basalt and underlying bedrock (up to 1000 m along the Fraser Valley), and divided the plateau into a patchwork of erosional remnants (Figure 3b) (Bevier, 1983b; Mathews, 1989). Late Cenozoic uplift in the Coast belt tilted the westernmost lavas to the northeast (Bevier, 1983b; Mathews, 1989). As eruption of

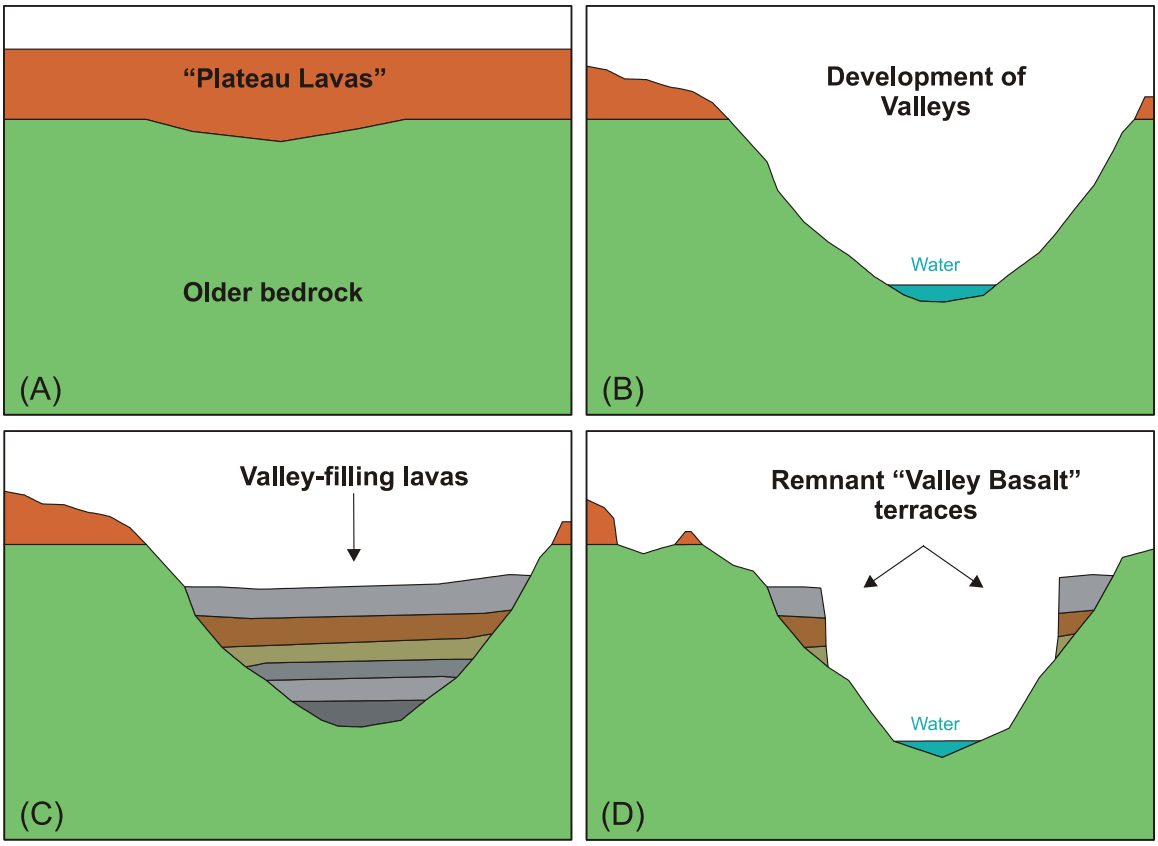

Figure 3. Generalized evolution of a typical valley basalt exposure
(A) Typical low-lying relief of the Neogene interior plateau, covered by flat-lying Chilcotin Group plateau lavas. B) Glacial and fluvial erosion following the eruption of the Chilcotin group plateau basalts leads to creation of valleys in the Merritt and Kelowna regions. C) Valley lavas erupt, and fill local valleys. D) Glacial and fluvial activity following valley lava eruption re-incises valleys. Valley lavas are preserved as terraces along valley walls.

the Chilcotin Group continued into the Quaternary, lavas flowed not only onto the plateau but into the valleys, forming what some researchers have referred to as "valley basalts" (Figure 3c) (Rice, 1947; Mathews, 1988; 1989). Pleistocene glaciation and fluvial erosion further denuded the plateau and deepened the valleys, preserving the valley lavas as terraces along the valley walls (Figure 3d), notably towards the southern extent of the volcanic field (Mathews, 1988; 1989). Mathews (1989) excluded these valley lavas from the formal definition of the Chilcotin Group as they postdate major plateau incision, however, the continuity in ages, and similar physical and geochemical characteristics outlined below suggest they should be included as an informal division of the Chilcotin Group.

2.4 The Valley Lavas: Physical Volcanology

The valley lavas of southern British Columbia are divisible geographically into two units: the Lambly Creek basalts (Church, 1980) and the Quilchena lavas (first described by Lambert, 1963). The Lambly Creek basalts are preserved on both sides of the Bear (Lambly) Creek valley, and for 1.5 km along the west bank of Okanagan Lake near Kelowna (Figure 4). The Quilchena lavas are preserved as discontinuous terraces in valleys east and south of Merritt (Figure 5). The Lambly Creek basalts are separated from the Quilchena lavas by a 70 km-wide highland that serves as a topographic divide.

Detailed examinations of lava sections within each region were completed, including measurements of elevation, lava and section thicknesses and flow morphology. Although separated geographically, the two units display similar morphology and geochemistry. Exposed sections are composed of flat-lying, subaerial flows that are

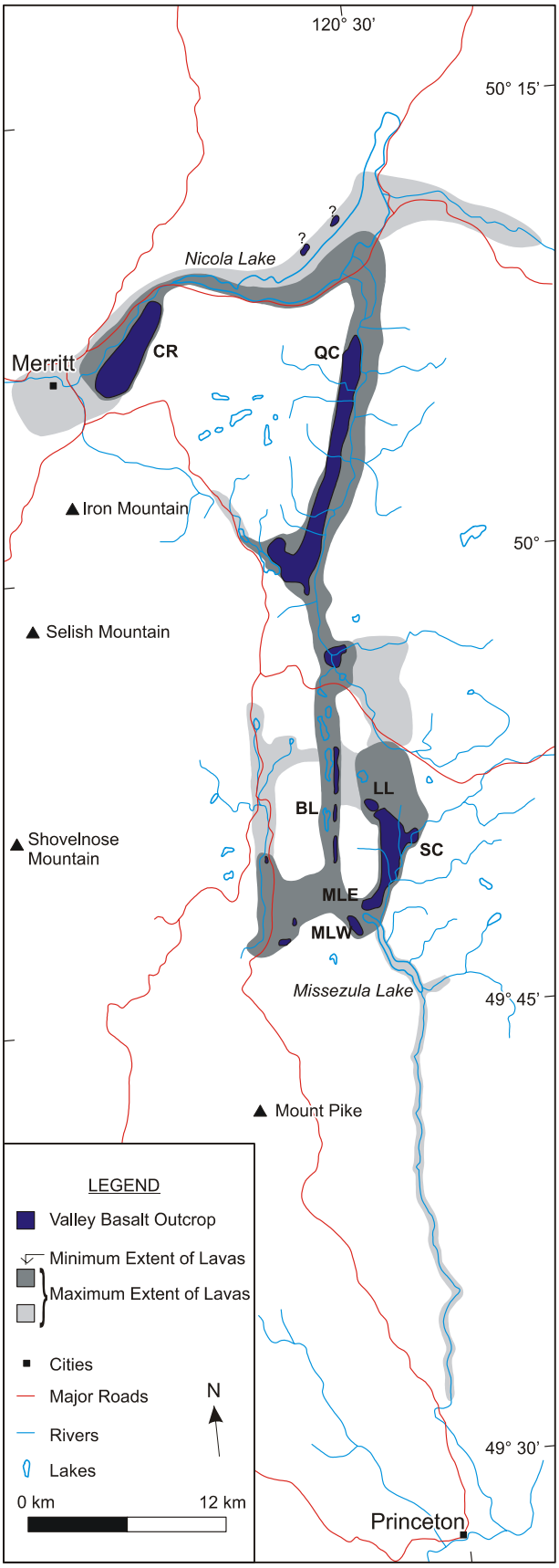

Figure 4. **Map showing the present-day and estimated original extent of the valley lavas (Quilchena lavas) in the Merritt region**

Existing outcropping of Quilchena lavas are shown in blue (from Preto, 1979; Monger, 1989a, 1989b). The estimated minimum extent of the Quilchena lavas (at the time of eruption) is shown in dark grey, and the estimated maximum extent of the Quilchena lavas (at the time of eruption) is shown as the combined dark and light grey shading. Mapped sections (see Appendix A) are labelled as follows: BL, Bluey Lake; CR, Chutter Ranch; LL, Loon Lake; MLE, Missezula Lake East; MLW, Missezula Lake West; SC, Shrimpton Creek, QC, Quilchena Creek.

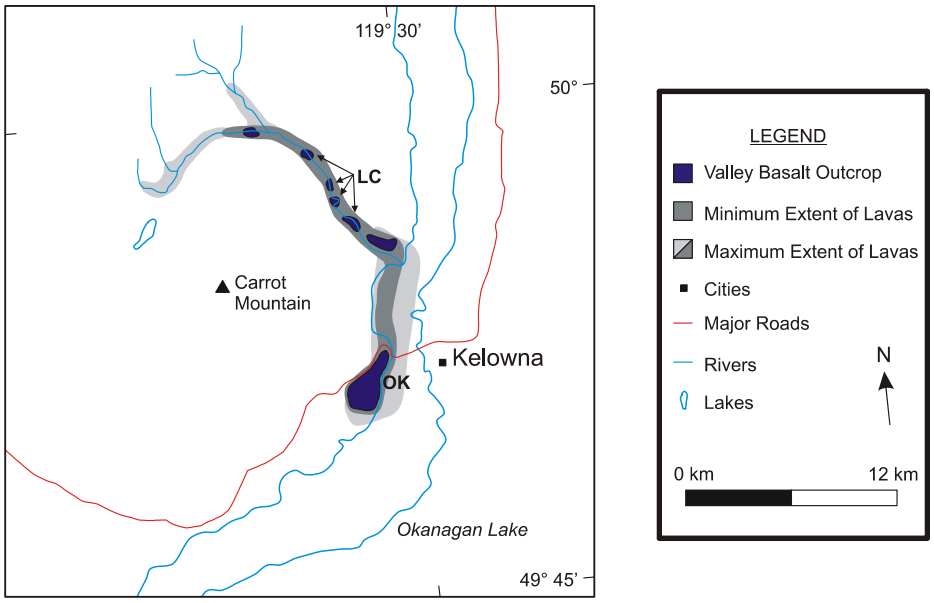

Figure 5. Map showing the extent of the valley lavas (Lambly Creek basalts) in the Kelowna region

Existing outcropping of Lambly Creeks lavas are shown in blue (after Tempelman-Kluit, 1989). The estimated minimum extent of the Lambly Creek lavas (at the time of eruption) is shown in dark grey, and the estimated maximum extent of the Lambly Creek lavas (at the time of eruption) is shown as the combined dark and light grey shading. Mapped sections (see Appendix A) are labelled as follows: SC, Shrimpton Creek, OK, Okanagan Lake.

typically 1–16 m thick. Crude columnar jointing is common in the thicker flows. The lava is fresh, and textures such as ropes, chisel marks, and vesicle cylinders and sheets are well preserved. In both regions the basalts unconformably overlie Triassic to Eocene volcanic and sedimentary rocks that dominate much of the southern interior of British Columbia. Appendix A contains locations and brief descriptions of sections from both regions.

2.4.1 Distribution and Volume

2.4.1.1 Establishment of Quaternary paleodrainages in the Merritt and Kelowna regions

Prior to the eruption of the plateau lavas during the Miocene–Pliocene, British Columbia's southern interior was dominantly composed of northwest-trending plateaus and plains, locally cut by deep paleodrainages (Tribe, 2005). Fluviolacustrine basins in the Merritt, Nicola Lake and Okanagan Lake valleys existed since at least Middle Eocene time (Tribe, 2005); however as base level increased during the Miocene, these valleys were partially infilled with Oligocene and Miocene strata (Tribe, 2005). The plateau lavas also erupted in the Miocene, disrupting paleodrainages (Mathews and Rouse, 1984; Tribe, 2004; Andrews and Russell, 2007). Base level fell during the Pliocene, creating new drainages and exhuming valleys that were previously buried (Tribe, 2004). During this time southward drainage was established in the Okanagan Valley south of Kelowna (Tribe, 2004).

During the Pleistocene, the repeated growth and decay of the Cordilleran ice sheet across most of British Columbia contributed to the evolution of the southern interior landscape (Ryder and Clague, 1989; Clague, 2000). Eight major climatic cycles are

recognized during this time period, some of which were accompanied by the development of a continental ice sheet in the interior of British Columbia (Ryder and Clague, 1989; Clague, 2000; Booth et al., 2003). These glaciations contributed to the restructuring of drainage systems and erosion of the landscape, and created large lakes in the interior (Clague, 2000). Between glaciations, erosion and deposition on the interior plateau was generally limited to near streams and areas of high relief (Clague, 2000). The last major glaciation in British Columbia's interior ended at approximately 10 ka. As a result of the repeated glaciation of this region up to the Holocene, few deposits from glaciations of Middle Pleistocene age and older remain (Clague, 2000; Booth et al., 2003).

The valley lavas erupted into an evolving landscape, one that continued to be modified by both glaciers and evolving fluviolacustrine drainages after eruption of the lavas ceased. Following valley lava volcanism, rivers and glaciers cut down through the valley lavas and into the underlying bedrock, preserving the lavas as terraces above the valley bottom. Although much of the lava was removed, the remaining sections can be used to estimate the volume of the lavas, and give insight into the environment the lavas erupted into and the nature of the volcanism.

2.4.1.2 Thickness of Preserved Sections

The thickness of preserved sections of Quilchena lava ranges from 15 m (Chutter Ranch) to ~130 m (Quilchena Creek), with most sections averaging ~30 m. The Lambly Creek basalts, in contrast to the Quilchena lavas, are preserved within a much smaller area along the narrow Lambly Creek valley, with exposed sections extending to the

valley floor. Sections along Lambly Creek are up to 40 m thick, whereas along Okanagan Lake (OK) sections are up to 25 m thick.

2.4.1.3 Estimation of Volume of Basalt Erupted

The main factors used to determine original lava volumes are the dimensions of the valleys at the time of eruption, the regional continuity and extent of the lavas, and lava thicknesses. In some areas, such as at Missezula Lake and Lambly Creek, the lavas are preserved on opposing valley walls. In such cases, the valley width at the time of eruption is equivalent to the distance between the contacts separating the valley lava from the adjacent bedrock on opposing valley walls. Similarly, in the valleys north of Missezula Lake, the lavas are preserved as discontinuous terraces on both sides of the valley, suggesting that the current valley width is a reasonable approximation of the original valley width. In contrast, in some areas the lavas are preserved on only one side of the valley, for example along Okanagan Lake and in the Nicola Valley, so the width of the valley at the time of eruption is unconstrained.

To estimate the volume of lava erupted, the preserved sections within the Quilchena or Lambly Creek regions are considered to be erosional remnants of a once-continuous valley-filling lava field. The current local topography was used to identify areas into which lava might have flowed, but where no lavas are preserved today. The minimum and maximum extents of the lava were estimated, with the minimum estimate restricted to low-lying areas between and near preserved sections, and the maximum extent including predictions of areas where the basalts might have once existed (Figure 4 and Figure 5). The Quilchena and Lambly basalts are estimated to have a combined volume of 8.8–21.1 km^3, less than one percent of the estimated volume (3300 km^3) of the

Chilcotin Group (Bevier, 1983b). For comparison, the Columbia River Basalt Group has an estimated total volume of 174,300 km^3, with individual flow volumes ranging from less than 1 km^3 to over 2000 km^3 (Tolan et al., 1989). Most of the calculated valley lava volume represents the Quilchena lavas, which are preserved over a much larger area than those near Lambly Creek. The detailed method used to determine the volume of the Quilchena and Lambly Creek basalts is described in Appendix B.

2.4.2 Lava Morphology and Internal Features

2.4.2.1 Physical Characteristics of Lavas

Exposures of both the Quilchena and Lambly Creek lavas are composed of nearly flat-lying, dominantly subaerial flows, which number between two and eighteen flows in a given section. The flows range in thickness from <1 m to ~16 m, with a given exposure being composed of flows of similar thickness. For example, the Quilchena Creek exposure is composed of flows 5–15 m thick that each extend for over 100 m along the section (Figure 6). In contrast, the Missezula section is composed of thin (1–2 m thick) flows at the base, and thicker flows (up to 18 m) interlayered with thin flows near the top. Individual flows at Missezula Lake extend laterally from a few meters to >500 m, although actual flow lengths are likely to be even greater (Figure 7). Thicker flows (e.g. the 18 m-thick flow at Missezula Lake) likely are "simple" flows, but some of the thinnest may be "compound" flows, forming multiple similar-sized lobes (Self et al., 1998). Individual flows cannot be followed with confidence from section to section.

The lavas display well-defined textures due to a lack of significant weathering and alteration. On fresh surfaces the lavas range from medium-grey to black, and on weathered surfaces from grey to red-brown. Vertical columnar jointing is common in

Figure 6. Photograph of flat-lying lava flows at the Quilchena Creek exposure
White dashed lines indicate contacts between lava flows.

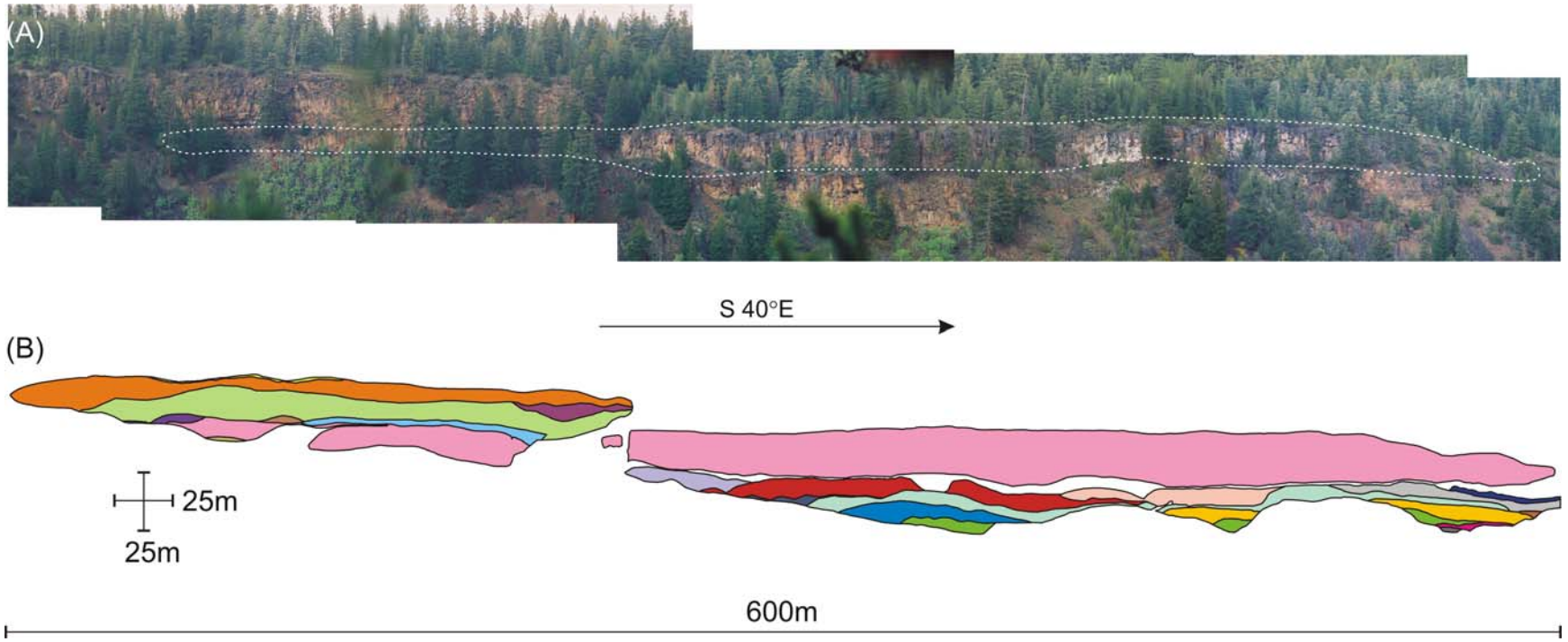

Figure 7. Quilchena lava flows north-east of Missezula Lake ("Missezula Lake section")
(A) Stitched photograph of the Missezula Lake section, with a single lava flow outlined by a white dashed line. (B) A map of the same section, with each individual lava flow identified in the section shown in a different colour. The pink flow (midway up the section) corresponds to the outlined flow in (A). Map modified from unpublished fieldwork by R. Fitton in 2000.

thicker flows, and commonly extends through the entire flow thickness (Figure 8a). Only one flow near Quilchena Creek has a possible intervening entablature (Figure 8b). The columnar jointing ranges from crude to well-defined, with individual columns ranging from 30–70 cm wide. Some columns display evenly spaced horizontal chisel marks (Figure 8a).

Generally, the lavas are most vesicular at the base and top of a given flow, with a denser interior. The base is usually moderately vesicular and locally ropey, and grades up into the denser interior over 5–30 cm (Figure 8b–d). Pipe vesicles occur at the base of some flows, and locally have a consistent direction of tilt or curvature. The top of a flow is generally highly vesicular over a thickness of tens of centimetres to metres (Figure 8e). The flow-top may be crudely layered, with zones of denser lava between zones with greater vesicle abundances. Coarse autoclastic breccia or ropey pahoehoe defines the upper surface. Although most vesicles are open, locally they are filled by calcite or quartz, particularly in the Lambly Creek valley.

Flow interiors locally host vesicle cylinders and sheets. Vesicle cylinders, which range from 5 cm to >60 cm in height, are crudely cylindrical regions of densely-packed vesicles of uniform size (2–5 mm) (Figure 9a, b). Shapes range from tapered cylinders to mushrooms to upside-down tear-drops, and in some instances are tilted in a similar direction to that of pipe vesicles. Vesicle sheets are usually 2–3 cm thick and, where present, commonly occur more than once in the lava flow, separated by horizontal layers of denser lava (Figure 9c, d). The sheets are most abundant in flows that also contain vesicle cylinders. In one instance, the top of a mushroom-shaped vesicle cylinder merges

Figure 8. Photographs of valley lava physical features

(A) Vertical columnar jointing in a lava flow at the Missezula Lake exposure. Horizontal chisel marks cut across the columns. (B) Possible entablature observed in a lava flow at the Quilchena Creek exposure. The upper colonnade and lower colonnade (mostly hidden behind brush) are also indicated. Ropey texture is observed at the top of the columnar-jointed flow. (C) Pipe vesicles observed at the base of a flow at the Quilchena Creek exposure. The tops of the pipes are tilted in the direction of lava flow (i.e. away from where the lava erupted). (D) A contact between two flows, showing the highly vesicular flow top of the lower flow, and the vesicular base of the upper flow grading into dense flow interior, like the columns in (A). Small pipe vesicles are also present. (E) Top of lava flow, grading from mildly vesicular in the interior of the flow to highly vesicular at the top. Denser bands of vesicles are observed within the vesicular flow top.

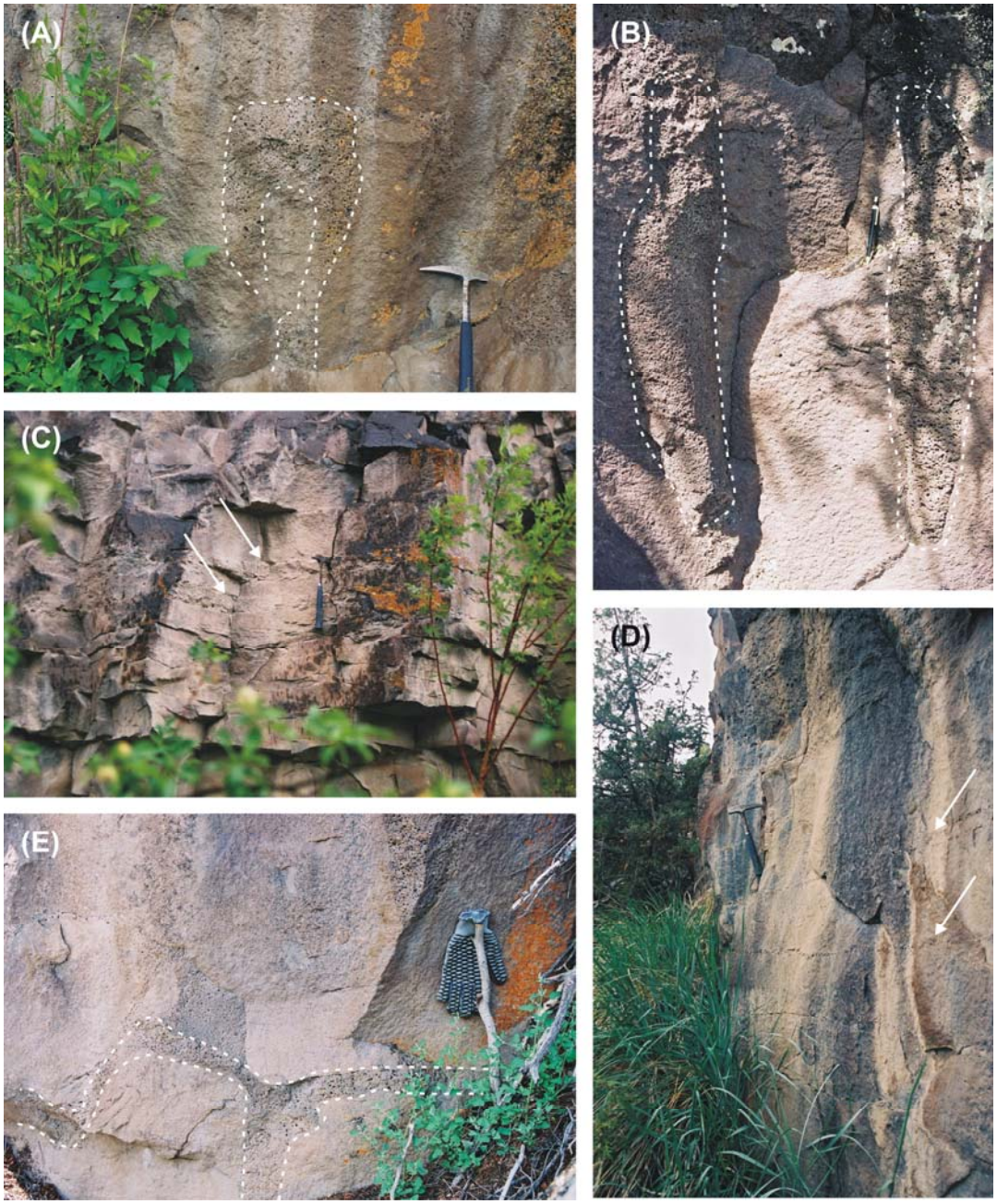

Figure 9. Photographs of vesicular features observed within valley lavas
(A) A diapir-shaped vesicle cylinder observed within the Quilchena lavas. (B) Tubular vesicle cylinders observed at the Quilchena Creek exposure. This is the most common shape of vesicle cylinder observed within the lavas. (C)&(D) Vesicle sheets observed at the Quilchena Creek exposure. (E) A mushroom-shaped pipe vesicle, observed at the Quilchena Creek exposure. The cylinder appears to have risen up into denser lava, and then spread out. The two ends of the vesicle cylinder (exiting the left and right of the picture) thin out into a horizontal vesicle sheet.

with a vesicle sheet (Figure 9e). The contact between two flows is typically near-horizontal except where a flow pinches out or abutts a pile of scoriaceous autobreccia.

Thin layers (<10 cm) of friable grey-brown silt are commonly trapped within or at the basal unconformity of lava successions (Figure 10a, b). In some cases, the sediment has been lithified into an indurated siltstone, probably through contact metamorphism with the hot lava (e.g., Bluey Lake, Figure 10a). In others, sediment at the base of a flow extends upward into a localized zone of autobreccia where it serves as the matrix to a jumble of vesicular lava clasts (Figure 10c–e). These pockets of autobreccia range from 20–40 m wide, and may extend through the entire thickness of the flow. Figure 11 illustrates the range in textures observed in the valley lavas, and their relation to one another within a given flow.

2.4.2.2 Interpretation and Significance of Lava Morphology and Internal Features

The physical features of the valley lavas provide evidence of their depositional environment and eruptive history. As the lavas erupted in the Quilchena and Lambly Creek regions, they flowed into and then along valleys, covering the Triassic to Eocene bedrock and Pleistocene surficial deposits (Figure 12a, b) and accumulating to form successions up to 130 m thick. Where lava flowed over moist sediment or ponded water, the water boiled explosively, quenching the lava into a localized a'a-like breccia, and forming spiracles and explosion tubes. Sediment entrained in the water shot up into the brecciating lava, coating and supporting the lava clasts and in some cases becoming thermally lithified into siltstone.

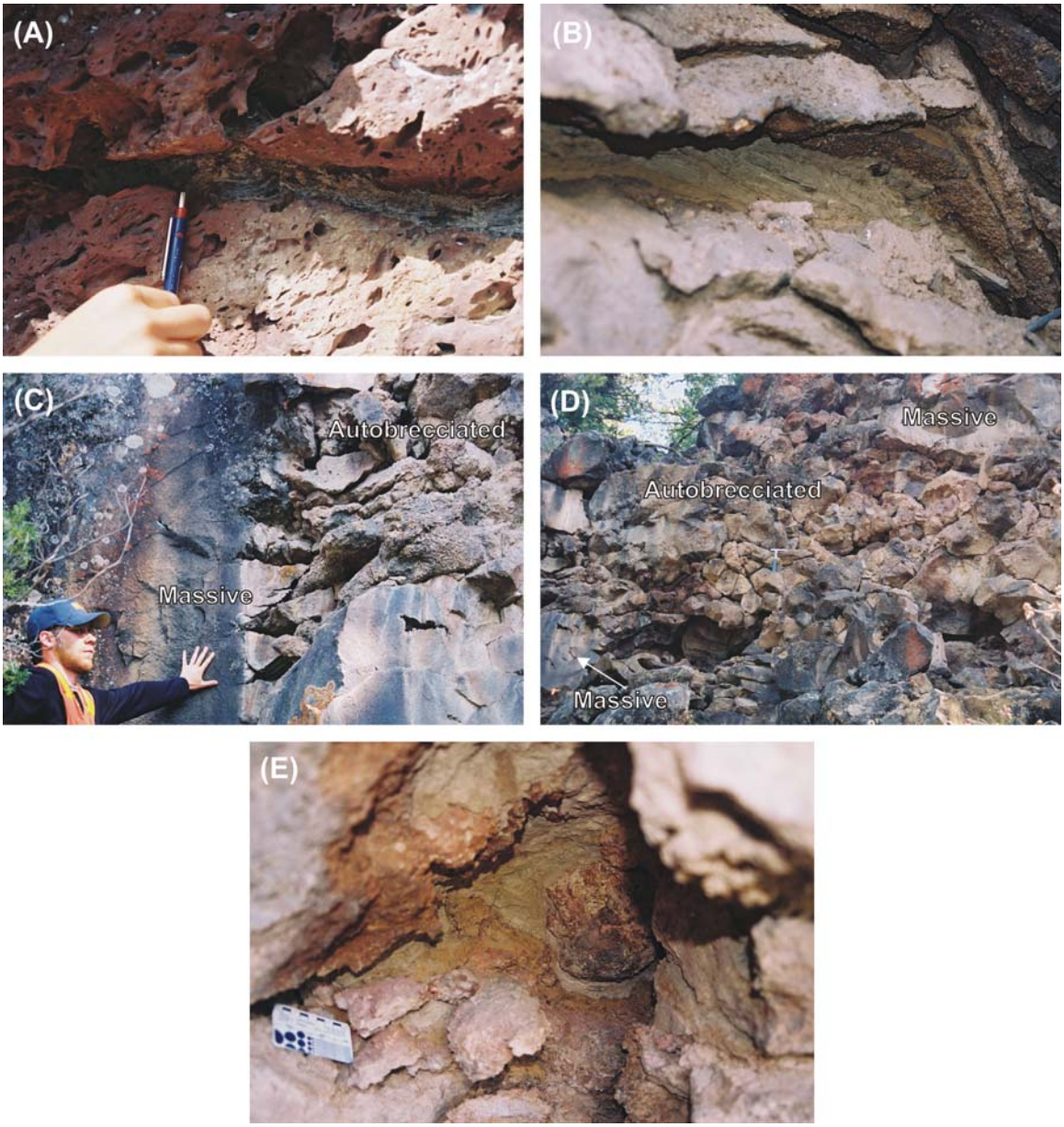

Figure 10. Photographs of sediment layers observed between lava flows
(A) Silt layer between two flows in the Bluey Lake exposure. The silt has been baked by the upper flow into an indurated siltstone. (B) Silt layer between two flows in the Okanagan Lake exposure. (C) A massive lava flow abruptly transitions into an autobrecciated flow at Missezula Lake. (D) The same flow as in (C), showing the entire autobrecciated section. In this case, the flow is typically massive, with this isolated autobrecciated section that over a restricted distance encompasses the entire flow. (E) A close-up view of the autobrecciated section, showing a vesicular lava clast supported by unaltered sediment.

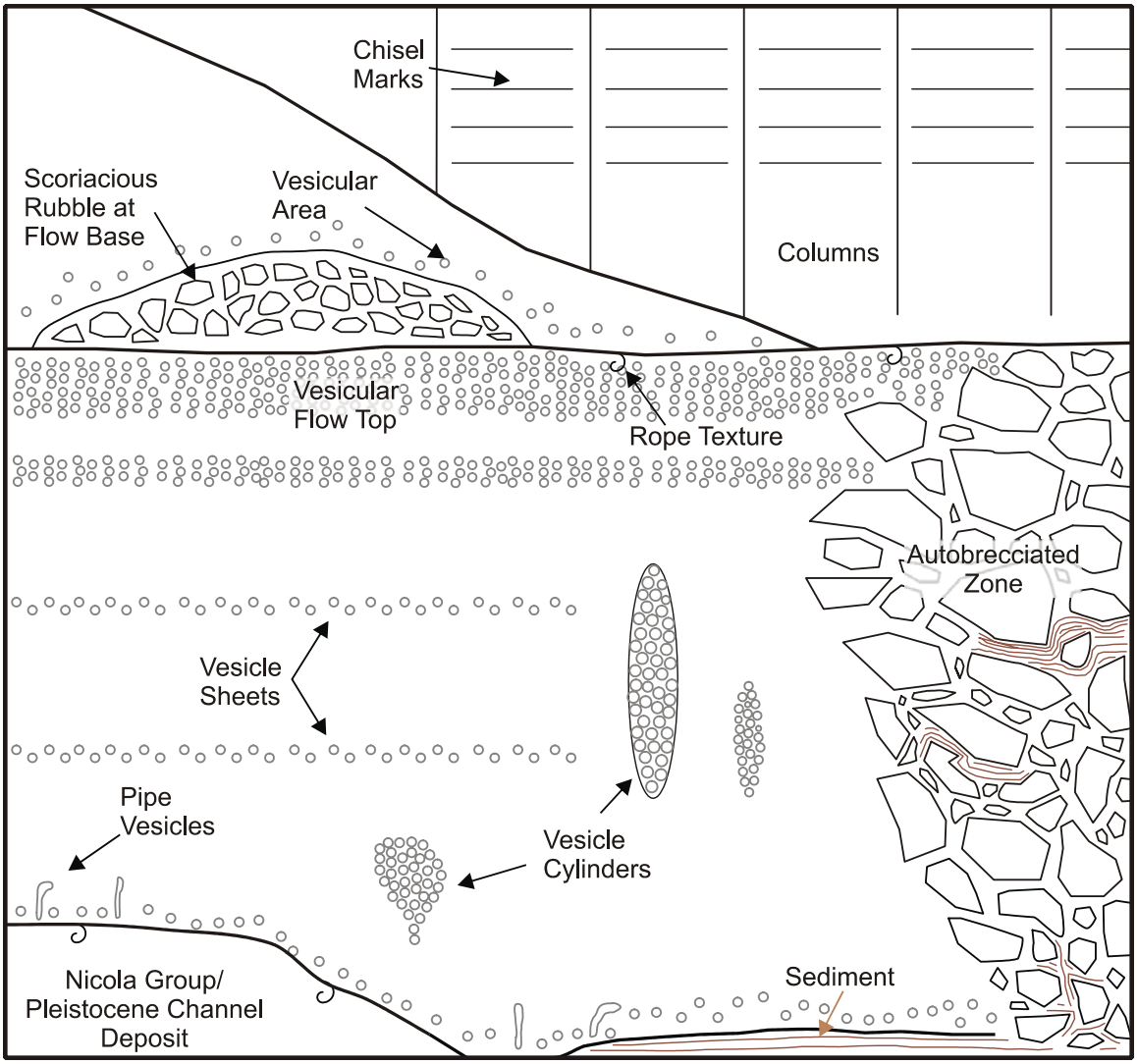

Figure 11. Hypothetical section of through valley lavas, showing the textures and features observed

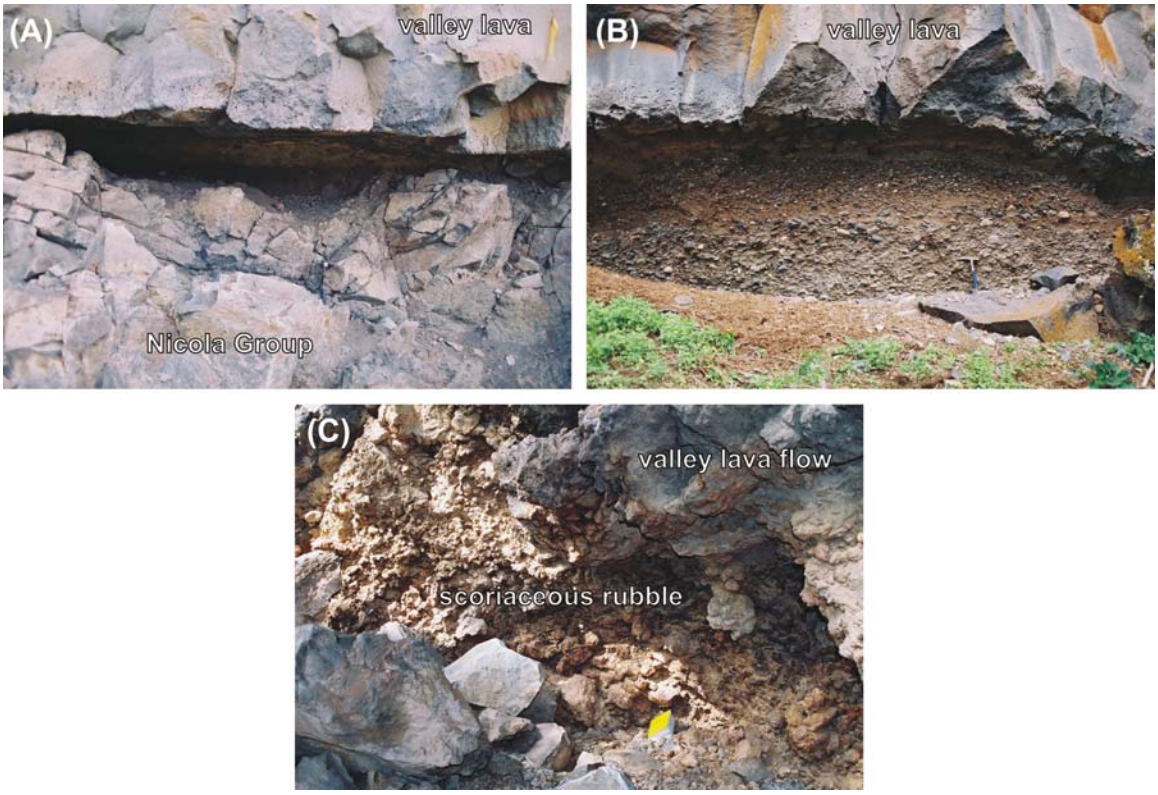

Figure 12. Photographs of basal contacts of valley lavas
(A) Valley lavas unconformably overlying Nicola Group volcanic rocks at the Missezula Lake exposure. A silt layer containing pebble and cobble-sized clasts of Nicola Group volcanic rocks can be observed between the two units. (B) Valley lavas overlying a Pleistocene channel deposit at the Chutter Ranch exposure. (C) Valley lava at the Missezula Lake exposure overlying a layer of scoriaceous lava rubble, which lies directly above another lava flow.

As a lava flow moved along the valley, its base and top cooled much more quickly than its interior, freezing bubbles of gas in place along the flow margins. The chilled, vesicular flow top was locally cycled underneath the still-moving flow interior, and became preserved as scoriaceous rubble at the flow base (Figure 12c). Pipe vesicles formed at the flow base as a result of bubbles of gas rising up through the lava or exsolved gas bubbles trapped on the rising lava solidification front (Philpotts and Lewis, 1987; Walker, 1987; Godinot, 1988). The upper tips of these pipe vesicles were sometimes distorted (tilted) by motion of the hotter, still-flowing flow interior, preserving the local flow direction.

As the lava flow continued to move away from its source and cool, pulses of hotter, more volatile-rich lava were injected into the core of the flow, increasing its thickness by inflation, and leading to bands of alternating vesicle-poor and vesicle-rich zones (Hon et al., 1994; Self et al., 1998). Progressive solidification of the basaltic lava produced pockets of a more felsic and volatile-rich residual liquid, which moved upwards through the flow as vesicle cylinders (Self et al., 1998). Most of these rose until they reached a cooler, rheologically impermeable front and then spread out laterally into thin vesicle sheets, although some became solidified in-place as vesicle cylinders (Self et al., 1998). In many flows, this sequence of events occurred more than once, leading to multiple vesicle sheets. Columnar joints formed in some of the thicker flows that ponded prior to solidification.

2.4.3 Flow Direction

Flow directions for both the Lambly Creek basalts and the Quilchena lavas can be inferred using flow base elevations coupled with paleoflow indicators such as pipe vesicles and vesicle cylinders (cf., Schmincke, 1967). The Quilchena lavas most likely flowed south to north, as the base of the lavas progressively decreases from an elevation of 1070 m near Missezula Lake to 600 m near Merritt. Tilted pipe vesicles in lavas preserved west of Quilchena Creek support this interpretation (Figure 8c). Pipe vesicles in the Shrimpton Creek valley are less conclusive, although the direction of flow in this region may have been more complex as it is close to a proposed lava source (the Loon Lake intrusive sample). Although not identified in the field, it is likely that there are other vents in the Quilchena region, possibly near the Quilchena Creek section where the lavas are thick (130 m-thick section of valley lava).

The Lambly Creek basalts flowed southeast along Lambly Creek towards Okanagan Lake, and south through the Okanagan Valley, as indicated by north-dipping vesicle cylinders along Okanagan Lake, and the decrease in flow base elevation along this path. No vents were identified in the Lambly Creek region, but flow direction suggests at least one vent was present near the Lambly Creek headwaters west of Okanagan Lake.

2.5 Sampling

Thirty-six samples were collected for mineralogical and geochemical analysis, including five samples of older plateau lava. A subset of these samples was selected for ^{40}Ar–^{39}Ar dating. Of the twenty-eight geochemical samples collected from the Quilchena lavas, nineteen are from a section on the north-east side of Missezula Lake, with the

purpose of facilitating a more detailed study through a typical section of valley lava. The nine other Quilchena lava samples were selected from five other sites in which detailed studies had been completed; one of the sites is the location of a possible intrusive equivalent of the valley lavas. Three samples of Lambly Creek lavas were also collected from sites which had undergone a detailed study. A pilot paleomagnetic study was also completed, details of which are presented in Appendix C.

2.6 Petrography

The valley lavas range from aphyric to moderately porphyritic, with phenocrysts (0.5–2 mm) of olivine ± plagioclase ± augite occupying up to 20% of the rock volume. The phenocrysts are set in a groundmass that ranges from subophitic to intergranular to hyalo-ophitic. Olivine microphenocrysts sometime display resorbtion features (e.g. embayments), and may contain inclusions of spinel/chromite. Many of the larger olivine crystals display growth zoning. Accessory minerals include magnetite, ilmenite and apatite. Vesicles are common and occupy up to 75% of rock volume; samples collected for petrographic and geochemical analysis are composed of less than 15% vesicles. Alteration is generally limited to iddingsite on the rims and fractures of olivine crystals, and calcite and quartz infilling of vesicles. Interstitial glass is generally unaltered. The Lambly Creek lavas are slightly more altered than the Quilchena lavas. Appendix D shows the mineralogical composition of each sample, including five plateau basalt samples collected as part of this study.

Two petrographic types of valley lava are recognized. The main type is characterized by a low phenocryst content (generally <10%) consisting of almost entirely olivine. The olivine phenocrysts, some of which exhibit resorption features (Figure 13a),

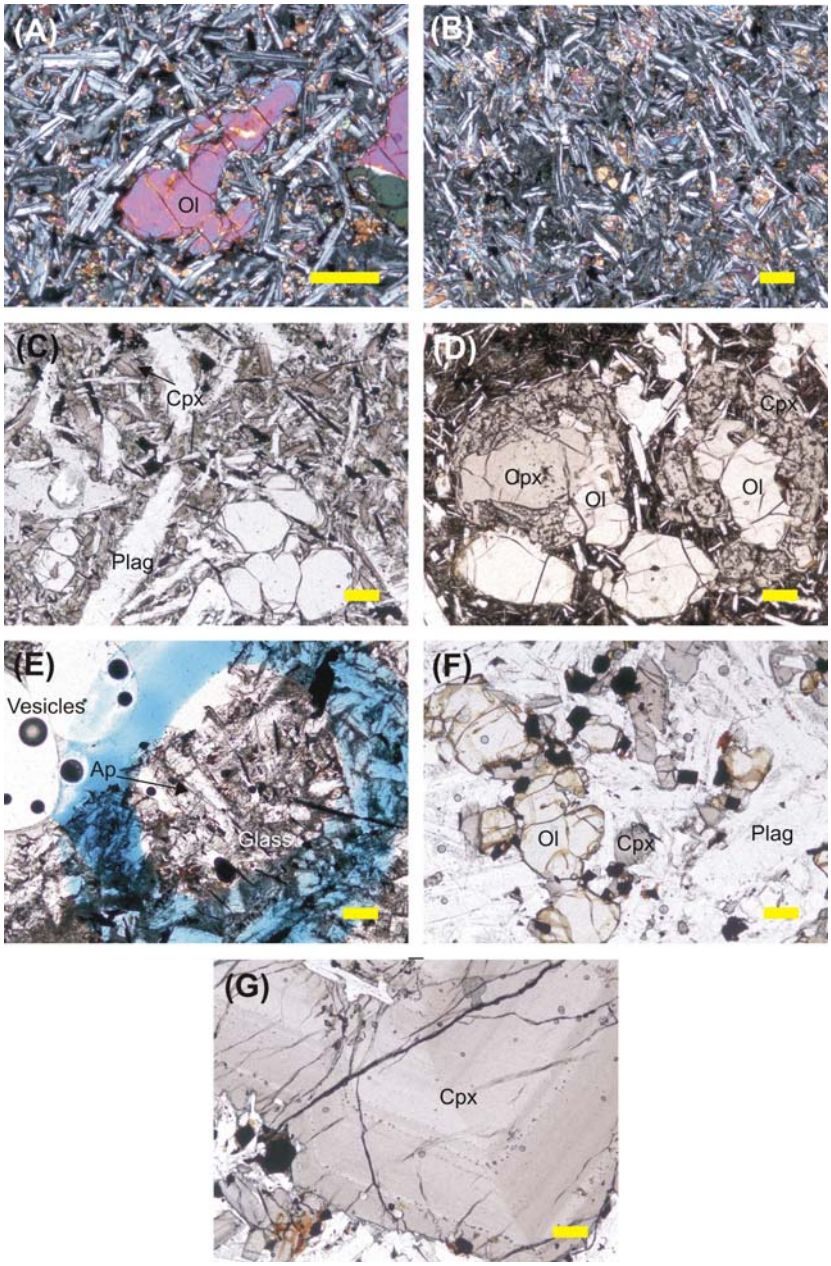

Figure 13. Representative photomicrographs of valley lava samples
Length of yellow bar on each photomicrograph = 20 μm. Labels: Ol, olivine; Plag, plagioclase; Cpx, clinopyroxene (generally augite); Ap, apatite needles. (A) RF-4-1-2, partially-resorbed iddingsitized olivine crystal in plag+ol+cpx groundmass, cross-polarized light. (B) RF-4-8-1, phenocryst-poor lava, with plag+ol+cpx groundmass, cross-polarized light. (C) RF-4-6-2, olivine and plagioclase phenocrysts, with smaller augite crystals in the groundmass, plane polarized light. (D) RF-4-12-1, olivine phenocrysts with augite rims, plane polarized light. (E) CS-05-2-2-1, apatite needles, magnetite, ilmenite and glass beside vesicle cylinder. (F) CS-04-3-1-1, representative image of the possible valley lava intrusive equivalent, with olivine, plagioclase and augite crystals, plane polarized light. (G) CS-04-3-1-1, large zone and partially-resorbed augite crystal in possible valley lava intrusive equivalent, plane polarized light.

are set in a uniformly sized fine-grained groundmass (plagioclase + clinopyroxene ± olivine with minor magnetite/ilmenite and apatite). Some samples have no phenocrysts, and are composed entirely of groundmass crystals (Figure 13b). The groundmass plagioclase ranges from weakly aligned isolated grains to radiating clusters. Glass is rare, but where present is commonly interstitial.

The other petrographic type is limited to some flows in the Missezula Lake and Shrimpton Creek sections of the Quilchena lava. It is characterized by a relatively high phenocryst content (≥14%; olivine, plagioclase and augite) and more glass and apatite (Figure 13c–d). The phenocrysts commonly occur as glomerocrysts, surrounded by a seriate groundmass composed of plagioclase + augite + glass ± olivine and accessory magnetite/ilmenite and apatite (particularly well-observed in the contact between the host lava and a vesicle cylinder; see Figure 13e). Some olivine phenocrysts are partially resorbed (resorbed rims or embayments), and some display augite rims or are enclosed by augite phenocrysts. Augite and plagioclase display sub-ophitic texture, however in a few samples augite completely surrounds plagioclase. A few samples (Missezula Lake and Bluey Lake sections) are intermediate to the two main types, with rare plagioclase and augite phenocrysts accompanying the olivine phenocrysts, and set in a fine groundmass similar to the second group.

One possible intrusive equivalent to the valley lavas occurs south of Loon Lake in the Quilchena lava region. The unit is composed of equigranular augite + olivine + plagioclase, with accessory magnetite/ilmenite and apatite (Figure 13f–g). The augite crystals are visually striking in hand sample and occupy 20% of rock volume. The augite grains are generally 0.5–1 mm (up to 3 mm) across, strongly zoned with embayed edges,

and commonly form glomerocrysts with olivine. The olivine grains contain opaque minerals, and tend to be smaller than the augite grains. Plagioclase laths (≤ 2 mm long), which comprise half the rock, exist between the glomerocrysts, and have sieve-textured interiors. Untwinned plagioclase (15%) is interstitial to the twinned plagioclase laths. Spherical vesicles occur in low proportion toward the top of the unit. Alteration of the sample is generally limited to olivine, which is partially to completely iddingsitized.

2.7 Geochronology

The Chilcotin Group has been extensively dated, with over one hundred published dates, most of which were determined using the K–Ar method as reported in Breitsprecher and Mortensen (2004). However, only five K–Ar dates exist for the Lambly Creek and Quilchena lavas, two of which are poorly constrained. In this study, the ^{40}Ar–^{39}Ar laser fusion technique was used to determine the age of seven valley lava samples, from both the Quilchena and Lambly Creek regions. Paleomagnetic analyses have also been used in previous studies to constrain the ages of the valley lavas (Church, 1980), and are used in the same fashion in this paper with the new isotopic results. The ^{40}Ar–^{39}Ar analyses were performed at the Pacific Centre for Isotopic and Geochemical Research, Department of Earth and Ocean Sciences at the University of British Columbia. Age spectra used to determine age of sample are shown in Figure 14; both the plateau and inverse isochron plots for each sample are shown in Appendix E, along with relevant sample descriptions and analysis, previous K–Ar dates on the section, and analytical data.

2.7.1 Quilchena Lavas

Six samples were analyzed to constrain the timing of eruption of the Quilchena lavas. Of these, three samples are from the Missezula Lake section, from near the base, middle and top. The base of the section (CS-04-28-1-1) is interpreted to have a crystallization age of 660 ± 30 ka (Figure 14a). The middle (CS-04-2-14-1) and top (CS-04-2-29-1) of the section are interpreted as 400 ± 100 ka and 180 ± 50 ka, respectively (Figure 14b and c), although the plateaus are of poorer quality than that from the basal sample. The analysis from the top of the section appears to have a low-temperature plateau at ~350 ka, likely a result of excess Ar, and so has been discounted. A sample collected from the possible intrusive equivalent of the Quilchena lavas near Loon Lake, 6.5 km north of Missezula Lake, has a plateau age of 460 ± 40 ka (Figure 14d), which correlates well with results at Missezula Lake. Therefore, volcanic activity at the southern end of the Quilchena lavas appears to have occurred from at least 660 ± 30 ka, and continued until as recently as 180 ± 50 ka.

Two samples were also analyzed from the northern extent of the Quilchena lavas, from sections that had previously documented K–Ar and paleomagnetic results. The $^{40}Ar/^{39}Ar$ analysis of a sample from west of Quilchena Creek (CS-04-8-3-1) produced a plateau age of 900 ± 100 ka, but because excess Ar was present in the sample (initial $^{40}Ar/^{36}Ar$ = 323.4 ± 9.5), the isochron age of 800 ± 100 ka is accepted as the igneous crystallization age (Figure 14e and f). Paleomagnetic data collected from the same flow indicates that the sample has a magnetic normal signature, and therefore most likely belongs to the Brunhes magnetic chron (<780 ka), as had been previously suggested by Fulton et al. (1992) (time scale from Cande and Kent, 1995). Therefore, the igneous

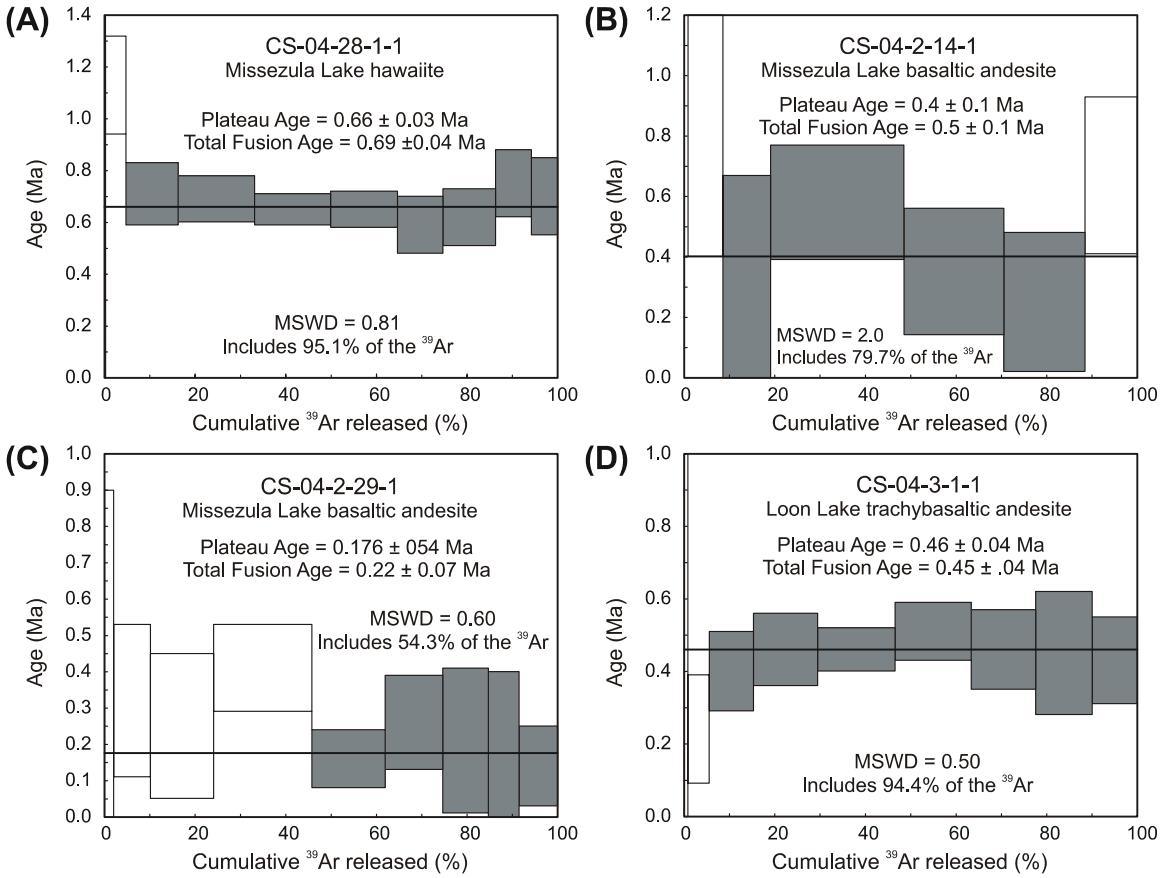

Figure 14. ^{40}Ar–^{39}Ar degassing spectra for six Quilchena lava and one Lambly Creek lava samples

The data was processed and results plotted using Isoplot 3.09 (Ludwig 2003) by T. Ullrich. The interpreted cooling age (which is likely the eruption age for these lavas) was determined from the plateau for all samples except CS-04-8-3-1, where the inverse isochron method was used. Only the shaded plateau steps were used in the plateau calculation. All uncertainties are reported at 2σ confidence limits. Only whole rock material was used in these analyses. (A) CS-04-28-1-1, base of Missezula Lake section; (B) CS-04-2-24-1, middle of Missezula Lake section, (C) 04-2-29-1, top of Missezula Lake section; (D) CS-04-3-1-1, possible Quilchena lava intrusive equivalent.

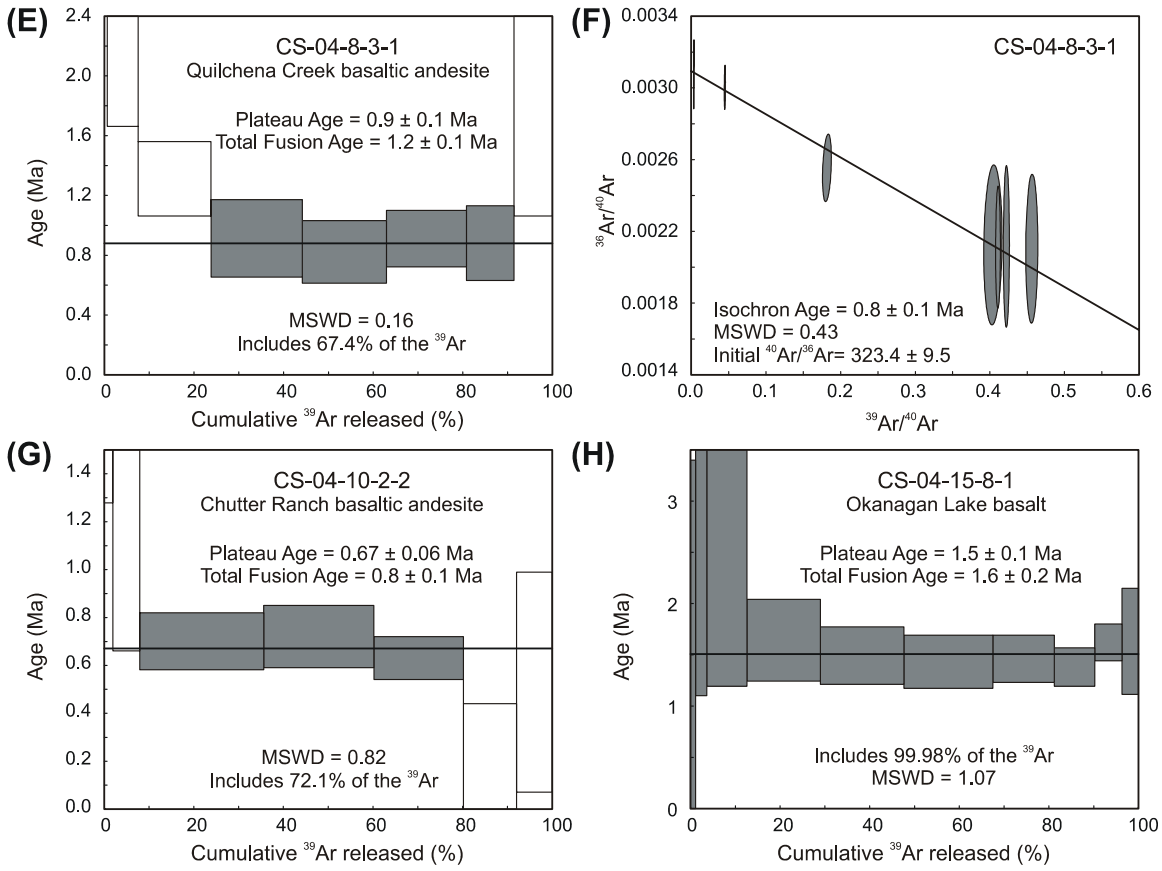

Figure 14. **^{40}Ar–^{39}Ar degassing spectra for six Quilchena lava and one Lambly Creek lava samples (continued)**

(E) and (F) CS-04-8-3-1, Quilchena section (isochron age taken as cooling age; (G) CS-04-10-2-2, Chutter Ranch section; (H) CS-04-15-8-1, Okanagan Lake section (only Lambly Creek lava sample).

crystallization age of this sample is constrained to be between 700 and 780 ka. The second sample was obtained from the Chutter Ranch, 2 km east of Merritt (CS-04-10-2-2), and yielded a date of 670 ± 60 ka (Figure 14g).

These six age determinations suggest that deposition of valley lavas in the Quilchena succession commenced at least as early as 780 ka in the north, possibly 100 ka earlier than volcanic activity in the south. The similarity in ages and chemistry (see geochemistry) between the Loon Lake occurrence and the base of the Missezula Lake section suggests that they are related, possibly with the basaltic flows in the southern end of the Quilchena lava field originating from a volcanic centre at Loon Lake. The lavas at the northern end of the Quilchena lava field probably originated south of the Quilchena section (based on paleo-flow indicators). Read (2000) suggested the valley lavas in the Merritt area originated from north of Courtney Lake and flowed south towards the Nicola valley, and this scenario is likely based on the decrease in elevation and section thickness to the north, and northward paleo-flow indicators.

2.7.2 Lambly Creek Lavas

One sample of the Lambly Creek lavas was analyzed, complementing previously determined K–Ar ages. The previous K–Ar and paleomagnetic results indicate that the lavas are less than 780 ka, in both the Lambly Creek and Okanagan Lake (Church, 1980; Mejia et al., 2002). However, the ^{40}Ar–^{39}Ar analysis of a flow from the Okanagan Lake section yields an age of 1.5 ± 0.1 Ma (Figure 14h). Paleomagnetic analysis of the same flow suggests it cooled during a magnetic normal period, but the ^{40}Ar–^{39}Ar age falls in the middle of a magnetic reversal (Cande and Kent, 1995). This inconsistancy between

the paleomagnetic and ^{40}Ar–^{39}Ar might be explained by a total resetting of the system, or the error on the analysis being larger than reported. An initial ^{40}Ar–^{36}Ar ratio of 298.9 ± 3.9) suggests that the sample was not in equilibrium with excess Ar.

2.8 Geochemistry

Major and trace element compositions were determined for thirty-six samples of Chilcotin Group volcanic rocks. Quilchena lava samples were collected from the previously described sections at Missezula Lake (n=19), Bluey Lake (n=3), Quilchena Creek (n=2), Chutter Ranch (n=2), as well as individual samples from Loon Lake and Shrimpton Creek. Lambly Creek lava samples were collected from along Lambly (Bear) Creek (n=2) and along Okanagan Lake (n=1). Five samples of plateau basalt were also collected. Sample locations are presented in Appendix A.

All selected samples were vesicle-poor, and free of amygdules. Weathered surfaces were chipped off in the field. Geochemical analyses were determined by ACTLABS (n=34) and ALS Chemex (n=2); analytical techniques used by both labs are outlined in Appendix F. Major and trace element compositions for all samples are in Table 1. Appendix F also presents analytical uncertainty analysis methods and results.

Neodymium isotopic ratios for seven whole-rock samples (and one duplicate) were determined at the Pacific Centre for Isotopic and Geochemical Research (PCIGR) at the University of British Columbia in Vancouver, Canada. Analytical techniques are outlined in Weis et al. (2005). The average $^{143}Nd/^{144}Nd$ value of the La Jolla standard run during the analytical session was 0.511853±6 (n=11).

Table 1. Major element oxide (wt.%) and trace element (ppm) concentrations for the valley lavas, and five plateau lavas

Sample	CS-04-2-26-1	RF-4-6-2b	RF-4-5-2	RF-4-5-3	RF-4-6-1	RF-4-10-2	RF-4-11-1	RF-4-12-1	CS-04-2-9-1
Unit	Quil. Lava	Quil. Lava	Quil. Lava	Quil. Lava	Quil. Lava	Quil. Lava	Quil. Lava	Quil. Lava	Quil. Lava
Type	A	A	A	A	A	A	A	A	CA-type 3
Location	Miss. Lk.	Miss. Lk.	Miss. Lk.	Miss. Lk.	Miss. Lk.	Miss. Lk.	Miss. Lk.	Miss. Lk.	Miss. Lk.
Rock Type	Tr. Basalt	Tr. Basalt	Tr. Basalt	Tr. Basalt	Tr. Basalt	Tr. Basalt	Tr. Basalt	Tr. Basalt	B.And.
SiO_2	48.72	48.24	48.33	48.64	48.80	48.27	49.15	48.42	52.43
Al_2O_3	15.83	15.54	14.95	15.75	15.71	15.58	15.03	15.70	15.38
Fe_2O3	9.34	9.16	9.30	9.28	9.23	9.17	9.43	9.25	8.16
MnO	0.13	0.13	0.13	0.13	0.13	0.13	0.13	0.13	0.11
MgO	6.57	7.04	7.62	6.59	6.84	6.66	7.39	6.72	7.69
CaO	8.78	9.21	9.41	8.85	9.15	8.99	9.07	9.00	8.65
Na_2O	4.57	3.76	4.15	4.33	3.85	3.82	3.86	3.87	3.60
K_2O	1.97	1.66	1.74	1.89	1.64	1.79	1.76	1.73	1.00
TiO_2	2.58	2.33	2.50	2.55	2.41	2.41	2.43	2.44	1.49
P_2O_5	0.73	0.63	0.69	0.72	0.65	0.65	0.67	0.68	0.38
LOI	-0.23	1.18	-0.18	0.03	0.70	0.60	0.43	0.70	0.05
TOTAL	99.00	98.89	98.63	98.75	99.12	98.07	99.34	98.63	98.94
Mg#[1]	62	64	66	62	63	63	65	63	69
Cs	0.2	b.d.	0.2	0.2	0.2	0.1	0.2	0.2	0.4
Rb	20	15	18	19	16	16	17	17	14
Ba	341	338	313	339	370	334	344	335	253
Th	2.98	2.73	2.85	2.84	2.65	2.62	2.68	2.64	2.21
U	1.09	1.01	1.09	1.11	0.89	0.98	1.05	0.99	0.71
Nb	50.1	45.8	47.9	52.1	48.8	49.7	48.9	50.9	28.2

***Quil. Lava**, Quilchena Lava; **Miss. Lk.**, Missezula Lake; **A**, Alkaline; **CA**, Calc-Alkaline; **Tr. Basalt**, Trachybasalt; **B. And.**, Basaltic Andesite, **b.d.**, below detection limit*

[1]Mg # = $Mg^{2+}/(Mg^{2+} + Fe^{2+})$

Table 1. Major element oxide (wt.%) and trace element (ppm) concentrations for the valley lavas, and five plateau lavas (continued)

Sample	RF-1-1-2	RF-4-1-2	RF-4-1-1	RF-4-1-3	CS-04-2-5-1	RF-4-2-2	RF-4-8-1	RF-4-2-3	CS-04-2-14-1
Unit	Quil. Lava	Quil. Lava	Quil. Lava	Quil. Lava	Quil. Lava	Quil. Lava	Quil. Lava	Quil. Lava	Quil. Lava
Type	CA-type 3	CA-type 3	CA-type 3	CA-type 2	CA-type 2	CA-type 2	CA-type 1	CA-type 1	CA-type 1
Location	Miss. Lk.	Miss. Lk.	Miss. Lk.	Miss. Lk.	Miss. Lk.	Miss. Lk.	Miss. Lk.	Miss. Lk.	Miss. Lk.
Rock Type	B.And.	B.And.	B.And.	B.And.	B.And.	B.And.	B.And.	B.And.	B.And.
SiO_2	52.79	51.99	52.64	52.57	52.65	53.01	52.90	53.36	53.67
Al_2O_3	15.73	15.40	15.72	15.21	15.66	15.52	15.06	15.46	15.66
Fe_2O3	8.05	8.30	8.11	7.70	7.93	7.79	8.61	8.79	8.97
MnO	0.11	0.11	0.11	0.11	0.11	0.11	0.13	0.11	0.12
MgO	6.97	7.85	6.84	7.84	7.69	7.99	7.00	7.36	7.50
CaO	8.59	8.72	8.55	9.00	8.86	8.73	8.96	8.72	8.80
Na_2O	3.81	3.61	3.76	3.26	3.25	3.36	3.26	3.36	3.34
K_2O	1.09	1.00	1.14	0.84	0.73	0.79	0.60	0.60	0.57
TiO_2	1.47	1.51	1.47	1.21	1.25	1.20	1.34	1.35	1.38
P_2O_5	0.40	0.38	0.39	0.26	0.27	0.26	0.19	0.20	0.19
LOI	-0.33	0.34	-0.03	0.65	0.22	0.10	0.64	-0.17	-0.28
TOTAL	98.66	99.21	98.71	98.65	98.62	98.85	98.68	99.13	99.91
Mg#[1]	67	69	66	70	69	71	66	66	66
Cs	b.d.	b.d.	b.d.	0.1	0.1	0.1	b.d.	b.d.	b.d.
Rb	13	6	13	9	8	9	6	6	6
Ba	226	237	238	180	188	175	146	137	147
Th	2.00	2.21	2.08	1.48	1.53	1.49	0.79	0.90	0.89
U	0.78	0.59	0.77	0.59	0.52	0.55	0.29	0.31	0.31
Nb	28.0	28.8	27.4	18.2	19.0	18.1	11.9	11.0	10.8

***Quil. Lava**, Quilchena Lava; **Miss. Lk.**, Missezula Lake; **A**, Alkaline; **CA**, Calc-Alkaline; **B. And.**, Basaltic Andesite, **b.d.**, below detection limit*

[1]Mg # = $Mg^{2+}/(Mg^{2+} + Fe^{2+})$

Table 1. Major element oxide (wt.%) and trace element (ppm) concentrations for the valley lavas, and five plateau lavas (continued)

Sample	RF-4-2-1	CS-04-3-1-1	CS-04-6-2-1	CS-04-7-1-1	CS-05-2-1-2	CS-05-2-2-1	CS-04-8-3-1	CS-04-8-4-1	CS-04-10-1-1
Unit	Quil. Lava	Quil. Lava	Quil. Lava	Quil. Lava	Quil. Lava	Quil. Lava	Quil. Lava	Quil. Lava	Quil. Lava
Type	CA-type 1	A	CA-type 3	CA-type 2	CA-type 2	CA-type 1	CA-type 1	CA-type 1	CA-type 1
Location	Miss. Lk.	Loon Lk.	Shrimp. Cr.	Bluey Lk.	Bluey Lk.	Bluey Lk.	Quil. Cr.	Quil. Cr.	Chutter Ra.
Rock Type	B.And.	B.T.And.	B.T.And.	B.And.	B.And.	B.And.	B.And.	B.And.	B.And.
SiO2	53.78	50.00	50.83	53.71	52.13	51.92	52.36	54.30	53.75
Al2O3	15.75	16.46	15.11	15.32	16.17	16.54	15.04	15.37	15.46
Fe2O3	7.80	8.71	9.05	8.62	8.25	8.54	8.97	7.84	8.32
MnO	0.10	0.12	0.12	0.11	0.11	0.11	0.11	0.10	0.11
MgO	7.53	5.52	7.59	7.15	8.12	7.57	8.44	7.81	7.33
CaO	8.79	8.44	9.06	8.58	8.84	8.70	8.72	8.69	8.63
Na2O	3.12	4.74	3.71	3.32	3.27	3.63	3.07	3.24	3.25
K2O	0.51	2.05	1.25	0.62	0.96	1.03	0.55	0.54	0.64
TiO2	1.09	2.34	1.66	1.37	1.31	1.35	1.37	1.17	1.29
P2O5	0.19	0.73	0.39	0.20	0.33	0.30	0.17	0.17	0.18
LOI	0.03	-0.12	-0.16	-0.19	0.51	-0.32	-0.07	-0.27	-0.18
TOTAL	98.69	98.99	98.62	98.81	100.10	99.49	98.72	98.96	98.77
Mg#[1]	69	60	66	66	70	67	69	70	67
Cs	b.d.	0.2	0.1	b.d.	0.1	b.d.	b.d.	b.d.	0.2
Rb	5	20	13	7	10	11	5	5	8
Ba	140	330	231	136	180.5	205	183	151	150
Th	0.84	3.06	1.58	0.82	2.00	1.00	0.53	0.59	0.90
U	0.30	1.23	0.62	0.31	0.70	0.60	0.20	0.24	0.38
Nb	11.1	53.1	27.6	11.5	21.0	21.0	9.9	10.3	10.1

***Quil. Lava**, Quilchena Lava; **Miss. Lk.**, Missezula Lake; **Shrimp. Ck.,** Shrimpton Creek; **Quil. Ck.**, Quilchena Creek; **Chutter Ra.**, Chutter Ranch; **A**, Alkaline; **CA**, Calc-Alkaline; **B. And.**, Basaltic Andesite; **B.T.And.**, Basaltic Trachyandesite, **b.d.**, below detection limit*

[1]Mg # = $Mg^{2+}/(Mg^{2+} + Fe^{2+})$

Table 1. Major element oxide (wt.%) and trace element (ppm) concentrations for the valley lavas, and five plateau lavas (continued)

Sample	**CS-04-10-2-2**	**CS-04-12-1-1**	**CS-04-13-4-1**	**CS-04-15-8-1**	**CS-04-24-1-1**	**CS-04-27-2-1**	**CS-04-28-1-1**	**CS-04-30-1-1**	**CS-04-31-1-1**
Unit	Quil. Lava	Lam. Lava	Lam. Lava	Lam. Lava	Plat. Bas.	Plat. Bas.	Plat. Bas.	Plat. Bas.	Plat. Bas.
Type	CA-type 1								
Location	Chutter Ra.	Lambly Cr.	Lambly Cr.	Okan. Lk.	Asp Ck.	Lillooet	Kamloops	Kelowna	Christ. Va.
Rock Type	B.And.	Basalt	Basalt	Basalt	Basalt	Basalt	Tr. Basalt	Tr. Basalt	Basalt
SiO2	52.48	49.04	48.05	49.36	46.78	50.73	47.46	48.30	47.65
Al2O3	15.50	13.96	13.85	14.43	14.65	13.76	15.09	15.53	14.52
Fe2O3	8.97	12.11	12.33	11.01	10.96	12.32	13.93	13.42	11.45
MnO	0.12	0.16	0.17	0.14	0.15	0.15	0.19	0.18	0.16
MgO	7.48	8.63	8.80	6.08	6.82	8.56	4.66	5.12	6.84
CaO	8.68	9.00	8.90	9.17	9.62	8.56	7.13	6.90	8.93
Na2O	3.43	3.26	3.17	2.93	2.39	3.31	3.76	4.44	2.63
K2O	0.64	0.87	1.15	1.01	0.69	0.58	1.42	1.13	0.84
TiO2	1.36	1.80	2.07	1.87	1.61	1.69	3.29	2.91	1.77
P2O5	0.21	0.33	0.49	0.36	0.28	0.28	0.59	0.58	0.33
LOI	-0.07	-0.27	0.08	2.79	4.86	-0.77	1.20	1.17	3.77
TOTAL	98.79	98.89	99.05	99.14	98.81	99.17	98.71	99.67	98.87
Mg#[1]	66	62	63	56	59	62	44	47	58
Cs	0.1	0.1	0.3	0.3	0.3	b.d.	0.4	0.3	b.d.
Rb	7	13	17	12	12	7	23	18	11
Ba	153	219	340	238	361	150	417	379	251
Th	0.87	1.77	2.80	1.94	1.46	1.00	2.80	2.28	2.17
U	0.38	0.55	0.93	0.38	0.54	0.36	1.03	0.81	0.67
Nb	10.8	22.3	35.0	24.1	9.8	14.7	44.8	36.6	25.6

***Quil. Lava**, Quilchena Lava; **Lam. Lava,** Lambly Creek Lava**; Plat. Bas.** Plateau Basalt**; Chutter Ra.,** Chutter Ranch; **Okan. Lk.,** Okanagan Lake**; Christ. Va.,** Christian Valley**; B. And.,** Basaltic Andesite**; Tr. Basalt,** Trachybasalt, **b.d.**, below detection limit*

[1]Mg # = $Mg^{2+}/(Mg^{2+} + Fe^{2+})$

Table 1. **Major element oxide (wt.%) and trace element (ppm) concentrations for the valley lavas, and five plateau lavas (continued)**

Sample	CS-04-2-26-1	RF-4-6-2b	RF-4-5-2	RF-4-5-3	RF-4-6-1	RF-4-10-2	RF-4-11-1	RF-4-12-1	CS-04-2-9-1	RF-1-1-2	RF-4-1-2	RF-4-1-1
Ta	3.17	2.85	3.00	3.17	3.01	2.99	3.01	3.05	1.76	1.66	1.98	1.70
La	29.0	26.6	27.5	30.8	28.8	28.7	29.4	29.6	18.1	17.2	17.8	17.3
Ce	60.1	53.9	56.9	63.4	59.9	59.8	61.5	61.9	37.1	35.2	36.6	36.1
Pb	9	b.d.	5	8	9	10	9	6	5	b.d.	3	b.d.
Pr	7.27	6.68	7.02	7.85	7.32	7.21	7.51	7.49	4.52	4.27	4.45	4.37
Sr	1,055	1,034	1,013	1,059	1,092	1,095	1,061	1,130	656	654	658	651
Nd	31.1	28.0	29.9	31.2	29.3	29.4	30.2	30.5	18.8	18.1	18.6	18.1
Zr	205	189	197	208	196	203	193	201	127	125	130	123
Hf	4.8	4.4	4.7	4.9	4.5	4.6	4.5	4.6	3.2	3.1	3.1	3.1
Sm	7.13	6.60	7.09	7.34	6.96	6.93	7.22	7.16	4.50	4.27	4.44	4.33
Eu	2.30	2.17	2.29	2.45	2.36	2.27	2.37	2.36	1.55	1.49	1.52	1.49
Gd	5.70	5.47	5.73	5.98	5.77	5.56	5.80	5.86	3.77	3.60	3.75	3.72
Tb	0.81	0.75	0.86	0.84	0.79	0.78	0.80	0.82	0.58	0.53	0.56	0.55
Dy	3.85	3.62	3.86	3.95	3.81	3.67	3.73	3.93	2.77	2.67	2.80	2.76
Y	17	15	16	17	16	16	16	16	12	13	12	13
Ho	0.60	0.57	0.60	0.65	0.62	0.60	0.63	0.63	0.45	0.45	0.46	0.45
Er	1.48	1.43	1.52	1.62	1.58	1.54	1.55	1.52	1.23	1.16	1.21	1.21
Tm	0.178	0.181	0.195	0.200	0.202	0.191	0.190	0.195	0.156	0.150	0.154	0.152
Yb	1.08	1.07	1.08	1.11	1.06	1.07	1.12	1.10	0.95	0.92	0.94	0.89
Lu	0.15	0.15	0.14	0.15	0.14	0.15	0.15	0.15	0.14	0.12	0.13	0.12
Zn	78	71	76	79	83	81	80	76	67	68	68	70
V	180	177	185	177	180	174	180	179	115	122	116	125
Sc	16.4	17.3	19.9	17.1	17.9	17.6	19.4	17.4	19.5	16.0	16.6	16.2
Co	39	40	42	40	40	40	44	40	46	37	40	37
Cu	54	52	51	58	67	66	59	48	39	42	45	47
Cr	169	256	358	194	239	229	304	219	286	180	270	200
Ni	79	87	103	81	91	87	100	87	165	128	171	130

***b.d.**, below detection limit*

Table 1. **Major element oxide (wt.%) and trace element (ppm) concentrations for the valley lavas, and five plateau lavas (continued)**

Sample	RF-4-1-3	CS-04-2-5-1	RF-4-2-2	RF-4-8-1	RF-4-2-3	CS-04-2-14-1	RF-4-2-1	CS-04-3-1-1	CS-04-6-2-1	CS-04-7-1-1	CS-05-2-1-2	CS-05-2-2-1
Ta	1.12	1.18	1.12	0.65	0.65	0.65	0.62	3.33	1.60	0.65	1.20	1.20
La	11.9	12.4	11.7	8.1	7.6	7.8	7.2	32.1	17.2	8.0	14.8	13.8
Ce	25.0	26.2	24.1	18.0	17.1	17.5	15.9	65.9	36.4	18.4	31.0	30.6
Pb	b.d.	5	b.d.	b.d.	b.d.	5	b.d.	7	b.d.	3	25	23
Pr	3.08	3.26	3.05	2.39	2.32	2.35	2.13	7.76	4.46	2.47	3.60	3.60
Sr	553	560	555	417	431	433	466	1127	708	436	597	655
Nd	13.1	14.0	13.1	10.7	11.0	10.9	9.5	30.6	18.2	11.0	16.0	16.3
Zr	88	92	88	75	75	76	63	207	120	76	101	101
Hf	2.2	2.3	2.3	2.1	2.1	2.2	1.8	4.8	3.0	2.2	3.0	3.0
Sm	3.28	3.38	3.25	3.17	3.05	3.18	2.58	6.82	4.53	3.37	3.60	3.80
Eu	1.19	1.22	1.22	1.21	1.21	1.21	1.04	2.31	1.54	1.22	1.20	1.20
Gd	2.89	2.95	2.82	3.10	3.11	3.16	2.51	5.53	3.92	3.20	3.20	3.20
Tb	0.44	0.49	0.45	0.49	0.49	0.51	0.39	0.73	0.56	0.51	0.50	0.50
Dy	2.20	2.37	2.25	2.59	2.62	2.63	2.07	3.49	2.81	2.64	2.50	2.40
Y	10	11	10	12	13	12	10	15	12	12	12.4	12
Ho	0.37	0.39	0.37	0.47	0.45	0.46	0.36	0.57	0.47	0.46	0.40	0.40
Er	1.04	1.08	1.02	1.22	1.23	1.24	0.96	1.40	1.26	1.25	1.20	1.20
Tm	0.138	0.140	0.136	0.162	0.166	0.168	0.131	0.172	0.162	0.168	0.100	0.100
Yb	0.86	0.85	0.82	0.96	0.93	1.01	0.80	0.92	0.96	1.00	0.90	0.80
Lu	0.11	0.12	0.11	0.15	0.14	0.14	0.10	0.14	0.13	0.14	0.10	0.10
Zn	67	65	74	77	72	73	64	77	75	74	142	134
V	107	110	107	121	124	129	104	154	158	124	112	120
Sc	16.5	20.3	16.9	18.5	17.9	17.7	16.9	15.2	18.5	19.0	n.d.	n.d.
Co	41	45	42	44	42	41	41	35	45	43	36	37
Cu	46	41	53	51	46	55	46	46	40	48	38	49
Cr	281	302	279	251	241	238	277	114	344	240	260	190
Ni	179	162	214	178	170	164	170	51	124	163	165	144

***b.d.**, below detection limit*

Table 1. Major element oxide (wt.%) and trace element (ppm) concentrations for the valley lavas, and five plateau lavas (continued)

Sample	CS-04-8-3-1	CS-04-8-4-1	CS-04-10-1-1	CS-04-10-2-2	CS-04-12-1-1	CS-04-13-4-1	CS-04-15-8-1	CS-04-24-1-1	CS-04-27-2-1	CS-04-28-1-1	CS-04-30-1-1	CS-04-31-1-1
Ta	0.56	0.58	0.60	0.62	1.37	2.15	1.48	0.56	0.84	2.85	2.32	1.51
La	6.5	6.8	7.7	8.1	16.3	23.1	16.3	13.5	11.8	31.7	26.9	19.0
Ce	15.2	15.5	17.6	18.2	33.9	47.4	34.0	31.1	26.1	67.7	59.6	39.7
Pb	b.d.	4	b.d.	b.d.	5	b.d.	6	b.d.	3	9	9	7
Pr	2.11	2.10	2.35	2.42	4.24	5.82	4.25	4.05	3.45	8.17	7.52	4.84
Sr	443	478	458	450	461	616	498	502	398	622	510	553
Nd	9.8	9.4	10.4	10.8	17.6	23.9	17.6	17.5	15.4	33.8	31.6	20.0
Zr	68	60	73	73	118	154	126	103	105	250	218	136
Hf	1.9	1.6	2.0	2.0	3.1	3.9	3.3	2.8	2.8	6.1	5.4	3.5
Sm	3.03	2.65	3.04	3.14	4.67	5.90	4.74	4.62	4.46	7.81	7.61	4.95
Eu	1.18	1.11	1.17	1.19	1.60	1.92	1.57	1.53	1.57	2.62	2.44	1.62
Gd	2.99	2.52	2.94	3.07	4.46	5.41	4.65	4.32	4.34	7.05	6.74	4.74
Tb	0.49	0.39	0.47	0.48	0.70	0.80	0.72	0.65	0.68	1.12	1.06	0.78
Dy	2.51	2.06	2.47	2.58	3.82	4.35	3.94	3.49	3.63	5.70	5.46	4.09
Y	11	9	11	11	18	20	19	18	17	26	25	20
Ho	0.45	0.36	0.43	0.47	0.68	0.75	0.70	0.66	0.65	0.98	0.96	0.73
Er	1.20	0.95	1.13	1.24	1.88	1.98	1.90	1.80	1.81	2.83	2.84	2.11
Tm	0.158	0.127	0.151	0.164	0.266	0.266	0.261	0.240	0.244	0.385	0.399	0.289
Yb	0.94	0.78	0.91	0.95	1.56	1.66	1.60	1.46	1.41	2.26	2.41	1.77
Lu	0.12	0.10	0.13	0.13	0.23	0.23	0.22	0.21	0.20	0.31	0.34	0.24
Zn	76	68	71	75	102	98	98	85	107	128	124	96
V	129	107	122	130	192	197	190	208	172	225	180	199
Sc	18.7	16.7	17.9	18.4	23.6	23.4	23.1	26.0	21.7	18.7	21.7	28.6
Co	46	42	43	43	53	55	43	46	54	40	45	48
Cu	48	49	38	51	50	46	54	35	35	18	21	36
Cr	342	294	267	243	321	288	241	211	312	12	48	255
Ni	250	214	187	190	178	171	92	69	214	8	24	69

***b.d.**, below detection limit*

2.8.1 Major Element Geochemistry

Using major elements, the Quilchena lavas can be separated into two distinct compositional types: a predominantly calc-alkaline type that occurs throughout the Quilchena succession, and a subordinate alkaline type, which was identified mainly in Missezula Lake area, at the base of the section, and in the Loon lake sample. The calc-alkaline type includes basaltic andesites and trachybasaltic andesites characterized by higher SiO_2 concentrations, sub-alkaline compositions, and a modest iron-enrichment trend (Figure 15). In contrast, the alkaline type consists of basalts and trachy-basalts with higher $Na_2O + K_2O$ values and a greater degree (tholeiitic style) of iron enrichment. The Lambly Creek lavas are transitional between the two Quilchena lava types, being composed of subalkaline basalt with increased iron concentrations relative to the Quilchena alkaline type. Magnesium numbers ($Mg\# = Mg^{2+}/[Mg^{2+} + Fe^{2+}]$) of the Quilchena lavas range from 58 to 71, with the calc-alkaline lavas from the Quilchena succession having the highest values (66–71), followed by the alkaline Quilchena lavas (60–66), and the Lambly Creek lavas (56–63) (Figure 16a). The valley lavas also have high Cr (114–358 ppm) and high Ni (51–225 ppm) concentrations.

CIPW normative mineralogy (calculated using $(Fe^{3+}/Fe^{2+})_{atomic} = 0.2$) also highlights the differences between the two compositional types, with the calc-alkaline Quilchena samples being either hypersthene or quartz normative (up to 3.7 wt.% quartz), and the alkaline samples being nepheline normative (up to 7.8 wt.% normative nepheline) (Figure 16b). The Lambly Creek lavas are all hypersthene normative. The geochemical

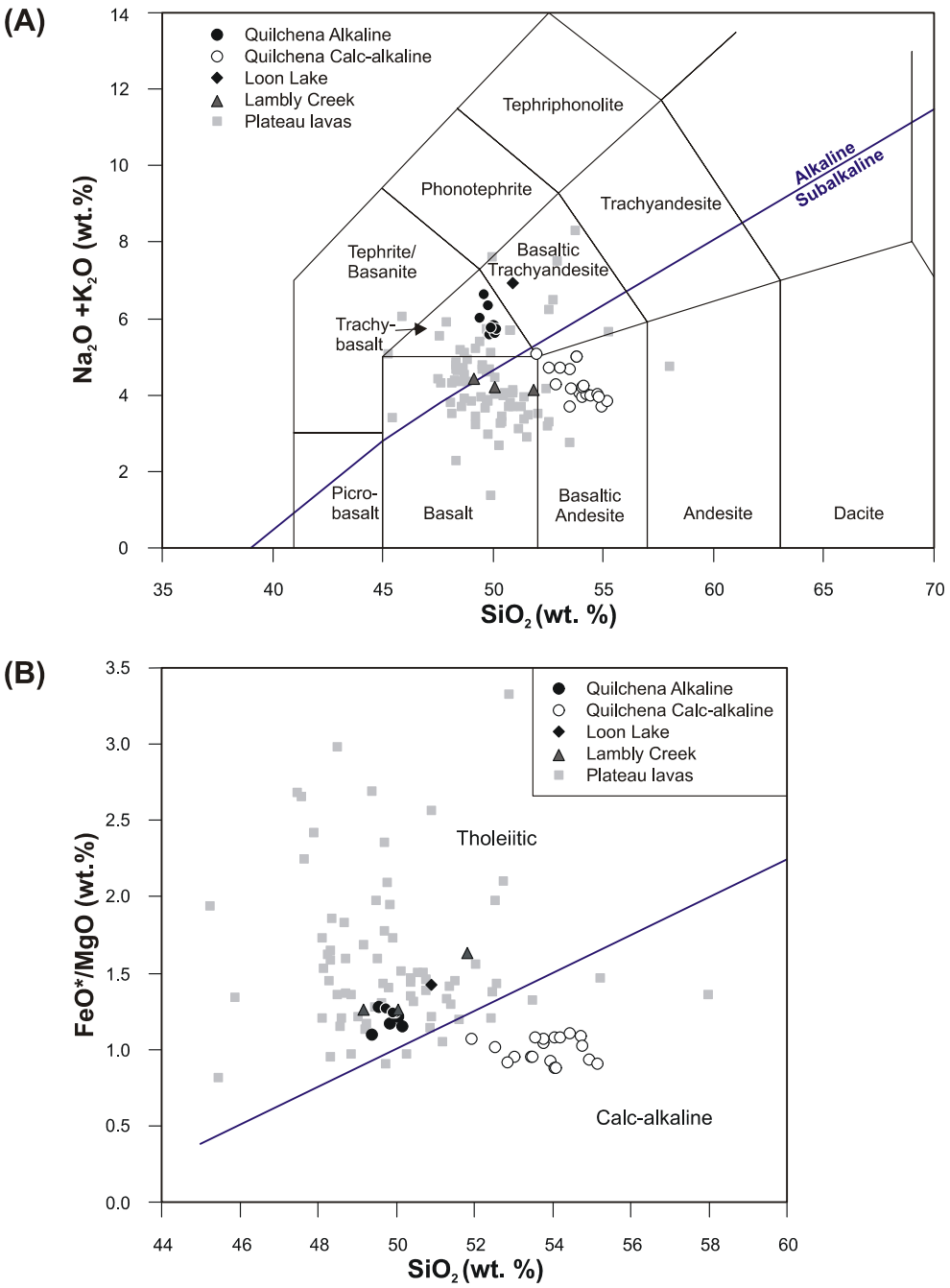

Figure 15. Classification of valley and plateau lavas using major elements
(A) Classification of lavas using the total alkalis versus silica diagram of LeBas et al. (1986) and the alkaline–subalkaline line of Irvine and Baragar (1971). (B) Classification of lavas using the calc-alkaline–tholeiitic diagram of Miyashiro (1974). Plateau lava samples from Bevier (1982), Smith (1986), and Dostal et al. (1996).

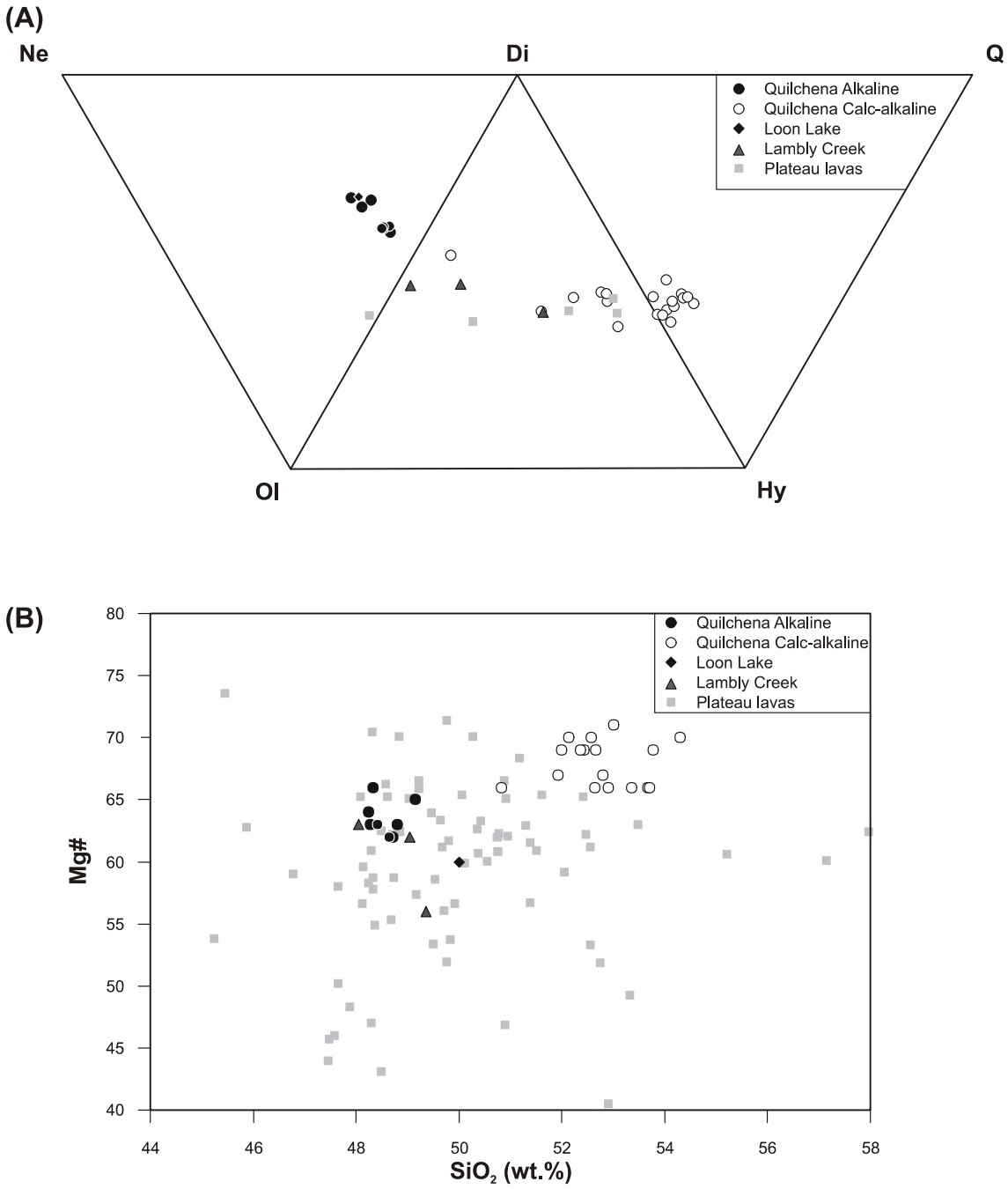

Figure 16. Classification of valley and plateau lavas using major elements
(A) Classification of valley lavas and plateau lavas collected in this study using their CIPW normative compositions (after Thompson, 1984). (B) Mg # versus SiO_2, where Mg # = $Mg^{2+}/(Mg^{2+} + Fe^{2+})$. Plateau lava samples from Bevier (1982), Smith (1986), and Dostal et al. (1996). Both the CIPW normative mineralogy and Mg# were calculated assuming $(Fe^{3+}/Fe^{2+})_{atomic} = 0.2$ (Middlemost, 1989).

types also correlate with the two main petrographic types described earlier in the paper: the calc-alkaline lavas are phenocryst-poor (only olivine phenocrysts), whereas the alkaline type and Lambly Creek lavas have more abundant phenocrysts (olivine–plagioclase–augite) and abundant accessory apatite.

In comparison, the older plateau lavas have a similar range in SiO_2 and alkalinity values, with most samples having basaltic or trachy-basaltic compositions. However, the lavas generally show tholeiitic iron-enrichment trends more strongly than the Quilchena alkaline type and the Lambly Creek basalts (Figure 15b). Magnesium numbers in the plateau lavas show a greater range in values (low 40's to over 70), (Figure 16a). Plateau lavas also range from slightly nepheline normative through to quartz normative (Bevier, 1983a), and the Miocene Cheslatta Lake suite at the northern end of the plateau lavas is alkaline and broadly nepheline normative.

2.8.2 Trace Element Chemistry of Valley and Plateau Lavas

Trace element concentrations for both the calc-alkaline and alkaline lava types are consistent with an intraplate environment and show little evidence of a subduction signature. On an N-MORB (normal mid-ocean ridge basalt) normalized trace element diagram, all samples display both a positive Nb and Ta anomaly relative to Th and La, or no anomaly, and none show the pronounced negative anomaly that characterizes most volcanic arc lavas (Figure 17, Pearce, 1996). The absence of volcanic arc character is also evident on plots of Ti–V (Shervais, 1982), Ti–Zr–Y (Pearce and Cann, 1973), Th–Zr–Nb (Wood, 1980) and Nb–Zr–Y (Meschede, 1986), which indicate a within-plate to E-MORB (enriched mid-ocean ridge basalt) affinity (Figure 18). Significant Pb spikes in

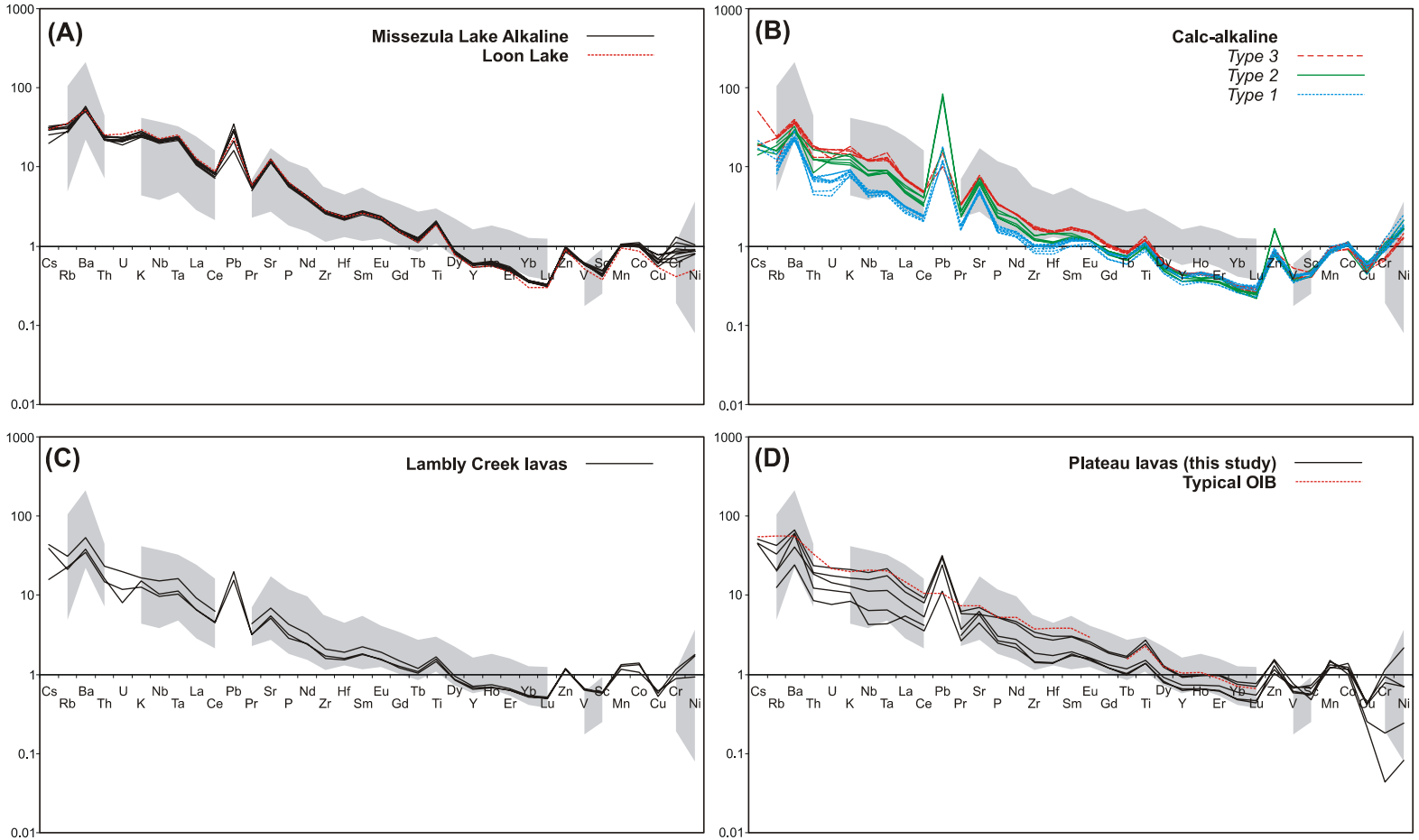

Figure 17. N-MORB normalized trace element diagrams for the valley lavas

(A) Alkaline Quilchena lavas from the Missezula Lake section(solid black lines) and the Loon Lake possible valley lava intrusive equivalent (dashed red line). (B) Calc-alkaline Quilchena lavas, subdivided into type 1 (, blue dashed line), 2 (green solid line) and 3 (red heavy-dashed line). (C) Lambly Creek lavas. (D) Plateau lavas collected in this study compared to typical OIB (red dashed line). Grey shading represents normalized trace element concentrations of the plateau basalts (Bevier, 1982; Smith, 1986; Dostal et al., 1996). N-MORB normalization factors and OIB after Sun and McDonough (1989).

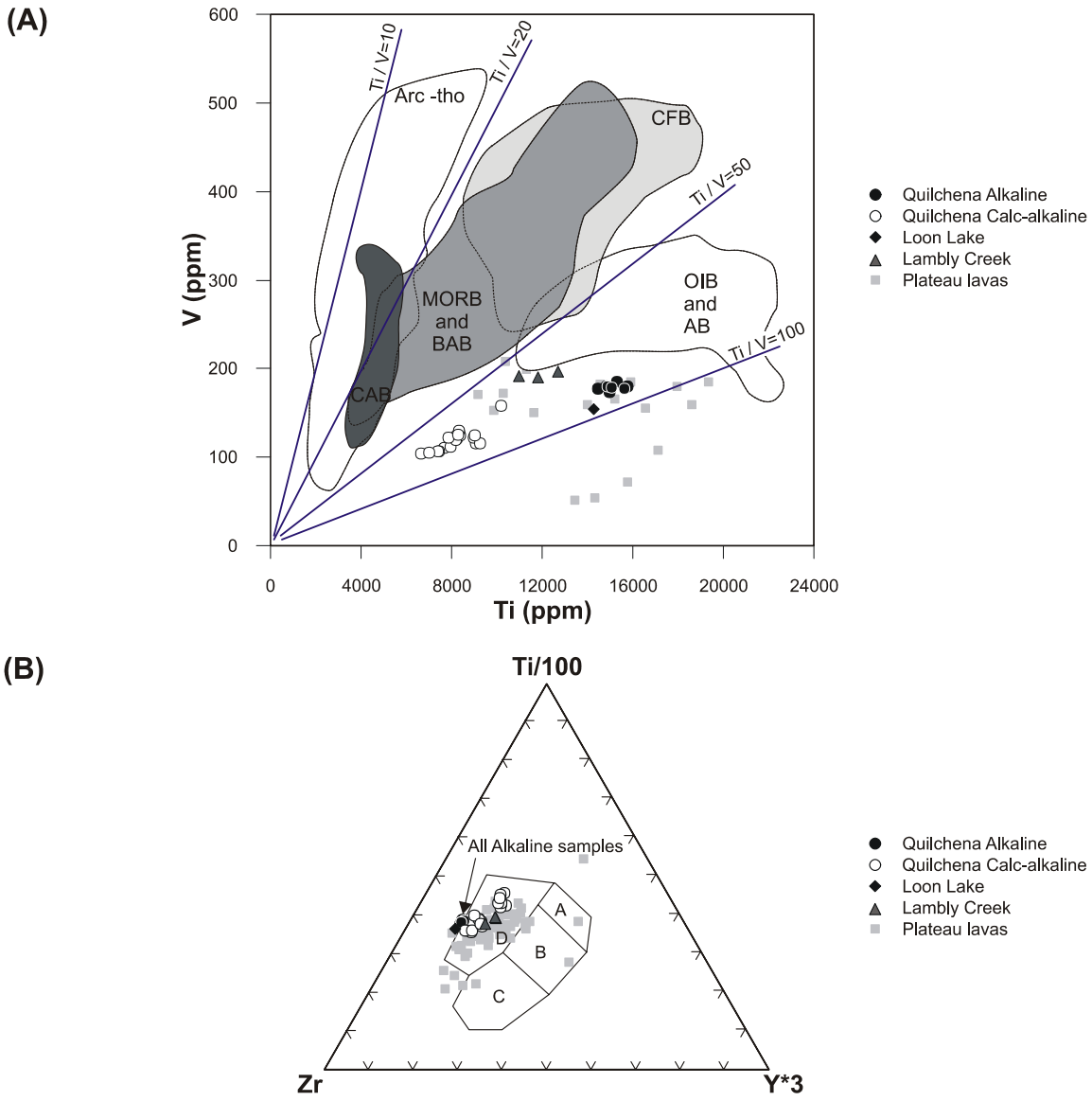

Figure 18. Trace element discrimination diagrams for the valley and plateau lavas
(A) Ti–V discrimination diagram (Shervais, 1982). The fields are as follows: Arc-tho, Arc Tholeiite; CAB, calc-alkaline basalts; MORB, mid-ocean ridge basalts; BAB, back-arc basin basalts; CFB, continental flood basalts; OIB, ocean-island basalts; AB, alkali basalts. (B) Ti–Zr–Y discrimination diagram for basalts (Pearce and Cann, 1973). The fields are as follows: A, island-arc tholeiite; B, mid-ocean ridge basalt; C, calc-alkaline basalt; D, within-plate basalt.

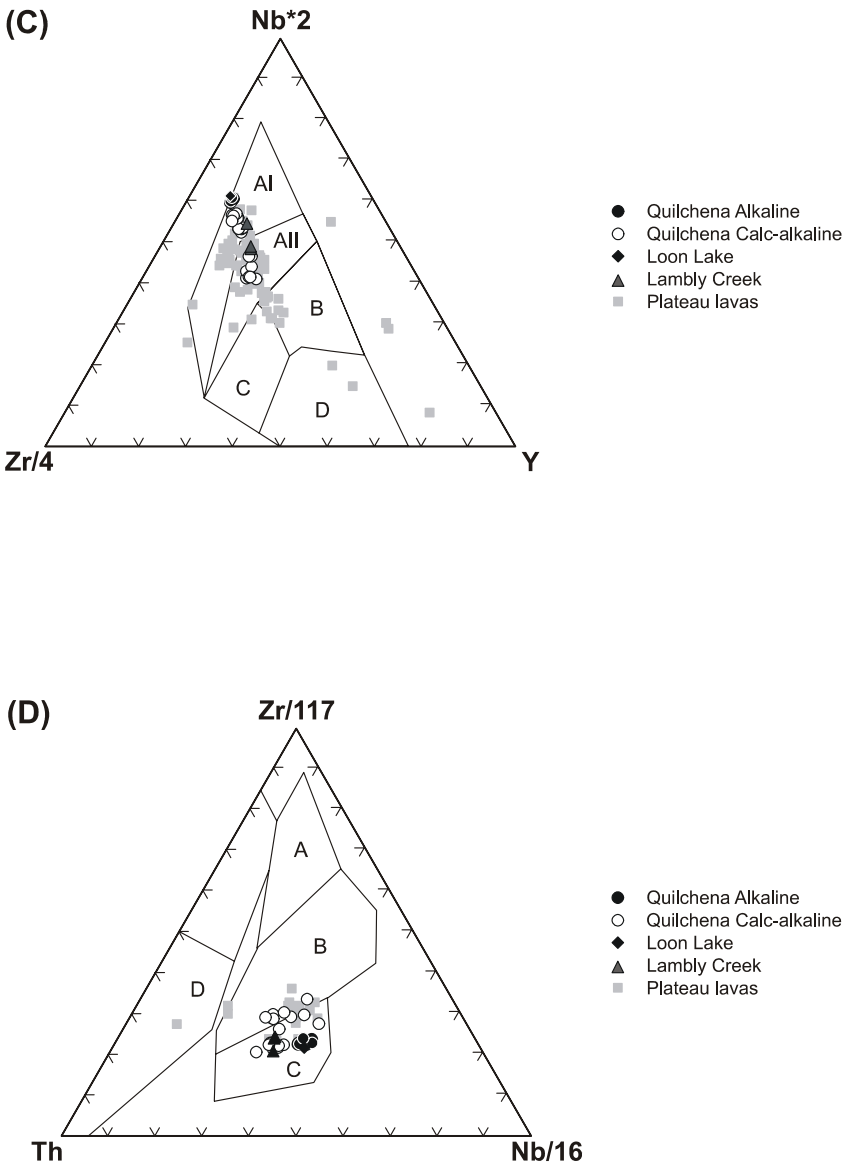

Figure 18. Trace element discrimination diagrams for the valley and plateau lavas (continued)

(C) Th–Zr–Nb discrimination diagram (Wood, 1980). The fields are as follows: A, N-MORB; B, E-MORB; C, Ocean Island Basalt or Rift; D, arc-basalts. (D) Zr–Nb–Y discrimination diagram for basalts (Meschede, 1986). The fields are as follows: AI, within-plate basalts; AII, within-plate alkali basalts and tholeiites; B, E-type MORB; C, within-plate tholeiites and volcanic-arc basalts; D, N-type MORB and volcanic-arc basalts.

the N-MORB normalized trace element patterns are due to high analytical error (Appendix F).

All the valley lavas have a N-MORB normalized trace element pattern similar to that of oceanic island basalts (OIB), with the LILE, LREE and HFSE elements being enriched (e.g. Sun and McDonough, 1989). Despite the overall similarity, consistent differences between the calc-alkaline and alkaline Quilchena lavas exist. The differences are most evident in the Missezula succession where the alkaline lavas generally show higher trace element concentrations relative to the calc-alkaline type (Figure 17). The alkaline type are the most enriched in the large ion lithophile (LILE) and light rare earth elements (LREE), with steep LREE to HREE patterns ($(La/Yb)_N$ =18–25).

The calc-alkaline type can be further subdivided into three distinct sub-types, each of which can be identified throughout the Quilchena region. The first type (type 1), which corresponds to the lavas directly above the alkaline type in the Missezula exposure, as well as lavas at Bluey Lake, Quilchena Creek and Chutter Ranch exposures, has the lowest LILE and LREE concentrations in the calc-alkaline type, higher middle REE (MREE; Sm to Ho) and HREE concentrations, with $(La/Yb)_N$ values of 5–6. Type 2 (corresponding to lavas stratigraphically higher than type 1 in the Missezula section as well as samples from Bluey Lake) has trace element concentrations higher than that of type 1 in the LILE and high field strength element (HFSE), but is the most depleted in the MREE and HREE ($(La/Yb)_N$=10–12). Finally, type 3 (corresponds to the top of Missezula section and Shrimpton Creek) is the least depleted of the three sub-types, with the exception of the HREE ($(La/Yb)_N$=13–14). This subdivision of the calc-alkaline type, although best defined using trace elements, is also evident in the major element

composition (each sub-type plots as a group, separate from the other subgroups) and in the petrography, where the type and proportion of phenocrysts are similar within a given subgroup.

The valley lavas have similar trace element and REE patterns to the older plateau lavas. The LILE and LREE concentrations of the alkaline Quilchena lavas are more enriched than most of the plateau lavas samples, and the same element concentrations in the calc-alkaline samples are at the low end of the range of the plateau lava samples. However, all the Quilchena lava samples show a greater trend in HREE depletion (particularly the calc-alkaline samples) compared to the plateau lavas (Figure 19a). The Lambly Creek lavas have similar trace element patterns to the Quilchena lavas, being LILE- and LREE-enriched, but less HREE-depleted ($(La/Yb)_N$=7–10), and are broadly similar to the plateau lavas (Figure 19b). The five new plateau lava samples are also shown in for reference in Figure 17. The valley lavas have broadly similar trace element patterns to the Cheslatta Lake suite and the Mount Noel Volcanic Province, both of which are contemporaneous to the older plateau basalts, but are more HREE-depleted (Coish et al., 1998; Anderson et al., 2001).

2.8.3 Comparison to Contemporaneous Volcanic Fields

The valley and plateau lavas of the Chilcotin Group erupted in a back-arc to intraplate environment in northwestern North America. This area, during the Late Cenozoic, has undergone both the arc-type volcanism of the Cascades–Garabaldi belt, as well as the intraplate-composition volcanism of the Anahim Volcanic Belt, the Wells Gray–Clearwater Complex, the Northern Cordilleran Volcanic Province (NCVP), the Cheslatta Lake Suite, the Mount Noel Volcanic Complex and the Columbia River

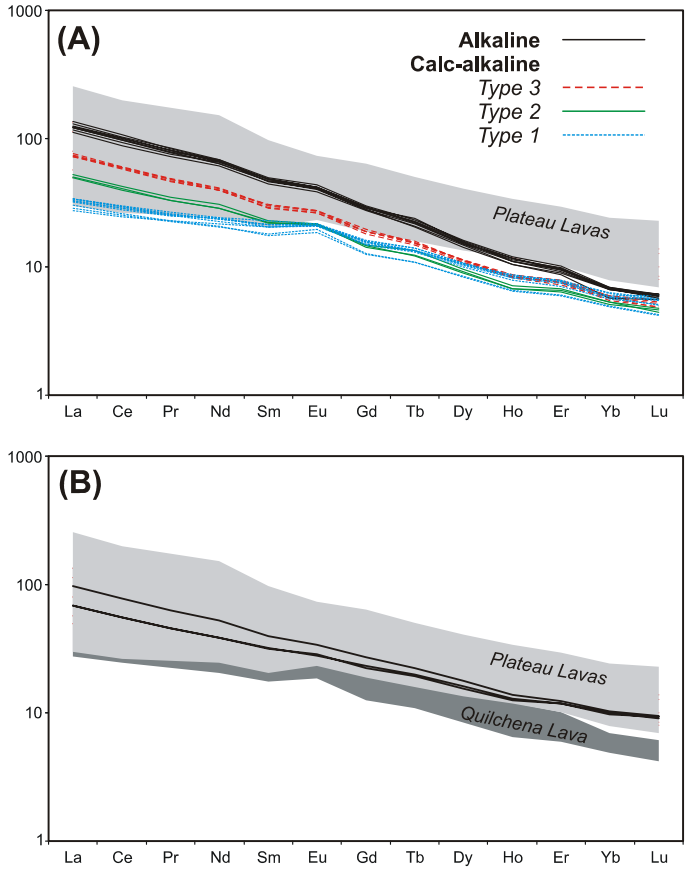

Figure 19. Chondrite-normalized rare earth element (REE) plots for the valley lavas
(A) Chondrite-normalized REE patterns for the Quilchena lavas. (B) Chondrite-normalized REE patterns for the Lambly Creek lavas. Light grey shading in both figures shows normalized REE concentrations from plateau lavas (including samples from this study), and dark grey shading in (B) shows normalized REE concentrations for the Quilchena lavas. Normalization factors from McDonough and Sun (1995).

Basalts. These volcanic fields are compared on a plot of La/Nb versus MgO (Figure 20), which highlights the difference in chemistry between Cordilleran arc-related (Cascade and Garabaldi) and intraplate volcanism. The valley lavas are generally the most similar to the plateau lavas of the Chilcotin Group as well as the intraplate Wells Gray–Clearwater Complex, Anahim Volcanic Belt, and the NCVP, as all three have a similar range in La/Nb values over a range of MgO concentrations. The valley lavas and the other intraplate volcanics are generally more MgO-rich (primitive) than the arc-related lavas, which have higher La/Nb ratios. Spanning the gap between the intraplate and arc-related volcanics are the Columbia River lavas, which demonstrate a broad range in composition.

2.8.4 Nd Isotopes

Nd isotopic ratios were determined on seven valley lava samples (Table 2), six from the Quilchena lavas and one from the Lambly Creek lavas. Sm and Nd concentrations from these seven samples are 3.147.09 ppm and 10.930.6 ppm respectively. The $^{147}Sm/^{144}Nd$ range from 0.1346 to 0.1769. The εNd values for the valley lavas analyzed in this study ranged from +8.0 to +8.4, with the alkaline samples from the Quilchena lavas and Loon Lake having slightly higher εNd values (+8.3 to +8.4) in comparison to the subalkaline samples (+8.0 to +8.1 at Missezula Lake, 8.3 farther north at the Chutter Ranch locality east of Merritt). Two additional samples of Quilchena basalt (alkaline group) from near Quilchena Creek were analyzed by Smith (1986), both of which had εNd of +8.5. The Lambly Creek basalt sample has a εNd value of +8.0.

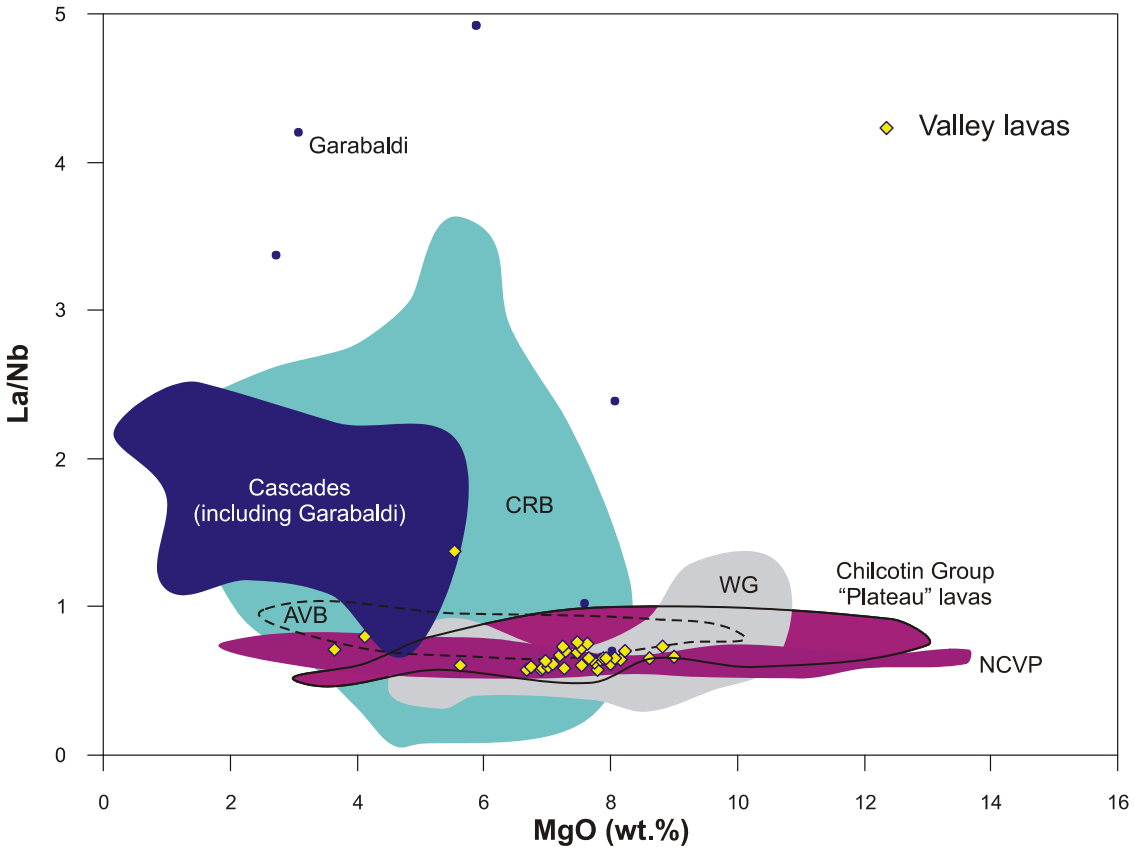

Figure 20. Graph of La/Nb versus MgO, comparing the valley and plateau lavas of the Chilcotin Group to other contemporaneous volcanic fields in northwestern North America

AVB, Anahim Volcanic Belt (dashed outline); CRB, Columbia River Basalt; NCVP, Northern Cordilleran Volcanic Province; WG, Wells Gray–Clearwater Suite. The Cheslatta Suite has been included in the Chilcotin Group for figure clarity (solid outline). Includes samples from Green (1981), Bevier (1982), Souther and Hickson (1984), Hickson (1986), Smith (1986), Souther (1992), Charland and Francis (1993), Dostal et al (1996), Anderson et al. (2001), Edwards et al. (2002), Hildreth et al. (2003). Columbia River Basalt analyses and Cascade analyses (other than those listed above) are from precompiled datasets downloaded from GEOROC on 21 April 2005 and 30 Nov 2005 (http://georoc.mpch-mainz.gwdg.de/georoc/Start.asp).

Overall, the Nd compositions of the valley lavas are strikingly similar, in contrast to the differences within the major and trace elements between the calc-alkaline and alkaline types. The small amount of variation in the εNd values, particularly between the alkaline and subalkaline types, does not correlate well with individual trace elements or element ratios, or with the Mg#. The εNd values suggest that the valley lavas were derived from mantle sources, and were not significantly contaminated by a crustal component. The values fall into the εNd range for Pacific MORB (+6 to +13; Lehnert, 2000: http://www.petdb.org).

Previous Nd isotope geochemistry studies on older Chilcotin plateau basalts (Smith, 1986; Grainger, 2000), indicate that the εNd values for the plateau basalts range from +3.7 to +7.5. Bevier (1983a) concluded that Sr and Pb isotopic compositions of the broader Chilcotin group, along with the lack of crustal xenoliths and silicic differentiates, provides no evidence for crustal contamination, a finding that was supported by the later Nd isotopic studies of Smith (1986) and Grainger (2000). The combined Nd isotopic values for the valley and plateau lavas suggest that the Chilcotin group as a whole is derived from a depleted source, with the valley lavas originating from a more depleted isotopic source than the plateau basalts.

Table 2. Nd isotopic compositions for six samples of Quilchena lavas and one sample of Lambly Creek lava

Sample	Unit	Location	Rock Type	$\frac{^{143}Nd}{^{144}Nd}$	Error (2σ)	$\frac{^{147}Sm}{^{144}Nd}$[2]	εNd_0[3]
CS-04-2-26-1	Quilchena Lava	Miss. Lk.	Trachybasalt	0.513071	0.000006	0.1426	8.4
RF-4-5-2	Quilchena Lava	Miss. Lk.	Trachybasalt	0.513063	0.000005	0.1431	8.3
CS-04-2-14-1	Quilchena Lava	Miss. Lk.	Basaltic Andesite	0.513052	0.000005	0.1769	8.1
CS-04-2-29-1	Quilchena Lava	Miss. Lk.	Basaltic Andesite	0.513049	0.000006	0.1429	8.0
CS-04-3-1-1	Quilchena Lava	Loon Lk.	Basaltic Trachyandesite	0.513068	0.000010	0.1346	8.4
CS-04-10-2-2	Quilchena Lava	Chutter Ra.	Basaltic Andesite	0.513064	0.000006	0.1752	8.3
CS-04-10-2-2[1]	Quilchena Lava	Chutter Ra.	Basaltic Andesite	0.513064	0.000005	0.1752	8.3
CS-04-15-8-1	Lambly Creek Lava	Okan. Lk.	Basalt	0.513049	0.000006	0.1631	8.0

***Miss. Lk.**, Missezula Lake East section; **Chutter Ra.**, Chutter Ranch section; **Okan. Lk.**, Okanagan Lake section*

[1]duplicate sample

[2]Sm-Nd ratios calculated from Sm and Nd concentrations reported in Table 1.

[3]εNd calculated using the present-day $^{143}Nd/^{144}Nd = 0.512638$ (Wasserburg et al., 1981)

2.9 Modelling of the Valley Lava Mantle Source

The nature of the mantle that melted to form the valley lavas was investigated using combined major element, trace element and isotopic geochemistry to constrain the minimum depth of melting and to estimate the composition of the mantle source. This mantle source was then contrasted with the inferred source of mantle xenoliths contained in late Cenozoic volcanic rocks in southern British Columbia. The results indicate that the mantle source for the valley lavas was deeper and more geochemically depleted than the mantle source for the xenoliths, but more geochemically enriched than typical depleted MORB source mantle.

The valley lavas are interpreted to be sourced from mantle that was garnet-bearing based on their LREE-enriched and consistently HREE-depleted patterns ($(La/Yb)_N$ >5; Thirlwall et al., 1994; Farmer, 2003). This agrees with conclusions reached by Dostal et al. (1996) who suggested that the plateau lavas were derived from a garnet-bearing source. The presence of garnet implies magma derivation from depths of at least 80 km (Robinson and Wood, 1998; Harder and Russell, 2006). These depths correspond to temperatures of at least 1100°C, according to the geothermal model of Harder and Russell (2006).

2.9.1 Geochemical Modelling: Procedure

Only the Quilchena lavas were used in the modelling because 1) the majority of samples collected in this study belong to this group, and 2) the Quilchena lavas can be divided into two distinct types (alkaline and calc-alkaline, as described above). Geochemical trends within the alkaline type and each calc-alkaline subtype are consistent

with fractional crystallization of olivine; therefore, it was assumed that the most "primitive" samples (with highest Mg#'s) from each of the types were related by olivine crystallization to a primary mantle-equilibrated melt. Ultimately, the alkaline and type 1 calc-alkaline types were modelled, with the type 1 calc-alkaline group chosen at is has high Ni concentrations and Mg#'s, and the sub-type was the most different of the three subalkaline subtypes when compared to the alkaline type. Detailed modelling procedure including formulas and partition coefficients are reported in Appendix G.

2.9.1.1 Calculation of Primary Magma Compositions

Calculation of primary magma compositions was accomplished by (1) selecting the most "primitive" compositions (highest Mg# and Ni abundance) for the alkaline and type 1 calc-alkaline geochemical types (samples RF-4-5-2 and CS-04-8-3-1 respectively), and (2) incrementally adding the composition of olivine to the primitive magma compositions. Olivine was used because it is the most abundant or sole phenocryst phase in the Quilchena lavas, and the addition of olivine to a primitive magma is a recognized way to generate a mantle-equilibrated primary magma (e.g. Albarede, 1992; Asimow and Longhi, 2004). Essentially, this method reverses the chemical effect that olivine fractionation had in the generation of primitive Quilchena lavas from their parental, primary magmas. Olivine accumulation was determined not to have been a factor, as there is not a linear relationship between increasing wt. % MgO and proportion of olivine phenocrysts in a given lava.

To estimate the amount of olivine fractionation between primary melt to the most primitive samples from each trend, the composition of melt-equilibrated olivine (Roeder and Emslie, 1970) was added to each sample of Quilchena lava to increase its Mg# to

~ 73 (approximate Mg# of primary melt in equilibrium with mantle olivine; Grove, 2000; Farmer, 2003). The composition of the olivine that was added to the primitive Quilchena compositions was based on the mineral–melt exchange coefficients for FeO and MgO and the methods described in Roeder and Emslie (1970), assuming an Fe_2O_3/FeO weight ratio of 0.2. The procedure works by (1) calculating the composition of olivine that would be in equilibrium with the primitive magmas, (2) adding 1% by weight of that olivine to the primitive magma to form a new (more primitive) composition, (3) calculating the composition of olivine that would be in equilibrium with the new magma composition, and (4) repeating the procedure iteratively until Mg# of the primitive samples is ~73, thus yielding the major element composition of the primary parent magma for each the two geochemical types.

The modelling shows that the alkaline suite of samples were derived from a primary parental magma that had undergone a minimum 11% fractional crystallization of olivine, and the type 1 calc-alkaline samples were derived from a primary magma that had undergone a minimum of 6% fractional crystallization of olivine. The trace element concentrations for the primary parent magmas were also calculated, using the degrees of fractional crystallization of olivine calculated above for each suite. Table 3 contains the major and trace element results of adding olivine into the most primitive alkaline and calc-alkaline samples, thereby calculating the primary magmas from which the alkaline and calc-alkaline types are derived (PL-A and PL-C1 respectively).

Table 3. Composition of primary magmas PL-A and PL-C1

	Alkaline Suite		Calc-Alkaline (Type 1) Suite	
	Daughter Magma	Primary Magma	Daughter Magma	Primary Magma
	RF-4-5-2	PL-A[2]	CS-04-8-3-1	PL-C1[3]
SiO_2	49.37	48.89	53.48	53.06
TiO_2	2.55	2.40	1.40	1.35
Al_2O_3	15.27	14.39	15.36	14.86
FeO	7.23	7.04	6.97	6.86
Fe_2O_3	1.45	1.37	1.39	1.35
MnO	0.13	0.13	0.12	0.11
MgO	7.78	10.40	8.62	10.06
CaO	9.61	9.06	8.91	8.62
Na_2O	4.24	3.99	3.14	3.03
K_2O	1.78	1.67	0.56	0.54
P_2O_5	0.70	0.66	0.17	0.16
Mg# (Fo[1])	65.7	72.5 (90)	68.8	72.3 (90)
Rb	18	16	5	4
Ba	313	282	183	173
Th	2.85	2.56	0.53	0.50
U	1.09	0.98	0.20	0.19
Nb	47.9	43.2	9.9	9.3
Ta	3.00	2.70	0.56	0.53
La	27.5	24.8	6.5	6.1
Ce	56.9	51.3	15.2	14.3
Pr	7.02	6.33	2.11	1.99
Sr	1013	913	443	418
Nd	29.9	27.0	9.8	9.3
Zr	197	178	68	64
Hf	4.7	4.3	1.9	1.8
Sm	7.09	6.39	3.03	2.85
Eu	2.29	2.06	1.18	1.11
Gd	5.73	5.16	2.99	2.82
Tb	0.86	0.77	0.49	0.46
Dy	3.86	3.47	2.51	2.37
Y	16	14	11	10
Ho	0.60	0.54	0.45	0.42
Er	1.52	1.37	1.20	1.13
Yb	1.08	0.97	0.94	0.88
Lu	0.14	0.13	0.12	0.12
V	185	167	129	122
Sc	19.9	18.2	18.7	17.8
Co	42	76	46	63
Cr	358	347	342	336
Ni	103	466	250	582

[1]Calculated Fo content of olivine in equilibrium with primary magma

[2]RF-4-5-2 + 11% olivine; [3]CS-04-8-3-1 + 6% olivine

2.9.1.2 Calculation of Mantle Source Composition

The mineralogical composition of the mantle source of these calculated primary magmas are unknown (other than that they contain garnet). For modelling purposes, a garnet lherzolite composed of 58% olivine, 19% orthopyroxene, 14% clinopyroxene and 9% garnet was used. This composition was selected after a review of literature that focused on non-cratonic mantle samples (McDonough, 1990; Ionov, 1993; McDonough and Rudnick, 1998; Walter 2003). The garnet lherzolite melting model of Walter (1998) was employed, which assumes a melting reaction at 3.0 GPa of 4 Ol + 84 Cpx + 12 Gt = 87 Melt +13 Opx, for the melting interval of 0–14%.

The primary magma trace element concentrations determined in the previous section (PL-A and PL-C1) were then used in non-modal melting models to calculate the composition of the mantle source from which they were derived. It was assumed that the primary magmas were derived from 5% partial melting of their mantle sources (continental alkaline basaltic primary magmas are generated by small degrees (≤5%), see Hirose and Kushiro, 1993; Farmer, 2003). Both equilibrium and fractional melting methods were tested, with the final model using non-modal fractional melting, as it allowed for a greater range in trace element concentrations in the resulting calculated primary magma over low degrees of partial melting. This choice made it easier to determine if the calc-alkaline subtypes could have been derived from a single source which had undergone variable degrees of partial melting.

2.9.2 Geochemical Modelling: Results

Using the procedure described above, estimated mantle source trace element concentrations of the Quilchena lava alkaline and type 1 calc-alkaline samples were calculated, herein referred to as MS-A (mantle source of the Quilchena alkaline suite) and MS-C1 (source of the type 1 calc-alkaline suite). The full trace element suite for each mantle source is presented in Table 4 with the exception of Pb, which is not included in the modelling because of high analytical error in the original analyses. The concentration of selected elements in MS-A and MS-C1 are compared to the calculated primary magmas for each suite (PL-A and PL-C1), and the most primitive Quilchena lava samples in the two suites (RF-4-5-2 and CS-03-8-3-1) in Figure 21, all normalized to primitive mantle (Sun and McDonough, 1989). Figure 22 shows the final modelling results for Ni and La, including the mantle source, partial melting curves, fractional crystallization curves, and Quilchena lava samples.

The modelling shows that the alkaline lavas within the Quilchena lavas require a mantle source (MS-A) that is more enriched compared to the calc-alkaline lavas, particularly in the HFSE and LREE, and with slightly higher concentrations of all modelled trace elements then primitive mantle (Figure 21). The profile of MS-A indicates that the mantle source of the alkaline Quilchena lavas is slightly enriched in all elements relative to primitive mantle, with anomalous enrichments in Nb, Ta and Sr. In contrast, the calculated mantle source of the type 1 calc-alkaline Quilchena lavas (MS-C1) is slightly depleted relative to primitive mantle, with Zr and LREE values close to that of depleted mantle (shading in Figure 22 after Salters and Stracke's (2004) estimate of depleted mantle and Workman and Hart's (2005) estimates of depleted MORB source

Table 4. Calculated trace element concentrations (ppm) in MS-A and MS-C1

	Mantle Source Composition[3]	
	MS-A[1]	MS-C1[2]
Rb	0.8	0.3
Ba	14	8
Th	0.13	0.02
U	0.05	0.01
Nb	2.1	0.5
Ta	0.13	0.03
La	1.2	0.3
Ce	2.6	0.7
Pr	0.37	0.12
Sr	45	21
Nd	1.7	0.6
Zr	15	5
Hf	0.4	0.2
Sm	0.51	0.23
Eu	0.19	0.11
Gd	0.56	0.31
Tb	0.10	0.06
Dy	0.55	0.38
Y	7	5
Ho	0.11	0.08
Er	0.33	0.27
Yb	0.4	0.37
Lu	0.07	0.06
V	95	70
Sc	9.1	8.9
Co	374	299
Cr	2229	2165
Ni	5554	6013

1Calculated composition of alkaline Quilchena lava mantle source

[2]Calculated composition of calc-alkaline Quilchena lava mantle source

[3]Mantle source compositions calculated assuming 5% non-modal fractional melting of the given mantle source would produce calculated primary magmas PM-A (alkaline suite) and PM-C1 (calc-alkaline type 1 suite). The mantle source was assumed to be 58% olivine, 19% orthopyroxene, 14% clinopyroxene and 9% garnet, and was assumed to melt following the reaction 4 olivine + 84 clinopyroxene + 12 garnet = 87 melt and 13 orthopyroxene (melt reaction from Walter, 1998). Partition coefficients are shown in Appendix G.

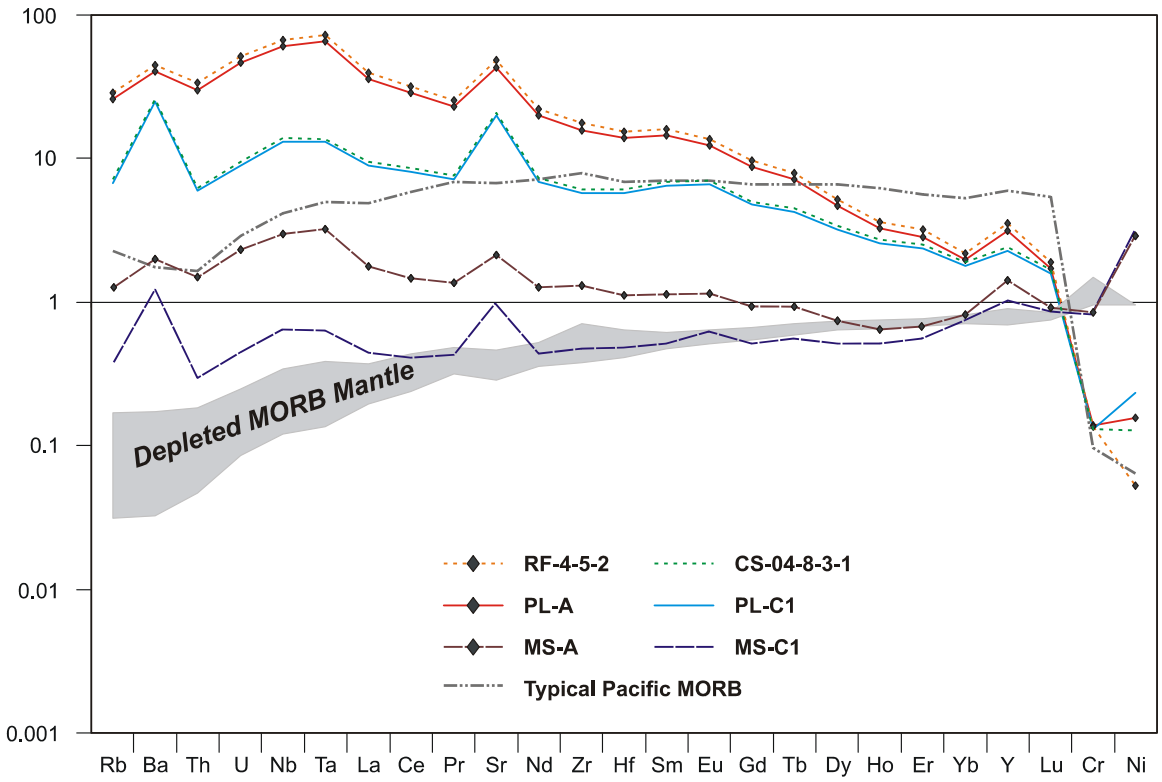

Figure 21. Results of modeling of valley lava mantle sources
Normalized to primitive mantle: Cr, Ni normalizing values from McDonough and Sun (1995), all other elements from Sun and McDonough (1989). Depleted MORB mantle (after Salters and Stracke (2004) and Workman and Hart (2005)) shown in grey shading. Pacific MORB from Klein (2003).

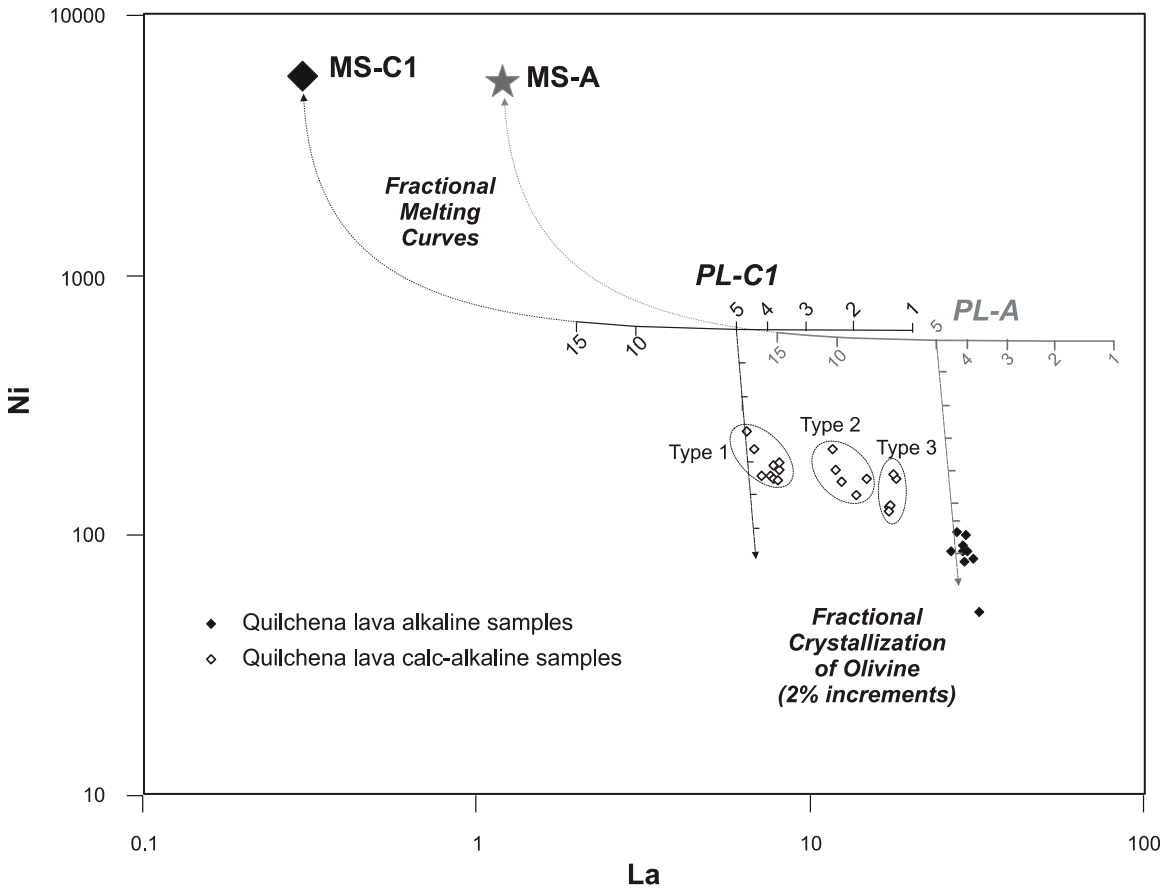

Figure 22. Bivariate Ni vs. La diagram, showing composition of mantle sources MS-A and MS-C1, partial melting curves, fractional crystallization of olivine curves and Quilchena lava samples

Solid and dotted curved lines represent fractional melting of mantle sources (black line for MS-C1, grey line for MS-A; solid lines for low degrees of partial melting, dotted lines for inferred higher degrees of partial melting). Compositions of melt after 1, 2, 3, 4, 5, 10, and 15% fractional melting of source are indicated. Vertical dashed lines descending from 5% fractional melting mark show pathway for fractional crystallization of olivine from melt (tick marks every 2%). Type 1, 2 and 3 calc-alkaline samples are circled.

mantle), and with peaks in Ba, Nb, Ta and Sr in a style similar to those in MS-A. The composition of Pacific MORB is also shown for comparison (northern East Pacific Rise; Klein, 2003).

The modelling results also indicate that the alkaline and subalkaline compositions could not reasonably be generated from the same mantle source. For example, assuming 5% partial melting of MS-A produces the alkaline primary magmas, a minimum of 20–30% melting is needed to produce most of the trace element concentrations observed in the type 1 calc-alkaline samples (partial melting at mid-ocean spreading centers is 5–20% by weight; Walter, 2003). Although smaller degrees of partial melting can produce a few of the observed trace element concentrations (e.g. ~14% melting of MS-A can produce the concentrations of Rb, Ba and HREEs calculated in PL-C1), it cannot reproduce the low Nb, Ta, and LREE/MREE concentrations. Partial melting of MS-A also cannot generate the complete set of trace element concentrations found in the type 2 and 3 calc-alkaline samples. Therefore, simple fractional melting of one mantle source cannot relate the primary alkaline and most depleted magmas, and the two main geochemical types must therefore derive from separate mantle sources.

2.10 Discussion

2.10.1 Mantle Source Implications

Previous studies have evaluated the mantle beneath British Columbia using ultramafic mantle xenoliths carried up in Cenozoic lavas (e.g., Littlejohn and Greenwood, 1974; Nicholls et al., 1982; Canil et al., 1987; Sun and Kerrich, 1995; Peslier et al., 2002; Harder and Russell, 2006), including the plateau lavas of the Chilcotin Group. Recent

models for the southern Canadian Cordilleran indicate that the base of the lithosphere is at 50–66 km depth and 1100–1200°C (Hyndman and Lewis, 1999; Currie et al., 2004; Harder and Russell, 2006). These xenoliths are typically spinel-bearing with calculated equilibration temperatures between 800–1100°C and depths of 30–40 km, placing their source region entirely within the lithospheric mantle (Nicholls et al., 1982; Canil et al., 1987; Peslier et al., 2002; Harder and Russell, 2006). The spinel–garnet transition is estimated at >80 km depth (Robinson and Wood, 1998; Hofmann, 2003), putting it well below the lithosphere–asthenosphere transition in the Canadian Cordillera. As the valley lavas are interpreted to be sourced from garnet-bearing mantle, their source must be below the source of the mantle xenoliths and the spinel–garnet transition. Therefore, the valley lavas have originated in the asthenosphere. This agrees with the conclusion of Dostal et. al (1996) that the OIB-like Chilcotin Group plateau lavas were derived from melting of the asthenosphere.

However, as discussed in the previous section, the valley lavas are interpreted to be derived from (at least) two separate mantle sources (MS-A and MS-C1). Dostal et al. (1996) proposed that upwelling of the asthenospheric mantle triggered melting of the subcontinental lithospheric mantle to create the quartz-normative tholeiites found in the plateau lavas. This solution is implausible for the origins of the valley lavas, which, based on their source depth and internally consistent εNd ratios (+8.0 to +8.4), have not had significant input from an old and enriched continental lithospheric mantle.

Based on the modelling in the previous section, the variations in the mantle sources for the valley lavas are likely to be entirely asthenospheric, suggesting that the asthenosphere beneath southern British Columbia is not uniform, but contains small

heterogeneities. This is further emphasized when examining the full Quilchena lava calc-alkaline suite. The type 1 calc-alkaline samples and the alkaline samples represent the two end-member compositions observed within the Quilchena lavas with the less LREE-depleted calc-alkaline samples (types 2 and 3) having trace elements compositions generally in-between those of the two end-member compositions. However, the type 2 and 3 calc-alkaline samples cannot be derived from mixing of partial melts of MS-A and MS-C1 as they are more depleted in the HREEs than both the most depleted and alkaline lavas. Therefore, the variation within the calc-alkaline suite cannot be explained by mixing of two asthenospheric sources, indicating that the small mantle heterogeneities proposed have a range of compositions (not just two). All of the mantle sources show anomalous enrichments in Sr, Nb and Ta.

An alternate scenario that could account for the valley lavas is the possibility of melting of the subducted Juan de Fuca slab. The valley lavas, particularly the calc-alkaline Quilchena lavas, have SiO_2 compositions above those expected from a pure asthenospheric melt (52–54 wt.% oxide). The calc-alkaline lavas also have high Ni, Cr and Sr concentrations, and Sr/Y values of 33–59, all of which are characteristic of adakites or sanukitoids (Martin et al., 2005), although at slightly lower SiO_2 compositions. Melting of the subducted Juan de Fuca / Explorer slab would also be consistent with εNd values (+8.0 to +8.4) found in the valley lavas.

As a slab subducts, it undergoes changes in pressure and temperature which cause its edges to melt (Thorkelson and Breitsprecher, 2005). As the slab moves into the garnet stability field, melting may continue (e.g. adakite), leaving behind garnet-bearing restite (Thorkelson and Breitsprecher, 2005). The valley lavas should not be interpreted as

melting of the subducted slab, as they do not display the typical Nb–Ta depletions observed in adakites. However, subsequent melting of garnetiferous restite would produce melts with no Nb–Ta depletions (as observed in the valley lavas, which have no or positive Nb–Ta anomolies), and therefore should be considered as a possible alternative to a pure asthenospheric model of valley lava genesis.

2.10.2 Relationship Between Geochemistry and Age

The relationship between the geochemical trends described in Sections 2.8 and 2.9 can also be examined in their geochronological context. At Missezula Lake (the most analyzed section), the base of the lava succession is composed of alkaline lavas, which have an age of 660 ± 30 ka. These lavas are also some of the most isotopically depleted, with εNd values of +8.3 to +8.4. Lying directly above these lavas are the type 1 calc-alkaline lavas (the most LREE-depleted), with an age of 400 ± 100 ka and εNd of +8.1. This abrupt change in lava composition correlates with an observed break in the lava succession, where sediment is trapped between two lava flows. Continuing up-section from the calc-alkaline type 1 lavas, the type 2 and overlying type 3 lavas are observed, the last dating at 180 ± 50 ka (εNd = +8.0).

The northern Quilchena lavas near Merritt all share the type 1 calc-alkaline chemistry, but are older than the type 1 lavas to the south (800 ± 100 ka and 670 ± 60 ka), indicating that the composition of the valley lavas changed over time, from calc-alkaline (in the north) to alkaline (Missezula Lake and Loon Lake samples in the south), and back to calc-alkaline (Missezula Lake), with all three calc-alkaline types observed. This alternation in composition over time is consistent with melting of a heterogeneous

mantle. Although a similar analysis has not been performed on the Lambly Creek lavas further to the east, it can be noted that their composition is very similar to the Chilcotin Group plateau lavas, with εNd values that are more radiogenic than the plateau lavas (+8.0), and at 1.5 ± 0.1 Ma is significantly older than the Quilchena lavas, but younger than most of the plateau lavas in the Okanagan region.

2.10.3 Tectonic Implications of the Valley Lavas

The Chilcotin Group is located behind the northern end of the modern Garibaldi (northern Cascade) arc, and its Neogene precursor, the Pemberton arc, and was regarded by Bevier (1983a, b) to be a field of back-arc lavas. A recent reconstruction by Madsen et al., (2006) indicates that the Chilcotin Group erupted mainly above the subducted slab of the Juan de Fuca plate, the northern portion of which separated into the Explorer plate at ca. 4 Ma (Riddihough, 1984). The range in isotopic compositions of the Chilcotin Group suggests that although some of the earliest lavas were contaminated by enriched subcontinental lithospheric mantle, most of the plateau lavas were derived solely from garnet-bearing asthenospheric mantle (Dostal et al., 1996).

Although our view of the valley lavas is broadly consistent with the previous interpretations of the Chilcotin Group as asthenosphere-derived back-arc lavas, we offer some elaboration and clarification. First, the calc-alkaline to alkaline (major element) and intraplate (trace element) signatures of the lavas, and the compositions of the calculated primary magmas, indicates that the underlying asthenosphere is likely to consist of enriched peridotite containing heterogeneous pods or streaks of less enriched mantle, some of which may reflect slight subduction-generated metasomatism, or garnet-bearing restite generated by melting of the subducted slabs. Second, the composition of

the valley lavas, and the Chilcotin Group as a whole, is remarkably consistent with other Neogene to Recent lavas that extend from central British Columbia to Yukon in the form of the Northern Cordilleran Volcanic Province and the Wells Gray and Anahim volcanic fields (Hickson, 1986; Souther, 1992; Charland and Francis; 1993; Edwards et al., 2002). The consistency of La/Nb ratios (Figure 20) and other geologically sensitive indices demonstrate the geochemical continuity of the back-arc / intraplate region as a whole. Third, the tectonic environment of the northern Cordillera during the Late Cenozoic is best understood as a slab window generated by the subduction of the Juan de Fuca spreading ridge (Thorkelson and Taylor, 1989).

The slab window is bounded by slabs of the northward-subducting Pacific plate to the northwest and the eastward-subducting Juan de Fuca plate to the south. At 4 Ma, the northern part of the Juan de Fuca plate jammed in the subduction zone and broke away to form the Explorer plate (Riddihough, 1977 and 1984; Rohr and Furlong, 1995). On the sea floor, the differential motion between the Explorer and Juan de Fuca plates was taken up by the Nootka fault, but the configuration of this fault as it continues into the subducted realm is uncertain. Madsen et al. (2006) suggested that the Nootka fault continued in a linear manner, allowing the subducted parts of the Explorer and Juan de Fuca slabs to tear apart at depth. In this configuration (or others like it), the southern edge of the slab window beneath British Columbia would consist of a thin and broken subducted plate, providing little separation between sub- and supra-slab mantle environments (cf. Thorkelson, 1996). Thermal erosion in the form of partial melting of the subducting crust and concomitant increasing ductility of the subducted mantle

(Thorkelson and Breitsprecher, 2005), is likely to have further reduced the physical and thermal significance of the Explorer and northern Juan de Fuca slabs.

In the context of a thin and broken slab edge, the geochemical continuity between the Chilcotin Group and the Northern Cordilleran / Anahim / Wells Gray volcanic field is rationalized by widespread upflow of dry, enriched "sub-slab" asthenosphere through the slab window and past an ineffective, permeable slab barrier. Partial melting of enriched asthenosphere affected much of the Canadian Cordillera with the notable exception of the Garibaldi-Pemberton arc, which remained affected by slab-derived metasomatism and hydrous mantle magmatism (Thorkelson et al., 2008). Thus, although the valley lavas lie above the Juan de Fuca slab, and the Nootka fault is projected to lie 200-300 km to the north, enriched asthenosphere has gained access to the base of the overriding North American lithosphere. In support of the Nootka fault as a breach in the slab, and thermal degradation of the Juan de Fuca and Explorer plates, we note that the youngest plateau lavas of the Chilcotin Group (≤5 Ma) are located near (and mainly south of) the projected trace of the Nootka fault (49.5–52°N and 119–122.5°W; data compilation from Breitsprecher and Mortensen, 2004).

2.11 Conclusions

The Quaternary valley lavas of southern British Columbia are part of the Chilcotin Group, a widespread succession of Late Cenozoic mafic "plateau" lavas in south-central British Columbia. The valley lavas can be divided into two distinct geographic units: the Quilchena lavas, found in the Merritt–Princeton corridor, and the Lambly Creek lavas, found west of Okanagan Lake in the Kelowna area. Lambly Creek

volcanism occurred at 1.5 ±0.1 Ma, and Quilchena lava volcanism occurred from 780 ka to 100 ka.

The valley lavas erupted subaerially from discrete centres (e.g., near Loon Lake) and flowed down or pooled in existing valleys. An estimated 8.8–21.1 km^3 of lava erupted, but glacial and fluvial erosion removed most of the lava, with what remains preserved as terraces along valley walls. The lavas are flat-lying with pahoehoe tops indicative of subaerial deposition, and well-preserved internal features including vesicle sheets and cylinders implying flow inflation, and local intercalations of silt indicating hiatuses in volcanic activity. Individual flows cannot be traced between sections, suggesting that numerous flows, perhaps hundreds, comprise the valley lava successions.

The valley lavas range from alkaline to calc-alkaline in major element composition, with intraplate trace element characteristics similar to that of ocean island basalts. Trace element characteristics and modelling of the alkaline and calc-alkaline end-members of the Quilchena lavas indicate that the two geochemical types were derived from a heterogeneous garnet-bearing asthenospheric source, with little subduction signature and no involvement of continental lithospheric mantle. The asthenospheric source was below the physically and thermally degraded Juan de Fuca and Explorer plates, south of the slab window formed from subduction of the Juan de Fuca spreading ridge. The Chilcotin Group is geochemically similar to most Late Cenozoic volcanic rocks in the Canadian Cordillera, except for the Cascade (Garibaldi-Pemberton) arc, and forms the southern part of a large intraplate volcanic field that is scattered throughout much of British Columbia and Yukon. The compositional similarity implies a common mantle source for the region and a common process involving asthenospheric

upwelling through the slab window and breaches in the Juan de Fuca / Explorer slab. Melting of restite created by melting of the subducted Juan de Fuca / Explorer slabs should be further explored as a possible source of the valley lavas.

REFERENCE LIST

Albarède, F. (1992): How deep do common basaltic magmas form and differentiate; Journal of Geophysical Research, v. 97(B7), p. 10997–11009.

Anderson, R.G., Resnick, J., Russell, J.K., Woodsworth, G.J., Villeneuve, M.E. and Grainger, N.C. (2001): The Cheslatta Lake suite: Miocene mafic, alkaline magmatism in central British Columbia; Canadian Journal of Earth Sciences, v. 38(1), p. 697–717.

Andrews, G.D.M. and Russell, J.K. (2007): Mineral exploration potential beneath the Chilcotin Group (NTS 092O, P; 093A, B, C, F, G, J, K), South-Central British Columbia: preliminary insights from volcanic facies analysis; in Geological Fieldwork 2006, Geoscience BC, Report 2007-1, p. 229–238.

Andrews, G.D.M. and Russell, J.K. (2008): Cover thickness across the Southern Interior Plateau, British Columbia (NTS 092O, P; 093A, B, C, F): constraints from water-well records; in Geoscience BC Summary of Activities 2007, Geoscience BC, Report 2008-1, p. 11–20.

Asimow, P.D. and Longhi, J. (2004): The significance of multiple saturation points in the context of polybaric near-fractional melting; Journal of Petrology, v. 45(12), p. 2349–2367.

Atwater, T. (1970): Implications of plate tectonics for the Cenozoic tectonic evolution of Western North America; Geological Society of America Bulletin, v. 81(1), p. 3513–3536.

BC Geological Survey (2008): MapPlace GIS internet mapping system; BC Ministry of Energy, Mines and Petroleum Resources, MapPlace website, URL http://www.MapPlace.ca [May 2008].

Bevier, M.L., Armstrong, R.L. and J.G. Souther (1979): Miocene peralkaline volcanism in west-central British Columbia – Its temporal and plate-tectonics setting; Geology, v. 7(1), p. 389–392.

Bevier, M.L. (1982): Geology and petrogenesis of Mio–Pliocene Chilcotin Group basalts, British Columbia; unpublished Ph.D. dissertation, University of California – Santa Barbara, 110 p.

Bevier, M.L. (1983a): Implications of chemical and isotopic composition for petrogenesis of Chilcotin Group basalts, British Columbia; Journal of Petrology, v. 24(2), p. 207–226.

Bevier, M.L. (1983b): Regional stratigraphy and age of Chilcotin Group basalts, south-central British Columbia; Canadian Journal of Earth Sciences, v. 20(4), p. 515–524.

Booth, D.B., Troost, K.G., Clague, J.J. and Waitt, R.B. (2003): The Cordilleran ice sheet; Chapter 2 in The Quaternary Period in the United States, A.R. Gillespie, S.C. Porter and B.F. Atwater (eds.), Developments in Quaternary Science, Elsevier, p. 17–43.

Bostock, M.G. and VanDecar, J.C. (1995): Upper mantle structure of the northern Cascadia subduction zone; Canadian Journal of Earth Sciences, v. 32(1), p. 1–12.

Breitsprecher, K. and Mortensen, J.K. (2004): BCAge 2004A – A Database of Isotopic Age Determinations for Rock Units from British Columbia; British Columbia Ministry of Energy and Mines, Open File 2004-3 (v. 3.0), CD-ROM.

Cande, S.C. and Kent, D.V. (1995): Revised calibration of the geomagnetic polarity timescale for the Late Cretaceous and Cenozoic; Journal of Geophysical Research, v. 100(B4), p. 6093–6095.

Canil, D., Brearley, M. and Scarfe, C.M. (1987): Petrology of ultramafic xenoliths from Rayfield River, south-central British Columbia; Canadian Journal of Earth Sciences, v. 24(1), p. 1679–1687.

Charland, A. and Francis, D. (1993): Stratigraphy and geochemistry of the Itcha Volcanic Complex, central British Columbia; Canadian Journal of Earth Sciences, v. 30, p. 132–144.

Church, B.N. (1980): A survey of Cenozoic magnetostratigraphy in south-central British Columbia; in Geological Fieldwork 1979, BC Ministry of Energy, Mines and Petroleum Resources, Paper 1980-1, p. 9–10.

Clague, J.J. (2000): Recognizing order in chaotic sequences of Quaternary sediments in the Canadian Cordillera; Quaternary International, v. 68, p. 29–38.

Coish, R.A., Kretschmar, L.M. and Journeay, J.M. (1998): Geochemistry of the Miocene Mount Noel Volcanic Complex, British Columbia and comparison with the Columbia River basalt; Journal of Volcanology and Geothermal Research, v. 83, p. 269–285.

Currie, C.A., Wang, K., Hyndman, R.D. and He, J. (2004): The thermal effects of steady-state slab-driven mantle flow above a subducting plate: the Cascadia subduction zone and backarc; Earth and Planetary Science Letters, v. 223, p. 35–48.

D'Orazio, M., Innocenti, F., Manetti, P., Haller, M.J., Vincenzo, G.D. and Tonarini, S. (2005): The Late Pliocene mafic lavas from the Camusú Aike volcanic field (~50˚S, Argentina): Evidence for geochemical variability in slab window magmatism; Journal of South American Earth Sciences, v. 18, p. 107–124.

Dostal, J., Hamilton, T.S. and Church, B.N. (1996): The Chilcotin basalts, British Columbia (Canada): Geochemistry, petrogenesis and tectonic significance; Neues Jahrbuch Mineralogie, Abhandlungen, v. 170, p. 207–229.

Dunn, T. and Sen, C. (1994): Mineral/matrix partition-coefficients for orthopyroxene, plagioclase, and olivine in basaltic to andesitic systems – a combined analytical and experimental study; Geochimica et Cosmochimica Acta, v. 52(2), p. 717–733.

Dziak, R.P. (2006): Explorer deformation zone: Evidence of a large shear zone and reorganization of the Pacific–Juan de Fuca–North American triple junction; Geology, v. 34(3), p. 213–216.

Edwards, B.R. and Russell, J.K. (2000): Distribution, nature, and origin of Neogene–Quaternary magmatism in the northern Cordilleran volcanic province, Canada; Geological Society of America Bulletin, v. 112(8), p. 1280–1295.

Edwards, B.R., Russell, J.K. and Anderson, R.G. (2002): Subglacial, phonolitic volcanism at Hoodoo Mountain volcano, northern Canadian Cordillera; Bulletin of Volcanology, v. 64(3–4), p. 254–272.

Engebretson, D.C., Cox, A. and Gordon, R.G. (1985): Relative motions between oceanic and continental plates in the Pacific Basin; Geological Society of America, Special Paper 206, 59 p.

Farmer, G.L. (2003): Continental basaltic rocks; Chapter 3 in The Crust, R.L. Rudnick (ed.), Treatise on Geochemistry, v. 3, p. 85–121.

Farrell, R.E., Andrews, G.D.M., Russell, J.K. and Anderson, R.G. (2007): Chasm and Dog Creek lithofacies, Chilcotin Group basalt, Bonaparte Lake map area, British Columbia; Geological Survey of Canada, Current Research 2007-A5, 11 p.

Frederiksen, A.W., Bostock, M.G., VanDecar, J.C. and Cassidy, J.F. (1998): Seismic structure of the upper mantle beneath the northern Canadian Cordillera from teleseismic travel-time inversion; Tectonophysics, v. 294, p. 43–55.

Fujimaki, H., Tatsumoto, M. and Aoki, K.-i. (1984): Partition coefficients of Hf, Zr, and REE between phenocrysts and groundmasses; Journal of Geophysical Research, v. 89, p. 662-672.

Fulton, R.J., Irving, E. and Wheadon, P.M. (1992): Stratigraphy and paleomagnetism of Brunhes and Matuyama (>790 ka) Quaternary deposits at Merritt, British Columbia; Canadian Journal of Earth Sciences, v. 29, p. 76–92.

Gibbard, P. and Kolfschoten, T.V. (2004): The Pleistocene and Holocene epochs; Chapter 22 in A Geologic Time Scale 2004, F. Gradstein, J. Ogg and A. Smith (eds.), Cambridge University Press, Cambridge, p. 441–452.

Godinot, A. (1988): Pipe vesicles in Hawaiian basaltic lavas – their origin and potential as paleoslope indicators – Comment; Geology, v. 16(1), p. 90.

Gordee, S., Andrews, G., Simpson, K.A. and Russell, J.K. (2007): Subaqueous channel-confined volcanism within the Chilcotin Group, Bull Canyon Provincial Park (NTS 093B/03), south-central British Columbia; in Geological Fieldwork 2006, Geoscience BC, Report 2007-1, p. 285–290.

Gorring, M.L., Kay, S.M., Zeitler, P.K., Ramos, V.A., Rubiolo, D., Fernandez, M.I. and Panza, J.L. (1997): Neogene Patagonian plateau lavas: Continental magmas associated with ridge collision at the Chile Triple Junction; Tectonics, v. 16(1), p. 1–17.

Gorring, M.L. and Kay, S.M. (2001): Mantle processes and sources of Neogene slab window magmas from southern Patagonia, Argentina; Journal of Petrology, v. 42(6), p. 1067–1094.

Grainger, N. (2000): Petrogenesis of Middle Jurassic to Miocene magmatism within the Nechako plateau, central British Columbia: Insight from petrography, geochemistry, geochronology and tracer isotope studies; unpublished M.Sc. thesis, University of Alberta, 125 p.

Green, N.L. (1981): Geology and petrology of Quaternary volcanic rocks, Garibaldi Lake area, southwestern British Columbia: Summary; Geological Society of America Bulletin, Part 1, v. 92(10), p. 697–702.

Green, N.L., Armstrong, R.L., Harakal, J.E., Souther, J.G. and Read, P.B. (1988): Eruptive History and K–Ar geochronology of the late Cenozoic Garibaldi volcanic belt, southwestern British Columbia; Geological Society of America Bulletin, v. 100, p. 563–379.

Grove, T.L. (2000): Origin of magmas; in Encyclopedia of Volcanoes, H. Sigurdsson, B. Houghton, S.R. McNutt, H. Rymer and J. Stix (eds.), Academic Press, San Diego, California, p. 133–147.

Haeussler, P.J., Bradley, D.C., Wells, R.E. and Miller, M.L. (2003): Life and death of the Resurrection plate: Evidences for its existence and subduction in the northeastern Pacific in Paleocene–Eocene time; Geological Society of America Bulletin, v. 115(7), p. 867–880.

Harder, M. and Russell, J.K. (2006): Thermal state of the upper mantle beneath the Northern Cordilleran Volcanic Province (NCVP), British Columbia, Canada; Lithos, v. 87, p. 1–22.

Hauri, E.H., Wagner, T.P. and Grove, T.L. (1994): Experimental and natural partitioning of Th, U, Pb and other trace elements between garnet, clinopyroxene and basaltic melts; Chemical Geology, v. 177, p. 149–166.

Hickson, C.J. (1986): Quaternary volcanism in the Wells Gray–Clearwater area, east central British Columbia; unpublished Ph.D. dissertation, University of British Columbia, 357 p.

Hildreth, W., Fierstein, J. and Lanphere, M. (2003): Eruptive history and geochronology of the Mount Baker volcanic field, Washington; Geological Society of America Bulletin, v. 115(6), p. 729–764.

Hirose, K. and Kushiro, I. (1993): Partial melting of dry peridotites at high pressures: determinations of compositions of melts segregated from peridotite using aggregates of diamond; Earth and Planetary Science Letters, v. 114, p. 477–489.

Hofmann, A.W. (2003): Sampling mantle heterogeneity through oceanic basalts: isotopes and trace elements; Chapter 3 in The Mantle and Core, R.W. Carlson (ed.), Treatise on Geochemistry, v. 2, p.

Hole, M.J., Rogers, G., Saunders, A.D. and Storey, M. (1991): Relation between alkalic volcanism and slab-window formation; Geology, v. 19, p. 657–660.

Hon, K., Kauahikaua, J., Denlinger, R. and Mackay, K. (1994): Emplacement and inflation of pahoehoe sheet flows: Observations and measurements of active lava flows on Kilauea Volcano, Hawaii; Geological Society of America Bulletin, v. 106, p. 351–370.

Hyndman, R.D. and Lewis, T.J. (1999): Geophysical consequences of the Cordillera–Craton thermal transition in southwestern Canada; Tectonophysics, v. 306, p. 397–422.

Ionov, D.A. (1993): Garnet peridotite xenoliths from the Vitim volcanic field, Baikal region – the nature of the garnet spinel peridotite transition zone in the continental mantle; Journal of Petrology, v. 34(6), p. 1141–1175.

Irvine, T.N. and Baragar, W.R.A. (1971): A guide to the chemical classification of the common volcanic rocks; Canadian Journal of Earth Sciences, v. 8, p. 523–548.

Jenner, G.A., Foley, S.F., Jackson, S.E., Green, T.H., Fryer, B.J. and Longerich, H.P. (1993): Determination of partition coefficients for trace elements in high pressure–temperature experimental run products by laser ablation microprobe-inductively coupled plasma-mass spectrometry (LAM-ICP-MS); Geochimica et Cosmochimica Acta, v. 57(23–24), p. 5099–5103.

Jicha, B.R., Scholl, D.W., Singer, B.S., Yogodzinski, G.M. and Kay, S.M. (2006): Revised age of Aleutian Island Arc formation implies high rate of magma production; Geology, v. 34(8), p. 661–664.

Klein, E.M. (2003): Geochemistry of the igneous oceanic crust; Chapter 13 in The Crust, R.L. Rudnick (ed.), Treatise on Geochemistry, v. 3, p. 433–463.

Lambert, M.B. (1963): The valley basalts in Quilchena Creek area, British Columbia; unpublished B.Sc. thesis, University of British Columbia, 39 p.

Lebas, M.J., Lemaitre, R.W., Streckeisen, A. and Zanettin, B. (1986): A chemical classification of volcanic rocks based on the total alkali silica diagram; Journal of Petrology, v. 27, p. 745–750.

Lehnert, K., Su, Y., Langmuir, C., Sarbas, B. and Nohl, U. (2000): A global geochemical database structure for rocks; Geochemistry Geophysics Geosystems, v. 1, doi: 10.1029/1999GC00026.

Littlejohn, A.L. and Greenwood, H.J. (1974): Lherzolite nodules in basalts from British Columbia, Canada; Canadian Journal of Earth Sciences, v. 11, p. 1288–1308.

Ludwig, K.R. (2003): Isoplot, A Geochronological Toolkit for Microsoft Excel (3.09); Special Publication No. 4; Berkeley Geochronology Center.

Madsen, J.K., Thorkelson, D.J., Friedman, R.M. and Marshall, D.D. (2006): Cenozoic to Recent plate configurations in the Pacific Basin: Ridge subduction and slab window magmatism in western North America; Geosphere, v. 2(1), p. 11–34.

Martin, H, Smithies, R.H., Rapp, R. Moyen, J.-F. and Champion, D. (2005): An overview of adakite, tonalitetrondhjemitegranodiorite (TTG), and sanukitoid: relationships and some implications for crustal evolution; Lithos, v. 79, p. 1–24.

Mathews, W.H. and Rouse, G.E. (1984): The Gang Ranch – Big Bar area, south-central British Columbia: Stratigraphy, geochronology, and palynology of the Tertiary beds and their relationship to the Fraser Fault; Canadian Journal of Earth Sciences, v. 18, p. 662–664.

Mathews, W.H. (1988): Neogene geology of the Okanagan Highland, British Columbia; Canadian Journal of Earth Sciences, v. 25, p. 725–731.

Mathews, W.H. (1989): Neogene Chilcotin basalts in south-central British Columbia: geology, ages, and geomorphic history; Canadian Journal of Earth Sciences, v. 26, p. 969–982.

McDonough, W.F. (1990): Constraints on the composition of the continental lithospheric mantle; Earth and Planetary Science Letters, v. 101, p. 1–18.

McDonough, W.F. and Sun, S.S. (1995): The composition of the Earth; Chemical Geology, v. 120(3–4), p. 223–253.

McDonough, W.F. and Rudnick, R.L. (1998): Mineralogy and composition of the upper mantle; in Ultrahigh-Pressure Mineralogy: Physics and Chemistry of the Earth's Deep Interior, R.J. Hemley (ed.), Reviews in Mineralogy, v. 37, Mineralogical Society of America, Washington, DC, p. 139–164.

McKenzie, D. and O'Nions, R.K. (1991): Partial melt distributions from inversion of rare earth element concentrations; Journal of Petrology, v. 32, p. 1021–1091.

Mejia, V., Barendregt, R.W. and Opdyke, N.D. (2002): Paleosecular variation of Brunhes age lava flows from British Columbia, Canada; Geochemistry Geophysics Geosystems, v. 3, 8801, doi: 10.1029/2002GC000353.

Meschede, M. (1986): A method of discriminating between different types of mid-ocean ridge basalts and continental tholeiites with the Nb–Zr–Y diagram; Chemical Geology, v. 56, p. 207–218.

Middlemost, E.A.K. (1989): Iron oxidation ratios, norms and the classification of volcanic rocks; Chemical Geology, v. 77, p. 19–26.

Miyashiro, A. (1974): Volcanic rock series in island arcs and active continental margins; American Journal of Science, v. 274(4), p. 321–355.

Monger, J.W.H. (1989a): Geology, Hope British Columbia; Geological Survey of Canada, Map 41-1989, scale 1:250 000.

Monger, J.W.H. (1989b): Geology, Ashcroft, British Columbia; Geological Survey of Canada, Map 42-1989, scale 1:250 000.

Mysen, B. (1978): Experimental determination of nickel partition coefficients between liquid, pargasite and garnet peridotite minerals and concentration limits of behavior according to Henry's Law at high pressure and temperature; American Journal of Science, v. 278, p. 217–243.

Neilsen, R.L., Gallahan, W.E. and Newberger, F. (1992): Experimentally determined mineral–melt partition coefficient for Sc, Y, and REE for olivine, orthopyroxene, pigeonite, magnetite and ilmenite; Contributions to Mineralogy and Petrology, v. 110, p. 488–499.

Neilsen, R. (2005): Geochemical Earth Reference Model Partition Coefficient (Kd) Database; http://earthref.org/GERM/index.html [November 2005].

Nicholls, J., Stout, M.Z. and Fiesinger, D.W. (1982): Petrologic variations in Quaternary volcanic rocks, British Columbia, and the nature of the underlying upper mantle; Contributions to Mineralogy and Petrology, v. 79, p. 201–218.

Nomade, S., Renne, P.R., Vogel, N., Deino, A.L., Sharp, W.D., Becker, T.A., Jaouni, A.R. and Mundil, R. (2005): Alder Creek sanidine (ACs-2): A Quaternary Ar/Ar dating standard tied to the Cobb Mountain geomagnetic event; Chemical Geology, v. 218, p. 315–338.

Pearce, J.A. and Cann, J.R. (1973): Tectonic setting of basic volcanic rocks determined using trace element analysis; Earth and Planetary Science Letters, v. 19, p. 290–300.

Pearce, J.A. (1996): A user's guide to basalt discrimination diagrams; in Trace Element Geochemistry of Volcanic Rocks: Applications for Massive Sulphide Exploration, D.A. Wyman (ed.), Geological Association of Canada Short Course Notes, v. 12, p. 79–113.

Pearson, D.G., Canil, D. and Shirley, S.B. (2003): Mantle samples included in volcanic rocks: xenoliths and diamonds; Chapter 5 in The Mantle and Core, R.W. Carlson (ed.), Treatise on Geochemistry, v. 2, p. 171–275.

Peslier, A.H., Francis, D. and Ludden, J. (2002): The lithospheric mantle beneath continental margins: melting and melt–rock reaction in Canadian Cordillera xenoliths; Journal of Petrology, v. 43(11), p. 2013–2047.

Philpotts, A.R. and Lewis, C.L. (1987): Pipe vesicles – an alternate model for their origin; Geology, v. 15(10), p. 971–974.

Preto, V.A. (1979): Geology of the Nicola Group between Merritt and Princeton; BC Ministry of Energy, Mines and Petroleum Resources, 90 p., 1 map at 1:50 000 scale.

Ramachandran, K., Dosso, S., Spence, G., Hyndman, R. and Brocher, T. (2005): Forearc structure beneath southwestern British Columbia: A three-dimensional tomographic velocity model; Journal of Geophysical Research, v. 110, B02303, doi: 10.1029/2004JB003258.

Read, P.B. (2000): Geology and Industrial Minerals of the Tertiary Basins, South-Central British Columbia; BC Ministry of Energy, Mines and Petroleum Resources, Geofile 2000-3, 110 p.

Reinecke, L. (1920): Mineral Deposits between Lillooet and Prince George, British Columbia; Geological Survey of Canada, Memoir 118, 129 p.

Renne, P.R., Swisher, C.C., Deino, A.L., Karner, D.B., Owens, T. and DePaolo, D.J. (1998): Intercalibration of standards, absolute ages and uncertainties in $^{40}Ar/^{39}Ar$ dating; Chemical Geology, v. 145(1–2), p. 117–152.

Rice, R.M.A. (1947): Geology and mineral deposits of the Princeton map-area, British Columbia; Memoir 243, 136 p.

Riddihough, R.P. (1977): A model for recent plate interactions off Canada's west coast; Canadian Journal of Earth Sciences, v. 14(3), p. 384–396.

Riddihough, R.P. (1984): Recent movements of the Juan de Fuca plate system; Journal of Geophysical Research, v. 89(8), p. 6980–6994.

Robinson, J.A.C. and Wood, B.J. (1998): The depth of the spinel to garnet transition at the peridotite solidus; Earth and Planetary Science Letters, v. 164, p. 277–284.

Roeder, P.L. and Emslie, R.F. (1970): Olivine–liquid equilibrium; Contributions to Mineralogy and Petrology, v. 29, p. 275–289.

Rohr, K.M. and Furlong, K.P. (1995): Ephemeral plate tectonics at the Queen Charlotte triple junction; Geology, v. 23(11), p. 1035–1038.

Rohr, K.M.M. and Currie, L. (1997): Queen Charlotte basin and Coast Mountains: Paired belts of subsidence and uplift caused by a low-angle normal fault; Geology, v. 25(9), p. 819–822.

Rollinson, H.R. (1993): Using Geochemical Data; Longman, Harlow, 352 p.

Ryder, J.M. and Clague, J.J. (1989): British Columbia (Quaternary stratigraphy and history, Cordilleran ice sheet); Chapter 1 in Quaternary Geology of Canada and Greenland, R.J. Fulton (ed.), v. 1, Geological Survey of Canada, p. (also Geological Society of America, The Geology of North America, v. K-1).

Salters, V.J.M. and Stracke, A. (2004): Composition of the depleted mantle; Geochemistry Geophysics Geosystems, v. 5, Q05004, doi: 10.1029/2003GC000597.

Schmincke, H.-U. (1967): Flow directions in Columbia River Basalt flows and paleocurrents of interbedded sedimentary rocks, South-Central Washington; International Journal of Earth Sciences, v. 56(1), p. 992–1020.

Self, S., Keszthelyi, L. and Thordarson, T. (1998): The importance of pāhoehoe; Annual Reviews of Earth and Planetary Science, v. 26, p. 81–110.

Shervais, J.W. (1982): Ti–V plots and the petrogenesis of modern and ophiolitic lavas; Earth and Planetary Science Letters, v. 59, p. 101–118.

Shi, L., Francis, D., Ludden, J., Frederiksen, A. and Bostock, M. (1998): Xenolith evidence for lithospheric melting above anomalously hot mantle under the northern Canadian Cordillera; Contributions to Mineralogy and Petrology, v. 131, p. 39–53.

Smith, A.D. (1986): Isotopic and geochemical studies of Terrane I, south-central British Columbia; unpublished Ph.D. dissertation, University of Alberta, 195 p.

Sobolev, A.V., Migdisov, A.A. and Portnyagin, M.V. (1996): Incompatible element partitioning between clinopyroxene and basalt liquid revealed by the study of melt inclusions in minerals from Troodos lavas, Cyprus; Petrology, v. 4(3), p. 307–317.

Souther, J. and Hickson, C. (1984): Crystal fractionation of the basalt comendite series of the Mount Edziza Volcanic Complex, British Columbia – major and trace-elements; Journal of Volcanology and Geothermal Research, v. 21(1-2), p. 76–106.

Souther, J.G. (1991): Volcanic regimes; Chapter 14 in Geology of the Cordilleran Orogen in Canada, H. Gabrielse and C.J. Yorath (eds.), Geology of Canada, v. 4, Geological Survey of Canada, p. 457–490 (also Geological Society of America, The Geology of North America, v. G-2).

Souther, J.G. and Yorath, C.J. (1991): Neogene assemblages; Chapter 10 in Geology of the Cordilleran Orogen in Canada, H. Gabrielse and C.J. Yorath (eds.), The Geology of Canada, v. 4, Geological Survey of Canada, p. 373–401 (also Geological Society of America, The Geology of North America, v. G-2).

Souther, J.G. (1992): The Late Cenozoic Mount Edziza Volcanic Complex, British Columbia, v. Memoir 420, 320p.

Sun, S.S. and McDonough, W.F. (1989): Chemical and isotopic systematics of oceanic basalts: implications for mantle composition and processes; in Magmatism in the Ocean Basins, A.D. Saunders and M.J. Norry (eds.), Geological Society of America Special Publication, v. 42, p. 313–345.

Sun, M. and Kerrich, R. (1995): Rare earth element and high field strength element characteristics of whole rocks and mineral separates of ultramafic nodules in Cenozoic volcanic vents of southeastern British Columbia, Canada; Geochimica et Cosmochimica Acta, v. 59(23), p. 4863–4879.

Tempelman-Kluit, D.J. (1989): Geology, Penticton, British Columbia; Geological Survey of Canada, Map 1736A, scale 1:250 000.

Thirlwall, M.F., Upton, B.G.J. and Jenkins, C. (1994): Interaction between continental lithosphere and the Iceland plume – Sr–Nd–Pb ssotope geochemistry of Tertiary basalts, NE Greenland; Journal of Petrology, v. 35(3), p. 839–879.

Thompson, R.N. (1984): Dispatches from the basalt front; Proceedings of the Geologists Association, v. 95, p. 249–262.

Thorkelson, D.J. and Taylor, R.P. (1989): Cordilleran slab windows; Geology, v. 17, p. 833–836.

Thorkelson, D.J. (1996): Subduction of diverging plates and the principles of slab window formation; Tectonophysics, v. 225, p. 47–63.

Thorkelson, D.J. and Breitsprecher, K. (2005): Partial melting of slab window margins: genesis of adakitic and non-adakitic magmas; Lithos, v. 79, p. 25–41.

Thorkelson, D., Madsen, J., Sluggett, C. and Breitsprecher, K. (2008): Late Cenozoic slab window and mantle upflow tectonics of the northern Canadian Cordillera; International Geological Congress, Oslo, Norway, Abstract CD-Rom.

Tipper, H.W. (1978): Geology, Taseko Lake (092O) map area, British Columbia; Geological Survey of Canada, Map 534, scale 1:125 000.

Tolan, T.L., Reidel, S.P., Beeson, M.H., Anderson, J.L., Fecht, K.R. and Swanson, D.A. (1989): Revisions to the estimates of the areal extent and volume of the Columbia River Basalt Group; in Volcanism and Tectonism in the Columbia River Flood-Basalt Province, S.P. Reidel and P.R. Hooper (eds.), Geological Society of America Special Paper 239, Boulder, Colorado, p. 1–21.

Tribe, S. (2004): Cenozoic drainage history of southern British Columbia; unpublished Ph.D. dissertation, Simon Fraser University, 147 p.

Tribe, S. (2005): Eocene paleo-physiography and drainage directions, southern Interior Plateau, British Columbia; Canadian Journal of Earth Sciences, v. 42, p. 215–230.

Walker, G.P.L. (1987): Pipe vesicles in Hawaiian basaltic lavas: Their origin and potential as paleoslope indicators; Geology, v. 15(1), p. 84–87.

Walter, M.J. (1998): Melting of garnet peridotite and the origin of komatiite and depleted lithosphere; Journal of Petrology, v. 36(1), p. 23–53.

Walter, M.J. (2003): Melt extraction and compositional variability in mantle lithosphere; Chapter 8 in The Mantle and Core, R.W. Carlson (ed.), Treatise on Geochemistry, v. 2, p. 363–394.

Wasserburg, G.J., Jacobsen, S.B., Depaolo, D.J., McCulloch, M.T. and Wen, T. (1981): Precise determinations of Sm/Nd ratios, Sm and Nd isotopic abundances in standard solutions; Geochimica et Cosmochimica Acta, v. 45, p. 2311-2323.

Weis, D., Kieffer, B., Maerschalk, C., Pretorius, W. and Barling, J. (2005): High-precision Pb–Sr–Nd–Hf isotopic characterization of USGS BHVO-1 and BHVO-2 reference materials; Geochemistry Geophysics Geosystems, v. 6, Q02002, doi: 10.1029/2004GC000852.

Wood, D.A. (1980): The application of the Th–Hf–Ta diagram to problems of tectonomagmatic classification and to establishing the nature of crustal contamination of basaltic lavas of the British Tertiary volcanic province; Earth and Planetary Science Letters, v. 50, p. 11–30.

Workman, R.K. and Hart, S.R. (2005): Major and trace element composition of the depleted MORB mantle (DMM); Earth and Planetary Science Letters, v. 231, p. 53–72.

APPENDICES

Appendix A: Sample Locations and Section Descriptions

Fieldwork for this study was completed in May–July 2004, and July 2005. Below is a brief description of each studied location, along with photographs and stratigraphic sections where appropriate. Sample locations for all samples (geochemical, isotopic and petrographic) referred to in this thesis are listed in Table 5.

Quilchena Lavas

The Quilchena lavas are easily accessed from forest service roads that run either along the base of valleys, or on top of the plateau created by the top of the lava cliffs. While the lavas in the Missezula Lake region are on Crown land, the lavas at the Chutter Ranch and Quilchena Creek exposures are on ranchland, and therefore permission was sought before accessing the rocks. All the described sections below form cliffs midway up or at the top of valley walls. Erosion of the lavas has produced steep talus slopes below the cliffs. The area is generally sparsely vegetated and both the cliffs and talus slopes are highly visible (e.g. Figure 7, Figure 23).

The Quilchena lava sections described below include only sections from which geochemical samples were obtained. Other locations were visited, where valley lava was mapped by Preto (1979) or Monger (1989a, b). These included Kentucky–Alleyne Provincial Park, north of Courtney Lake, north of Nicola Lake, and south-east of the Dillard Forestry Road–Highway 5A intersection (between Princeton and Merritt). Exposure in these areas was limited (Kentucky-Alleyne and Courtney Lake), or limited to basaltic boulders.

Table 5. Sample locations

		NAD 27		NAD 83			
Sample	**Locality**	***Easting***	***Northing***	***Easting***	***Northing***	**Latitude**	**Longitude**
Quilchena Lavas							
RF-1-1-2	Missezula (E)	676645	5521019	676551	5521220	49°N 49.0'	120°W 32.7'
RF-4-1-1	Missezula (E)	676670	5520983	676576	5521184	49°N 49.0'	120°W 32.7'
RF-4-1-2	Missezula (E)	676670	5520983	676576	5521184	49°N 49.0'	120°W 32.7'
RF-4-1-3	Missezula (E)	676670	5520983	676576	5521184	49°N 49.0'	120°W 32.7'
RF-4-2-1	Missezula (E)	676685	5520953	676591	5521154	49°N 49.0'	120°W 32.7'
RF-4-2-2	Missezula (E)	676685	5520953	676591	5521154	49°N 49.0'	120°W 32.7'
RF-4-2-3	Missezula (E)	676685	5520953	676591	5521154	49°N 49.0'	120°W 32.7'
RF-4-5-2	Missezula (E)	676797	5520836	676703	5521037	49°N 48.9'	120°W 32.6'
RF-4-5-3	Missezula (E)	676797	5520836	676703	5521037	49°N 48.9'	120°W 32.6'
RF-4-6-1	Missezula (E)	676824	5520815	676730	5521016	49°N 48.9'	120°W 32.6'
RF-4-6-2	Missezula (E)	676824	5520815	676730	5521016	49°N 48.9'	120°W 32.6'
RF-4-8-1	Missezula (E)	676890	5520755	676796	5520956	49°N 48.9'	120°W 32.5'
RF-4-10-2	Missezula (E)	676998	5520688	676904	5520889	49°N 48.9'	120°W 32.5'
RF-4-11-1	Missezula (E)	677026	5520701	676932	5520902	49°N 48.9'	120°W 32.4'
RF-4-12-1	Missezula (E)	677077	5520718	676983	5520919	49°N 48.9'	120°W 32.4'
CS-04-2-26-1	Missezula (E)	677077	5520718	676983	5520919	49°N 48.9'	120°W 32.4'
CS-04-2-9-1	Missezula (E)	676787	5520926	676693	5521127	49°N 49.0'	120°W 32.6'
CS-04-2-5-1	Missezula (E)	676685	5520953	676591	5521154	49°N 49.0'	120°W 32.7'
CS-04-2-14-1	Missezula (E)	676824	5520815	676730	5521016	49°N 48.0'	120°W 32.6'
CS-04-2-29-1	Missezula (E)	676645	5521019	676551	5521220	49°N 49.0'	120°W 32.7'
CS-04-2-28-1	Missezula (E)	676824	5520815	676730	5521016	49°N 48.0'	120°W 32.6'
CS-04-3-1-1	Loon Lake	677300	5527495	677206	5527696	49°N 52.5'	120°W 32.0'
CS-04-4-7-1	Missezula (W)	676209	5520577	676115	5520778	49°N 48.8'	120°W 33.0'
CS-04-6-2-1	Shrimpton Ck	678982	5525219	678888	5525420	49°N 51.3'	120°W 30.7'
CS-04-7-1-1	Bluey Lake	675107	5526730	675013	5526930	49°N 52.2'	120°W 33.9'
CS-05-2-1-2	Bluey Lake	675107	5526730	675013	5526930	49°N 52.2'	120°W 33.9'
CS-05-2-2-1	Bluey Lake	675107	5526730	675013	5526930	49°N 52.2'	120°W 33.9'
CS-04-8-3-1	Quilchena Cr.	677718	5554654	677624	5554856	50°N 07.2'	120°W 30.9'
CS-04-8-4-1	Quilchena Cr.	677718	5554654	677624	5554856	50°N 07.2'	120°W 30.9'
CS-04-10-1-1	Chutter Ranch	664213	5555807	664119	5556009	50°N 08.0'	120°W 42.2'
CS-04-10-2-2	Chutter Ranch	665158	5556049	665064	5556251	50°N 08.1'	120°W 41.4'
Lambly Creek lavas							
CS-04-12-1-1[1]	Lambly Creek	316526	5537587	316446	5537796	49°N 57.9'	119°W 33.6'
CS-04-13-4-1[1]	Lambly Creek	317146	5536336	317066	5536545	49°N 57.2'	119°W 33.0'
CS-04-15-8-1[1]	Okanagan Lk	317853	5526921	317773	5527130	49°N 52.1'	119°W 32.2'
Plateau basalts							
CS-04-24-1-1	Asp Creek	673660	5487033	673565	5487233	49°N 30.8'	120°W 36.1'
CS-04-27-2-1	Lillooet	574956	5646009	574859	5646214	50°N 57.8'	121°W 56.0'
CS-04-28-1-1	Kamloops	671274	5639207	671180	5639410	50°N 52.9'	120°W 34.0'
CS-04-30-1-1[1]	Kelowna	359476	5533381	359396	5533589	49°N 56.3'	118°W 57.6'
CS-04-31-1-1[1]	Christian Va.	374081	5505003	374001	5505212	49°N 41.2'	118°W 44.8'

[1]Samples in UTM Zone 11U (all other samples in UTM Zone 10U)

(E) or (W), *east or west bank of Missezula Lake,* ***Christian Va.,*** *Christian Valley*

Figure 23. Photograph of Chutter Ranch exposure east of Merritt, BC

Missezula Lake East (East side of Missezula Lake)

The Missezula Lake East section, located at the north-east end of Missezula Lake, can be accessed by a short hike off the Dillard Forest Service Road. A 660 m section of these lavas was the focus of detailed mapping and sampling by Richard Fitton in 2000, and so fieldwork from this study focused on verifying lava flow contacts and feature interpretation, and collecting samples for Ar–Ar and paleomagnetic analysis (and additional geochemical samples where required). The lavas on the east side of Missezula Lake are part of a 55 m-thick succession, with twenty-one individual flows identified. Most of the lava flows are 1–2 m thick, particularly at the base of the section, but a few flows near the top of the succession are up to 18 m thick. A few flows are only 10 m long, but many are exposed for upwards of 50–100 m, the longest for over 500 m. Figure 7 contains a stitched panoramic photograph of most of the mapped section, and a small sketch identifying most of the mapped flows. Figure 24 contains an idealized cross-section through the Missezula Lake East section, showing sample locations and geochemical changes.

The Missezula Lake East section contains excellent examples of flow textures (e.g. columnar jointing, flow top brecciation, ropey texture, pipe vesicles, vesicle cylinders), particularly in the thicker flows (Figure 8 and Figure 9). Two additional features are of particular note: silt trapped between (and in) lava flows, and the basal contact with the underlying Nicola Group. A ~3 cm layer of silt marks the base of the 500+ m-thick flow which runs most of the length of the mapped section. In places the sediment is also trapped around scoriaceous rubble trapped at the base of the flow (Figure 12c). At one locality (immediately north of sample RF-1-1-2), a massive flow abruptly

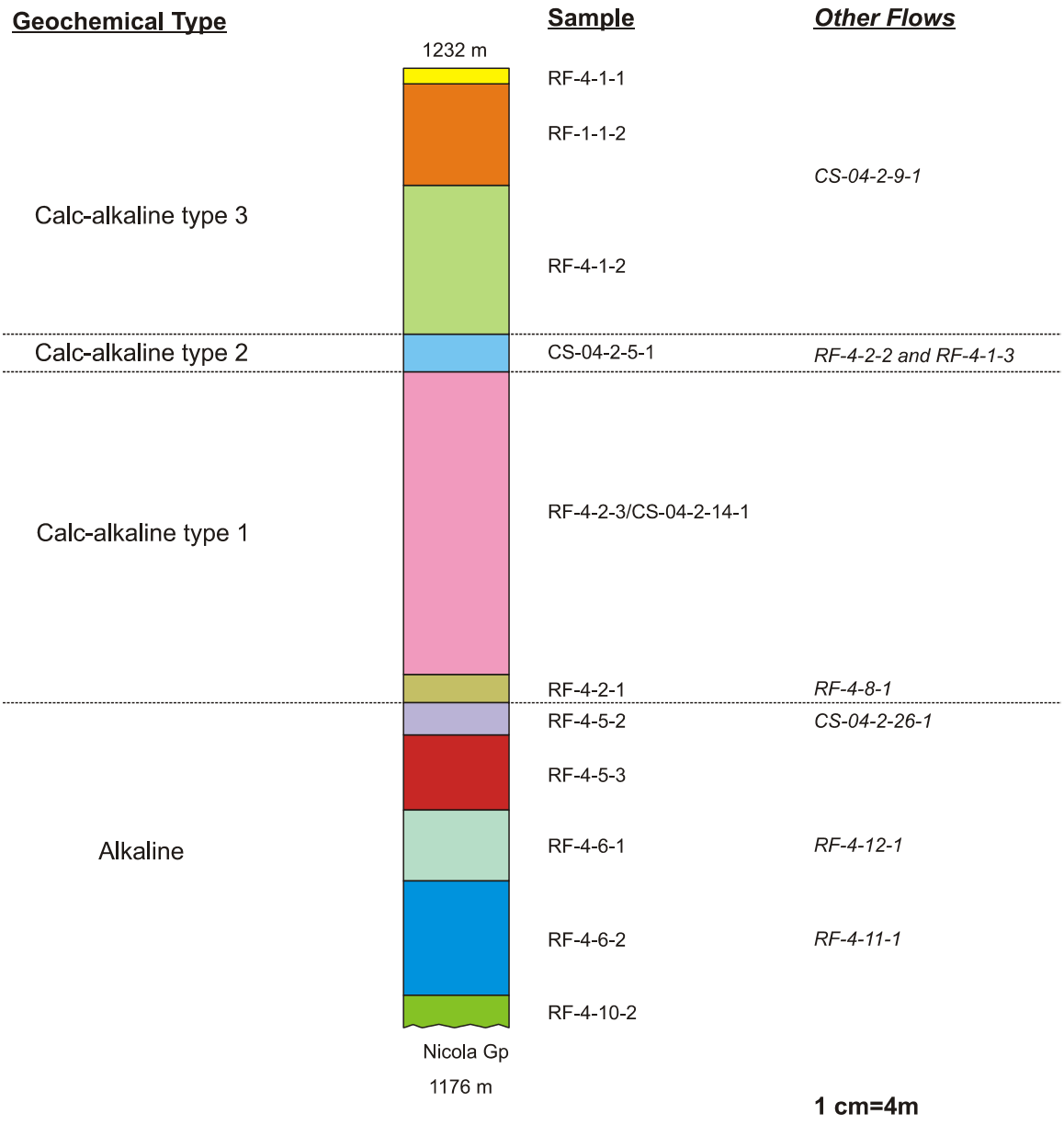

Figure 24. Idealized cross-section through the Missezula Lake East section
Sample numbers are shown next to the flow they were taken from, and samples that correspond to thin flows or flows of relatively short length are shown as "other flows", with the height of the sample number corresponding to their relative location in the section. Each flow is shown in a different colour. The base and top elevations of the cliff are shown (metres above sea level). Scale of 1 cm = 4 m for flow thickness**.**

transitions into a'a-like vesicular breccia clasts supported by silt across its full thickness, and then abruptly transitions back to a typical pahoehoe flow 15 m further along the section (Figure 10c–e). Below samples RF-4-6-1 and RF-4-6-2, the lava flows unconformably overlie the Triassic Nicola Group (Figure 12).

Samples for all but three of the lavas were analyzed for whole rock geochemical compositions and four samples were analyzed for Nd isotopic compositions. The lowermost eight lavas are alkaline, then the section transitions into the type 1, 2 and finally type 3 calc-alkaline Quilchena lavas at the top of the section. Three samples (from the base, middle and top) were dated using Ar–Ar methodology.

Missezula Lake West section (West side of lake)

The Missezula Lake West section, located at the northwest-end of Missezula Lake, can be accessed by a 500 m walk east of the Ketchan Lake Forest Service Road (which runs south off the Dillard Forest Service Road). A 140-m long cliff section was measured and sampled (although due to the high number of samples analyzed from the Missezula East section, only a single paleomagnetic sample was analyzed; see Table 5). The measured section is roughly 40 m high, and contains six lava flows, most between 4 and 10 m thick. Columnar jointing was noted in three of the flows, and all the flows had vesicular flow tops. Ropey texture was also observed on some flow tops. The contact between the lavas and older bedrock was not observed at this outcrop. The top of this section is at approximately the same elevation as the Missezula East section.

Loon Lake section

A 50 m-thick exposure of a likely intrusive equivalent of the Quilchena lavas, forms a hilltop northeast of Missezula Lake, just south of Loon Lake. The section is easily accessible from the Dillard Forest Service Road. Mapped by Preto (1979) as a medium-grained gabbro unit. The intrusive unit is characterized by phenocrysts of augite (1–5 mm across) surrounded smaller phenocrysts of olivine and plagioclase (Figure 25). This unit weathers into tabular blocks up to 5 cm by 15 cm in size. Epidote- and iron-staining is visible along fractures on the north and east faces of the outcrop, respectively. Small vesicles were observed near the top of the unit, suggesting that this is a high-level intrusive unit. No valley lava was observed on top of this unit (only boulders at the base of the hill), but geochemically it is very similar to the alkaline lava flows found at Missezula Lake. The Loon Lake section is higher in elevation than the valley lavas flows in the region.

As the Loon Lake exposure is unique in the valley lava sections mapped, samples from the section were included in all analytical studies completed as part of this project. Chemically, the Loon Lake section is very similar to the alkaline lava flows exposed at the base of the Missezula Lake east section.

Shrimpton Creek

Valley lava is exposed on both sides of the dry Shrimpton Creek valley for over 1.5 km southeast of the Loon Lake exposure. Further down the valley, the lavas are exposed along the west side of the valley until it terminates at Missezula Lake (where the lavas form a continuous section with the lavas exposed on the north-east side of Missezula Lake (Preto, 1979). Study of the Shrimpton Creek valley lavas was limited to

Figure 25. Photograph of Loon Lake possible intrusive equivalent of the Quilchena lavas
Sample shows small black augite phenocrysts (1–2 cm across), surrounded by plagioclase and olivine (olivine not visible in photograph).

the northern-most section of lavas on both sides of the dry creekbed (~400 m along each side), which are a short hike off the Dillard Forest Service Road, although active logging in the area over the last few years has re-opened up roads that come within 200 m of the northernmost lava cliffs. In this area, the lava outcrops are 20–30 m high, generally composed of between two and four flows (5–10 m thick), although the height of the cliffs increases heading south along the valley towards Missezula Lake (Figure 26). The lavas were coarsely mapped from the opposite cliff, with detailed examination of lowermost flows completed from the valley bottom. Some of the flows are roughly columnar jointed. Tilted pipe vesicles in some of the lavas indicate that the lavas flowed south towards Missezula Lake. The contact between the lava and basement rock is not exposed. One sample from the base of this section analyzed for its whole rock geochemical composition, which indicated it is part of the type 3 calc-alkaline suite of Quilchena lavas.

Bluey Lake

The Bluey Lake section is a 120 m-long section of valley lava on the east side of Bluey Lake. This valley runs from Missezula Lake north past Bluey, Kentucky and Alleyne Lakes (where only a 1–2 m-thick lava section is exposed), along Quilchena Creek to Nicola Lake, with valley lava outcropping sporadically along one side of the valley (east side in the south, west side in the north). At the Bluey Lake section, the valley lava flows are thin (mostly 1–3 m thick), and many are highly vesicular throughout. In at least one flow, vesicles form horizontal vesicle sheets, and pipe vesicles (up to 30 cm tall, 5 cm across) are common in two of the flows. One only flow (at the base of the section) is over 5 m thick and columnar-jointed. Between two flows, a

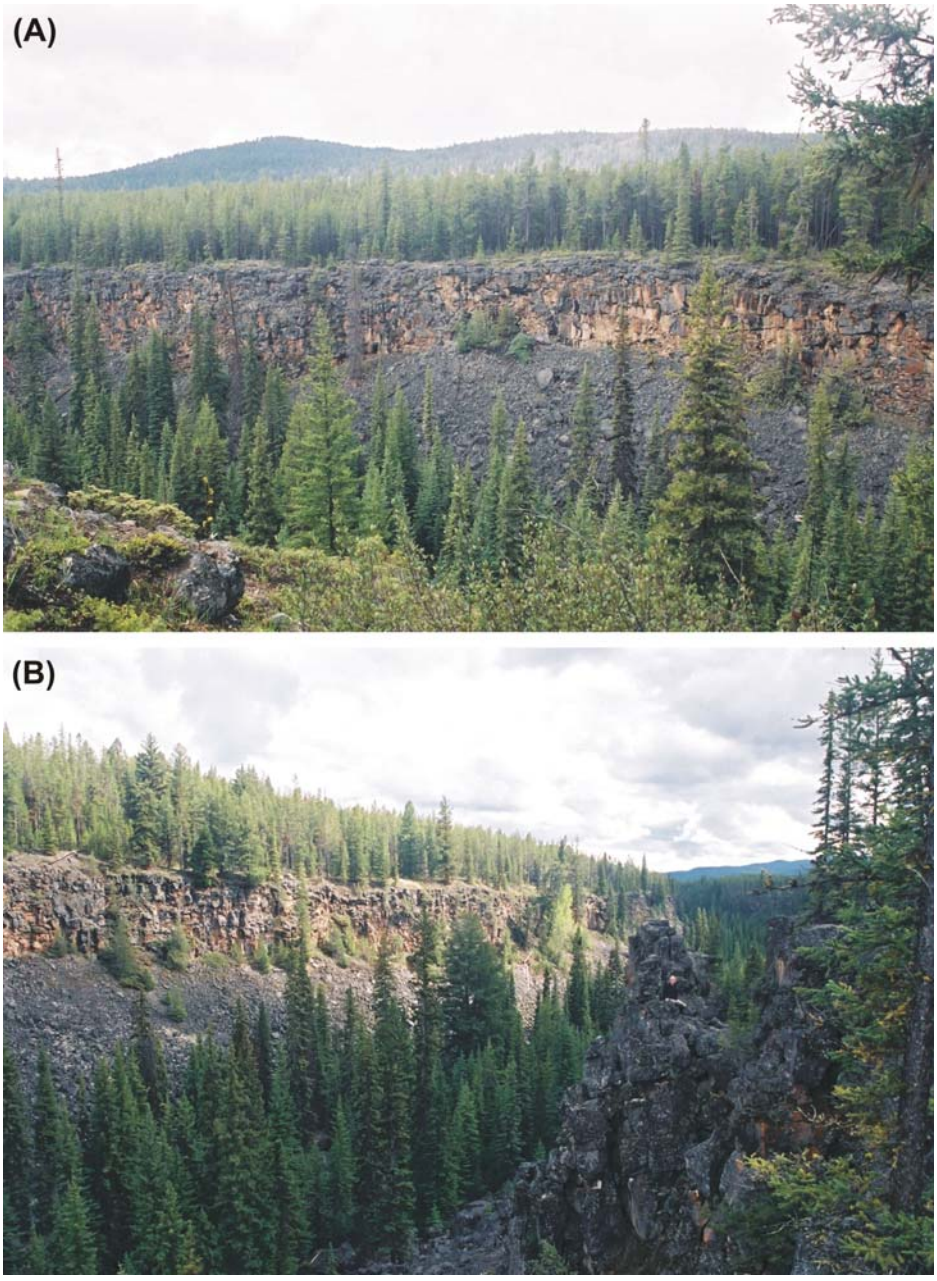

Figure 26. Photographs of Quilchena lavas in the Shrimpton Creek area

~3 cm-thick layer of silt has been thermally lithified into a grey-black siltstone (Figure 10a). In between other flows, the flow-top of the lower flow is broken into fist-sized vesicular clasts, whereas in other cases, the lower flow-top is quite ropey. Three samples from this section were geochemically analyzed, two (CS-05-2-1-2 and CS-05-2-2-1) from flows that had multiple pipe vesicles. The lowest sample from this section is part of the type 1 calc-alkaline suite, whereas the two other samples are part of the type 2 calc-alkaline suite of Quilchena lavas.

Quilchena Creek

The Quilchena Creek exposure is on the east side of the Quilchena Creek valley. The base of the cliffs can be accessed off the Quilchena Creek Road (south off Highway 5A at Quilchena). The exposure is over 3 km long, so fieldwork in this study focused on 150 m near the northern end of the exposure. In this area, the exposed lava cliffs are ~50 m high, with five to six flows of roughly equal thickness (6–10 m; Figure 6). Field observations suggest that the lavas may be up to ~130 m thick in the area studied. The contact between the lavas and underlying bedrock was not observed in this study, although was noted by Lambert (1963; location unknown) beneath cliffs ~50 m high, suggesting that the lavas at Quilchena in places are likely not much thicker than what is exposed. Many of the flows are roughly columnar-jointed, and one has possible entablature (Figure 8b). Pipe vesicles and vesicle sheets were also observed (Figure 9). Two geochemical samples were collected from lavas at this exposure, with the lowermost flow (CS-04-8-3-1) also included in the Nd isotope and ArAr geochronology studies. Both samples are chemically part of the type 1 calc-alkaline Quilchena lava suite.

Chutter Ranch

The Chutter Ranch exposure is located south of Highway 5A and the Nicola River, midway between Merritt and the community of Nicola. The north-east facing cliffs form the base of a flat-lying plateau visible from Highway 97C (Okanagan Connector and Highway 5 (Coquihalla) (Figure 23). Access to the cliffs, located on Chutter Ranch land, was provided by Dave Chutter.

A 1.5 km-long section of the cliffs was examined. The cliffs are generally 15 m high, typically one to two flows thick that are laterally continuous for much of the mapped section. The base of the lavas is exposed at the location of sample CS-10-2-2, where it overlies a Pleistocene channel deposit (Figure 12b). The upper flow is massive and columnar-jointed (6–8 m thick), whereas the lower flow is thinner and more vesicular (including pipe vesicles). Two geochemical samples were collected, with the lower sample (CS-04-10-2-2, from directly above the Pleistocene channel contact) also geochronologically and isotopically analyzed. Both samples are chemically part of the type 1 calc-alkaline Quilchena lava suite.

Lambly Creek Lavas

The Lambly Creek lavas were examined along Okanagan Lake, and in four different exposures along Lambly Creek (also known as Bear Creek). As the mapped exposures the furthest upstream from Okanagan Lake are poor (creek valley is only 4–6 m wide in places, with lava flows exposed right above the water), observations from along Lambly Creek are grouped together.

Lambly Creek

Lambly Creek is easily accessed from the Bear Creek Forest Service Road along the north side of the valley (turnoff just north of Bear Creek Provincial Park). The lava flows are all exposed along the valley floor, and numerous dirt-biking trails can be followed down to the top of the lava outcroppings. Upstream (where Bald Range Creek and Terrace Creek empty into Lambly Creek), the Lambly Creek valley is steep, narrow and moss-covered, and so the base of the lava flows is difficult to access (Figure 27). Here, generally two or three flows can be identified above the water, in exposures 5–15 m thick. Further downstream (see location of sample CS-04-13-4-1), five to seven flows are exposed in a 60 m-high cliff, with individual flows 4–12 m thick (Figure 28). The cliffs are all near-vertical, and in most places the highest flows cannot be examined or sampled. Generally, all the flows are flat-lying, some are columnar-jointed. Discrete pockets (6–8 m long, 2 m high) of scoriaceous rubble are locally found at the base of a flow. The lavas in Lambly Creek are slightly more weathered than the Quilchena lavas or those along Okanagan Lake. Two samples collected along Lambly Creek were included in the whole rock geochemical study.

Okanagan Lake

Lambly Creek lavas are also exposed along the west side of Okanagan Lake, just south of the W.R. Bennett Bridge, which connects Kelowna and Westbank. The lavas are on the land of the Westbank First Nation, who gave permission for the lavas to be studied. The lavas are easily accessed from below, along Cambell Road. The top of the lavas form a broad plateau, which is now a heavily developed residential neighbourhood (Figure 29). The lavas are fairly continuously exposed for over 1.5 km, forming outcrops 5–20 m

high, generally two to three flows thick. Flows are typically 6–8 m thick. Most of the flows show weak columnar jointing, and rough upper and lower colonnade is visible (with no entablature) in a couple areas (one just south of sample CS-04-15-8-1). Pipe vesicles are common, particularly in the lower flows, and may be tilted. Brown silt forms a 5 cm-thick horizontal layer at the base of one lava flow, and in one spot abruptly forms a vertical 3 m-high "chimney" into the overlying lava flow, before continuing of at the base of the same flow (Figure 30). The sediment appears to encase blocks of the lava (up to 20 cm in diameter); this feature is a possible spiracle (e.g. Schmincke, 1967).

One sample of the lavas at Okanagan Lake was collected and analyzed for its whole rock geochemical composition. Samples were also included in the Ar–Ar geochronology and Nd isotopic studies.

Figure 27. Photograph of Lambly Creek lava flows where Bald Range Creek intersects Lambly Creek

Figure 28. Photograph of Lambly Creek lava flows west of Blue Grouse Mountain (near sample CS-04-13-4-1)

Figure 29. Panoramic photograph of Lambly Creek lava flows above Okanagan Lake (Westbank, BC)

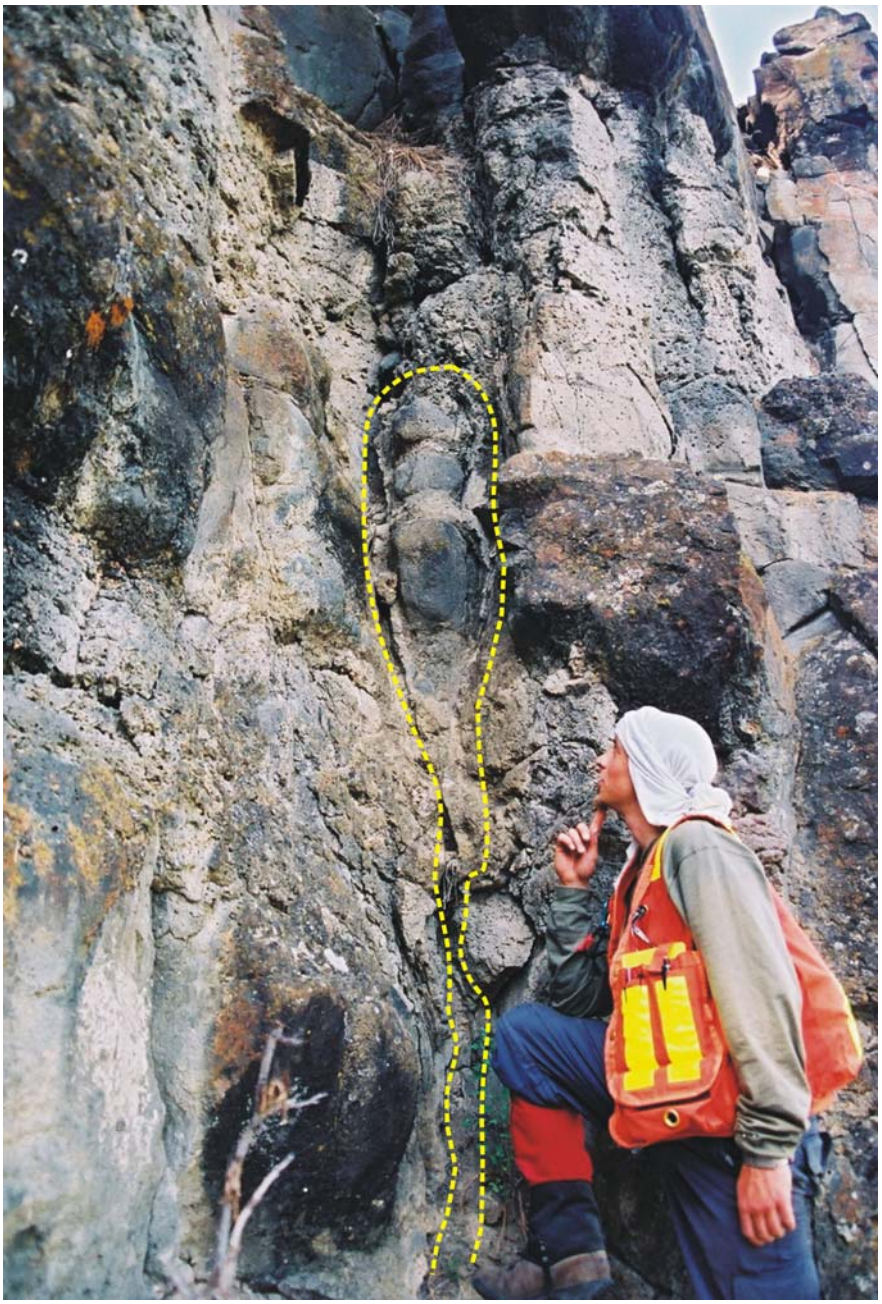

Figure 30. Photograph of possible spiracle in Lambly Creek lavas along Okanagan Lake

Appendix B: Volume Calculations

Minimum and maximum Quilchena and Lambly Creek lava volumes were determined using a combination of known outcrops and current valley extents. Results are reported in Table 6.

Calculation of Minimum Volume

To determine the minimum volume of each unit, the following procedure was used:

1. Known outcrops were drawn onto 1:50 000 maps. The exposed thickness of most outcrops was determined during fieldwork (where possible).
2. The lavas were then projected to extend to the opposite valley wall (i.e. using the current valley width as an approximation for original valley width). In areas such as Missezula Lake, Shrimpton Creek and Lambly Creek, this was not an assumption, as lavas crop out on both sides of the valley. Therefore, in areas such as Bluey Lake and Quilchena Creek, which lie further north along the same valley as Missezula Lake, the assumption that the original valley width is similar to the modern valley width appears valid. In all cases the 100 ft interval topographic contours on the 1:50 000 maps were used to project the lava outcrops across the valley. The one exception to this procedure involved the Lambly Creek basalt exposure along the west side of Okanagan Lake. In this case, the relationship between the flat-lying, subaerial lavas and the Okanagan Valley (which, at the time of eruption, was a major fluvial-lacustrine pathway) is unclear (Tribe, 2004).

Therefore, the width of the valley was assumed to be the width of the preserved lava field on the west bank of Okanagan Lake.

3. The topographic contours were followed to connect the various outcrops, using the modern valleys as a guide. Lava was assumed to have existed between outcrops, so that all the outcrops within either the Quilchena or Lambly Creek regions were connected to one another. For example, in the Nicola Valley the lavas were assumed not to have extended further west than the Chutter Ranch exposure, and not further east than where Quilchena Creek enters Nicola Lake. The lavas were also not projected into any valleys that currently intersect the main valleys where the basalts crop out.
4. To determine the area the lavas occupied, the valleys were then divided into sections based on the shape of the valleys and so that they included an outcrop of known thickness (see Figure 31). A grid was then drawn over each section, with each square have dimensions of 250 m by 250 m. The number of filled squares in each section (to the nearest ¼ square) were then added up and used to determine the aerial extent of the lavas.
5. To determine the minimum volume of the lavas, the known thickness of the lavas in a given outcrop was used as the thickness of the lavas, i.e. the valley was assumed to be rectangular in cross-section, and so the thickness of the lavas at the side of the valley is the same as the thickness of the lavas in the middle of the valley. The area of the lavas in a given section was then multiplied by the thickness of the lavas to give a volume for each section. The volumes of each

section were then added together to produce a minimum volume estimate for the Quilchena and Lambly Creek basalts.

Calculation of Maximum Volume

With the minimum aerial extent and volume of the lavas determined, the procedure was modified to determine the maximum volume.

Using the maps outlining the minimum aerial extent of the lavas, the lava field was then projected further along valleys in which lavas currently crop out (i.e. south of the Missezula Lake exposure) as well as into valleys that have no outcroppings of lava but, based on current valley morphology, may have been accessible to the lavas at the time of eruption.

1. As when determining the minimum volume, these new areas were covered in a 250 m by 250 m grid, and were included into the nearest sections used in the minimum volume calculation. The aerial extent of each section was then determined.
2. The maximum volume was calculated in two parts. First, a volume was calculated using the same method as in the minimum calculation, using the area and the known thickness of an outcrop contained within that section to give the volume of a rectangular prism. Then, the lavas were projected to occupy a V-shaped valley that extends down from the base of the known outcrops to the base of the modern valley, forming a triangular prism.
3. As the area of the base of the prism is known (the aerial extent of a given section) and the height of the triangle can be estimated from the map (using contours, the

elevation difference between the base of the modern valley/lake level and the base of the lava exposures), the volume of the prism can be determined (by multiplying the area by the height and dividing by 2). By adding the volume of the triangular prism to that of the rectangular prism, the maximum volume of a given section was calculated.

4. These volumes were then added together to determine the maximum volume of both the Quilchena and Lambly Creek basalts.

Neither the minimum or maximum calculation takes into consideration the possibility that significant erosion occured *between* eruptive events. Given that the valley lavas erupted over hundreds of thousands of years, this type of erosion is likely to have occured, but would be difficult to quantify beyond the volume calculations described above. However, it is likely that this erosion could have removed all traces of valley lava in some regions, indicating that the total volume of lava erupted might be under-estimated.

Table 6. Calculation of minimum and maximum valley lava volumes

Section	Section Thickness[1] (m)	Depth of Valley[2] (m)	Minimum		Maximum	
			Aerial Extent of Lavas (km^2)	Calculated Volume (km^3)	Aerial Extent of Lavas (km^2)	Calculated Volume (km^3)
Kentucky-Bluey	25	45	11.2	0.28	11.2	0.53
Swamps	1	30	17.9	0.02	30.1	0.48
Missezula Lake	55	110	9.6	0.53	12.5	1.38
Shrimpton Creek	40	2	9.6	0.38	9.6	0.39
Loon Lake	50	250	11.5	0.58	14.8	2.59
N. Kentucky	25	30	14.6	0.37	27.1	1.08
Courtney Lake	80	175	20.0	1.60	21.0	3.52
Quilchena	130	90	25.6	3.33	25.0	4.38
Chutter Ranch	15	150	31.0	0.47	31.0	2.79
Nicola Lake	25	90	25.6	0.64	38.0	2.66
Lambly Creek	60	1	6.5	0.39	10.0	0.61
Kelowna	20	80	12.0	0.24	12.0	0.72
TOTAL				**8.8**		**21.1**

[1] Measured thickness, with the exception of Courtney Lake, which is approximated from nearby sections

[2] Depth of present-day Valley (from 1:50,000 topographic map)

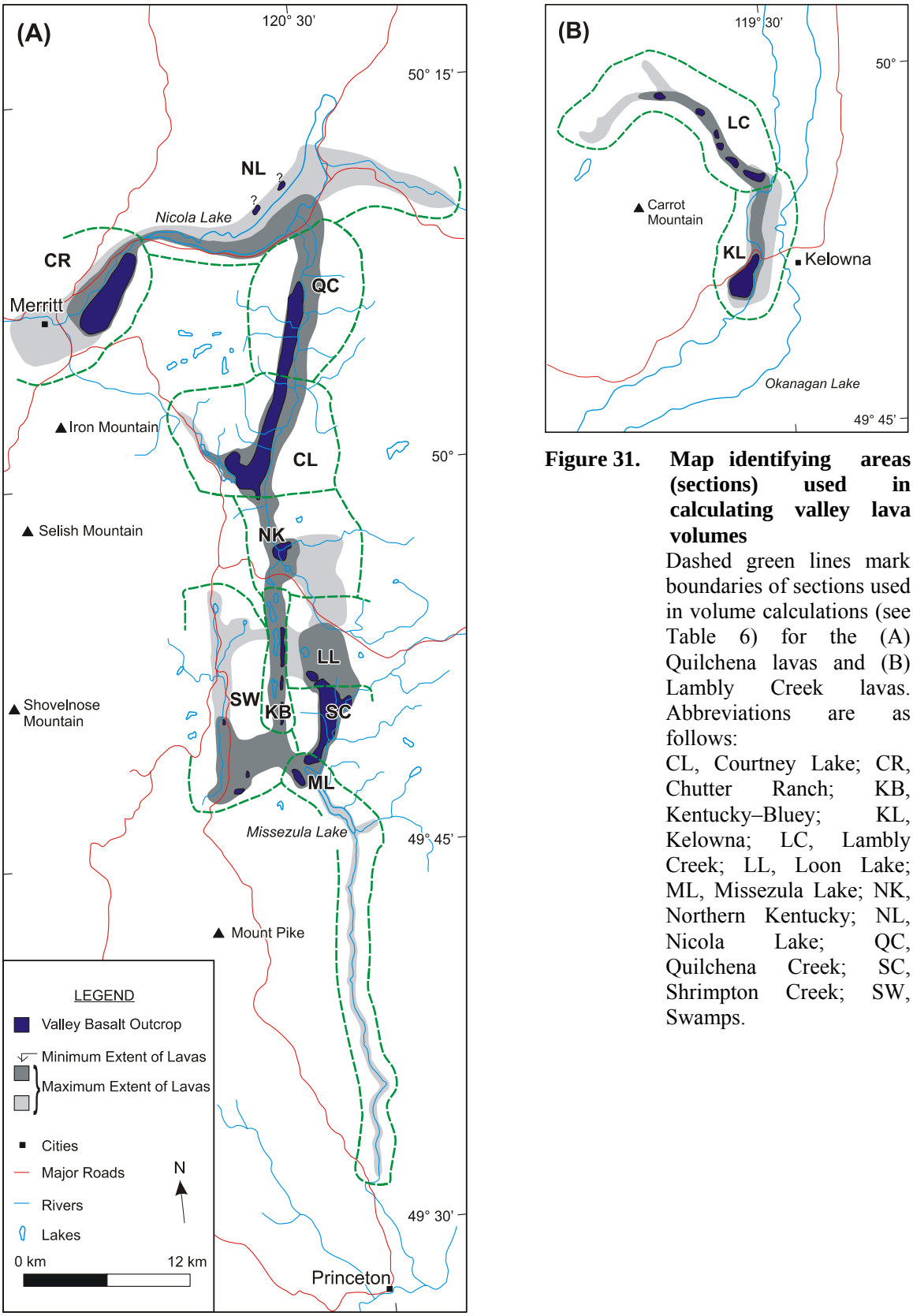

Figure 31. Map identifying areas (sections) used in calculating valley lava volumes

Dashed green lines mark boundaries of sections used in volume calculations (see Table 6) for the (A) Quilchena lavas and (B) Lambly Creek lavas. Abbreviations are as follows:

CL, Courtney Lake; CR, Chutter Ranch; KB, Kentucky–Bluey; KL, Kelowna; LC, Lambly Creek; LL, Loon Lake; ML, Missezula Lake; NK, Northern Kentucky; NL, Nicola Lake; QC, Quilchena Creek; SC, Shrimpton Creek; SW, Swamps.

Appendix C: Paleomagnetic Analysis

Samples for paleomagnetic analysis were collected from each lava flow that was sampled for Ar–Ar analysis (includes samples from flows from which ArAr samples were collected in the field, but ultimately not submitted for ArAr analysis). Paleomagnetic samples were collected as oriented hand samples (information included strike and dip measurements of one or more of the sample faces, as well as an indication of the "up" direction). All paleomagnetic samples were analyzed, although only seven of their accompanying Ar–Ar samples were analyzed.

Lab preparation and analysis of the samples took place May 4–6, 2005, at the Pacific Geoscience Centre in Sidney BC, under the supervision of Dr. Randy Enkin. All samples were oriented and then marked up all the way around the sample with a line perpendicular to the strike, and arrows indicating the dip direction. The sample was then drilled to produce a core one inch in diameter and at least two inches long. Once the cores were drilled for each sample, the core was marked up with the same line and arrows as the hand sample, so that the correct orientation of the core was maintained. Each core was then cut into one inch-high cylinders (with orientation markings maintained), and any rough breaks on the core edge smoothed down by a disc lathe.

The core down dip azimuths were then determined (generally 90° less than the strike value, with the exception of a few samples collected from overhanging ledges where 90° had to be added to the strike). The core dip angle is the same as the dip angle. Each individual cylinder was then relabelled with the sample number and an individual specimen label (e.g. A, B, C etc.), and then was analyzed using an Agico JR5-A spinning

magnetometer. All samples were analysed for paleomagnetic information and magnetic susceptibility.

All of the samples had inclinations consistent with both previously analysed valley lava samples in the Merritt area (Fulton et al., 1992) and the expected geocentric axial dipole field of 67.2° (R. Enkin, pers. comm. 2005), but had declinations that were inconsistent with the region and time frame. Therefore, one cylinder from each sample was then demagnetized using an alternation current of five milliteslas (mT) using a Schonstedt GSD-5 demagnetizer, and then renanalyzed. Some of the samples appeared to at first be displaying a possible magnetic overprint, and so subjecting the samples to demagnetization allowed the smallest and largest magnetite grains to become equally magnetized. This subset of samples were demagnetized using increasing currents of 10, 20, 40, 60 and 80 mT, with each sample reanalyzed between subsequent demagnetizations. All remaining samples were then demagnetized at 10 and 20 mT, again being reanalyzed after each demagnetization. However, the declination results for most of the samples remained poor.

After some deliberation regarding what could have caused the declination results to be inconsistent for the Merritt–Kelowna region, the following conclusions were reached:

1. The Quilchena and Lambly Creek lavas contain high fidelity single dipole carriers (magnetite), in unaltered, untilted to only minor tilted basaltic lava flows.
2. The inclination-only analysis of all the samples produced results consistent with normally magnetized rocks, therefore we can safely interpret that all the samples analyzed come from rocks that erupted in a normal-polarity cycle. For most of

the samples this most likely corresponds to the Brunhes normal polarity chron (0 to 780 ka), although the Jamarillo (0.99 to 1.07 Ma), Cobb Mountain (1.21 to 1.24 Ma), Gilså (1.68 Ma) and Olduvai (1.77 to 1.95 Ma) chrons may be possibilities for the older Lambly Creek lava sample(s) (refer to Appendix E for further age analysis; polarity chrons from Cande and Kent, 1995). The dispersion of inclination values is consistent with secular variation, indicating the lavas did not erupt all at once, but likely over 1000's of years.

3. The declination of the lavas is very inconsistent, and so should not be interpreted as accurate magnetic declination data for the valley lavas.

Possible explanations for the problematic declination data, and an evaluation of the each explanation are as follows:

1. **The rocks have been hit by lightening or are poor magnetic recorders**. This seems unlikely as all the rocks contain magnetite, and it is unlikely that all the samples (from eight different sample localities) were hit by lightning. In addition, the inclination distribution is tightly concentrated around the expected value for the region.
2. **The rocks produce a local magnetic anomaly, leading to incorrect azimuth orientations**. Although it would have been preferable to use a sun compass (or to sight the orientation from a short distance), it is unlikely that the measured magnetic remanences are high enough to deflect the compass. A deflection would also have most likely been noticed by the samplers at some point in the field season. However, this may be a possibility for some of the samples.

3. **The rocks have undergone large and very variable vertical axis-rotations.** There is no field evidence to support this.
4. **The compass was misread or the orientation lines (drawn in the lab) were confused**. The orientation lines were repeatedly reviewed by both the author and Dr. Enkin both before the samples were analyzed and afterwards, and both are confident that the error was not made then. Possible errors during sampling (the collection, orientation and marking-up of the samples in the field) cannot be refuted.

Therefore, at this time it must be assumed that problematic declination readings are the result of poor sampling procedures (collecting and labelling the samples), with possible local magnetic anomalies in some or all of the lavas contributing to the problem. Fortunately, as the main purpose behind the paleomagnetic study was to help constrain the Ar–Ar ages, the study is still useful as it constraints all seven Ar–Ar dates to periods of normal magnetic polarity. Based on this study, it is recommended that paleomagnetic analytical procedures (e.g. drilling and orienting cores from hand sample) be reviewed prior to sampling, as this may help clarify the field sampling procedure and reduce sampling error. Table 7 presents the paleomagnetic data collected in this study.

Table 7. Paleomagnetic data for nine Quilchena lava samples and two Lambly Creek lava samples

Sample Number	Sample Locality	s	N	NRM (A/m)	X_0 (SI/vol)	D (°)	I (°)	k	α95 (°)
[1]CS-04-2-28-1	Missezula Lk (E)	3	6	4.10	7.35E-04	198	64.9	0	1.4
[1]CS-04-2-14-1	Missezula Lk (E)	3	6	1.86	2.39E-03	346	63.1	0	0.8
[1]CS-04-2-29-1	Missezula Lk (E)	2	6	1.13	2.43E-03	303	72	0	2.3
[1]CS-04-3-1-1	Loon Lk	2	4	2.59	9.29E-03	284	71.6	0	2.7
CS-04-4-7-1	Missezula Lk (W)	2	4	13.2	6.62E-03	190	56.9	0	2.5
CS-04-7-1-1	Bluey Lk (E)	3	6	2.10	1.86E-03	235	73.9	0	1.6
[1]CS-04-8-3-1	Quilchena Cr	3	4	2.48	1.71E-03	234	63.2	0	1.9
CS-04-8-4-1	Quilchena Cr	2	6	1.43	1.66E-03	20.4	65	0	1.2
[1]CS-04-10-2-2	Chutter Ranch	3	6	3.53	3.95E-03	205	55.9	0	1.2
CS-04-12-1-1	Lambly Cr	2	6	2.21	9.90E-03	117	64.2	0	1.6
[1]CS-04-15-8-1	Westbank	1	6	2.11	3.78E-03	132	71.5	0	1.6

***(W)**, west side of lake; **(E)**, east side of lakes; **s**, number of oriented cylinders analyzed; **N**, number of demagnitization steps; **NRM**, mean intensity of the natural remnant magnitizations; **X_0**, mean magnetic susceptibility (SI/vol); **D**, mean site declination; **I**, mean site inclination; **k**, Fisher's estimate of precision (Fisher, 1953); **α95**, the radius of the circle of confidence*

[1]corresponding Ar-Ar sample analyzed as part of this study

Appendix D: Petrography

Table 8. Modal abundances of common minerals in the phenocryst and groundmass assemblages of lavas sampled in this study, based on petrographic analysis

Sample	Locality	Phenocrysts[1]				Groundmass[2]					
		(%)[3]	Ol	Plag	Cpx	Ol	Plag	Cpx	Mag	Gl	Ap
Quilchena lavas											
CS-04-2-26-1	Missezula Lk	14	36	64	-	9	41	35	6	7	2
RF-4-6-2	Missezula Lk	20	35	50	15	3	47	32	10	5	2
RF-4-5-2	Missezula Lk	30	30	50	20	8	44	23	15	7	3
RF-4-5-3	Missezula Lk	35	37	49	14	6	46	32	8	5	3
RF-4-6-1	Missezula Lk	21	24	62	14	1	47	39	4	6	3
RF-4-10-2	Missezula Lk	20	25	60	15	3	32	26	5	30	4
RF-4-11-1	Missezula Lk	16	13	75	13	5	26	33	5	27	4
RF-4-12-1	Missezula Lk	40	13	83	5	0	8	25	13	50	3
CS-04-2-9-1	Missezula Lk	6	100	-	-	16	51	29	3	1	tr
RF-1-1-2	Missezula Lk	22	27	55	18	10	58	26	6	-	tr
RF-4-1-2	Missezula Lk	5	100	-	-	21	63	11	5	-	-
RF-4-1-1	Missezula Lk	20	30	60	10	6	56	25	13	-	-
RF-4-1-3	Missezula Lk	5	100	-	-	19	42	19	5	15	tr
CS-04-2-5-1	Missezula Lk	2	100	-	-	4	55	26	3	12	tr
RF-4-2-2	Missezula Lk	5	100	-	-	11	42	26	3	18	tr
RF-4-8-1	Missezula Lk	0	-	-	-	4	55	36	3	2	-
CS-04-2-14-1	Missezula Lk	0	-	-	-	1	40	45	9	5	-
RF-4-2-1	Missezula Lk	1	100	-	-	10	47	22	4	16	tr
CS-04-3-1-1	Loon Lk	94	11	68	21	-	-	-	83	-	17
CS-04-6-2-1	Shrimpton Ck	38	53	39	8	-	56	32	5	5	2
CS-04-7-1-1	Bluey Lk	1	100	-	-	9	54	29	6	2	tr
CS-04-8-3-1	Quilchena Ck	5	100	-	-	11	42	11	21	16	0
CS-04-8-4-1	Quilchena Ck	5	100	-	-	23	53	16	3	5	tr
CS-04-10-1-1	Chutter Ra.	6	100	-	-	2	56	32	4	5	tr
CS-04-10-2-2	Chutter Ra.	2	100	-	-	14	52	3	7	23	tr
Lambly Creek lavas											
CS-04-12-1-1	Lambly Creek	5	100	-	-	6	48	34	9	2	tr
CS-04-13-4-1	Lambly Creek	7	100	-	-	3	47	42	5	2	tr
CS-04-15-8-1	Okanagan Lk	10	100	-	-	6	63	26	4	1	tr
Plateau lavas											
CS-04-24-1-1	Asp Creek	0	-	-	-	3	80	6	11	-	-
CS-04-27-2-1	Lillooet	10	100	-	-	11	73	13	2	-	tr
CS-04-28-1-1	Kamloops	4	-	100	-	4	72	7	16	-	1
CS-04-30-1-1	Kelowna	3	67	33	-	10	68	5	14	1	1
CS-04-31-1-1	Christian Va.	0	-	-	-	7	65	25	3	-	-

Abbreviations: Ol=Olivine; Plag=Plagioclase; Cpx=Clinopyroxene (generally Augite); Mag=Magnetite; Gl=Glass; Ap=Apatite; tr=trace; "-"=not noted

[1]Proportion of mineral in phenocryst assemblage

[2]Proportion of mineral in groundmass

[3]Volume modal abundance of phenocrysts in rock

Appendix E: Geochemical Analysis and Analytical Uncertainty Calculations

Geochemical Analysis Methodology

All samples were collected from massive (vesicle-poor) regions within a given flow, contained no amygdules and few fractures, and were not visibly altered (besides minor iddingsite on olivine). All weathered surfaces were chipped off in the field. Of the 36 samples, 34 were submitted in 2004 to ACTLABS (Ontario, Canada) for both major and trace element analysis, via package 4E-Research. For major element oxide and select trace element concentrations, 0.2 g of the sample was mixed with lithium metaborate/lithium tetraborate, fused in a graphite crucible until molten, and then dissolved in a 5% nitric acid solution. This sample was then analyzed on a Thermo Jarrell-Ash Enviro II ICP-OES (Inductively Coupled Plasma Optical Emission Spectrometer). Another 0.25 g of sample was digested by four acids and then analyzed by a Perkin Elmer Optima 3000 ICP-MS (Inductively Coupled Plasma Mass Spectrometer) to provide most of the trace element data. Select trace elements (Cu, Ni, Pb, Zn) were analyzed using INAA methods (Instrumental Neutron Activation Analysis), in which the sample was irradiated for 7 days in the McMaster Nuclear Reactor, and then analyzed on a Canberra Series 95 multichannel. A more detailed summary of the techniques, including their detection limits, can be found at www.actlabs.com.

Two samples were analyzed by ALS Chemex (Vancouver) in 2005 for both major element oxide and trace element concentrations. Samples underwent Lithium Metaborate fusion, and were analyzed by XRF (X-ray fluorescence) and ICP-MS to determine major

element oxide and trace elements respectively. A more detailed summary of the techniques used can be found at www.alschemex.com.

Geochemical Analytical Uncertainty

Geochemical error analysis was performed using a spreadsheet program provided and developed/modified by Dr. Thorkelson. The spreadsheet utilizes two types of data: duplicate analyses of samples, and analyses of reference standards and their published values. The duplicate data set is used to estimate the precision of the analyses, and the reference standards and their published values are used to estimate accuracy. Input into the spreadsheet is done on an element-by-element basis, with data in either wt.% or ppm. The spreadsheet displays results on a bivariate plot, in which each set of duplicate analyses form the X and Y co-ordinate for a particular sample, and measured reference standards and their corresponding certified value form the X and Y co-ordinate for a particular standard (Figure 32). Plotted with the data is a line of unity and an error envelope. If the analysis are both precise and accurate (i.e. the duplicate analyses have the same concentration value, as do the measured and accepted values of the reference standards), then the duplicates and standards will plot along the line of unity. However, this is generally not the case, and so the error envelope is used to estimate the analytical error at the 95% confidence interval.

The size and shape of the error envelope is controlled by a numerical estimate of the absolute and relative uncertainty. The absolute uncertainty (in wt.% or ppm) may be as small as the detection limit for a particular element, but is commonly somewhat larger. By increasing or decreasing the absolute uncertainty, the error envelope expands or

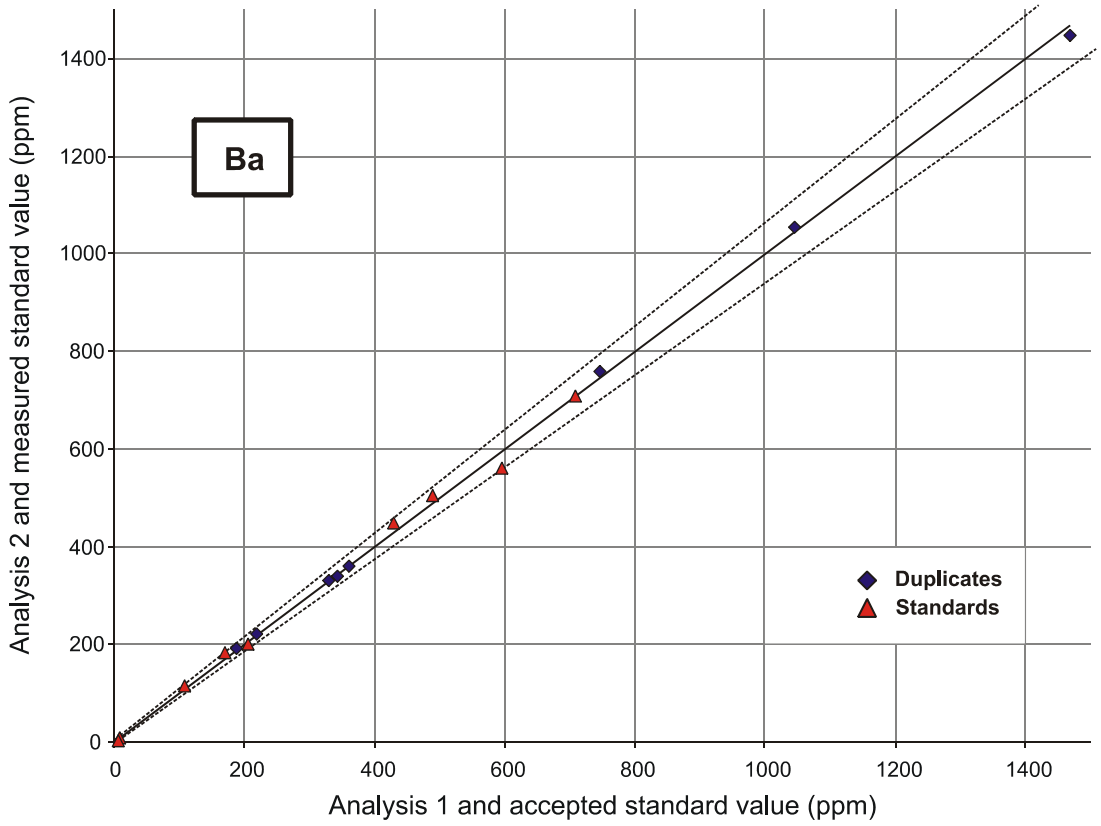

Figure 32. Example of graph used in determining the total analytical uncertainty for a given element

This plot examines the quality of Ba concentrations collected in this study by using eight duplicate analyses and nine standards. Duplicate analyses are shown by the blue diamonds (the X and Y co-ordinates correspond to the values of the two analyses) and the standards are represented by the red triangles (x-axis is the accepted standard value, y-axis is the measured value). The line of unity is flanked on either side by dashed lines representing the error envelope. The error envelope can be adjusted by changing the value of the absolute and relative errors until it includes 90% of the standards and duplicates, and thereby allows the user to visually estimate the error in their geochemical analyses. In this case, the absolute error is 3% and the relative error is 4%.

contracts, but stays parallel to the line of unity. This allows the envelope to account for imprecise data points sometimes observed in measurements near the detection limit of the analytical technique. By increasing or decreasing the relative error (%), the error envelope widens or narrows at its maximum, to account for the increase in scatter of data points at higher concentrations. By adjusting absolute and relative uncertainties (and therefore the error envelope) to contain 90% of the duplicate data analyses, an estimate of 2σ precision for the dataset can be reached. If the envelope is adjusted to also include 90% of the standards, an estimate of the combined precision and accuracy can be obtained. To obtain the numerical value of the uncertainty for a particular measurement, the measurement is multiplied by the relative error for that element, and then added to the absolute error for that element. Therefore, if an element has an absolute error of 1 ppm and a relative error of 5%, then a measurement of 100 ppm would have an error of 1 ppm +(100 ppm * 5%), or 6 ppm.

With the dataset presented in this thesis, error analysis was only performed on the results from ACTLABS, as no duplicate analyses were performed on the ALS Chemex samples. In general, most duplicate analyses plotted on or very close to the line of unity, indicating the precision of the analyses was good. However, for some elements (e.g. Ce, Dy, Ho) the standards plotted away from the line of unity, particularly at very low or very high concentrations (i.e. not in the range of the dataset). Depending on the number of standards analyzed for a given element (varied by analytical technique), a standard could be left out of the error envelope with the 95% confidence interval still maintained. In addition, in rare cases where a standard with an extremely high concentration fell off the line of unity (i.e. Ce, where the maximum value of a duplicate measurement was 40.0

ppm and the published standard value was 2200 ppm), that particular standard was ignored altogether. However, the majority of standards analyzed had concentrations similar to those of the duplicate measurements. Table 9 displays the absolute and relative errors for each element reported, the analytical uncertainty (combined absolute and relative errors), and the calculated net error at the mean of the data range for each element. As the reported error combines both absolute and relative errors, it is an overestimate of the precision of the analyses.

Table 9. Absolute and relative analytical uncertainty for each element analysed in this study
The mean concentration of each element is also given (average value of each element determined in the geochemical analyses used in this study), and the total error for that mean concentration has been calculated as an example.

Total error = absolute error + relative error*analyzed value,

so, using Ba again as an example with an absolute error of 3% and a relative error of 4%, the total error for a Ba value of 249 ppm would be:

Total error = 3 + 0.04*249 = ±13 ppm

	Absolute Error[1]	Relative % Error[2]	Mean data value (wt% or ppm)	Net error at mean (wt% or ppm)
SiO_2	0.03	1	50.7	0.5
TiO_2	0.01	0.5	8.12	0.05
Al_2O_3	0.03	1.2	15.26	0.2
Fe_2O_3	0.04	0.2	9.48	0.06
MnO	0.002	1	0.13	0.003
MgO	0.02	0.3	7.19	0.04
CaO	0.02	0.6	8.76	0.07
Na_2O	0.03	1.6	3.55	0.09
K_2O	0.01	0.8	1.09	0.02
P_2O_5	0.02	21	0.4	0.1
Cs	0.1	5	0.2	0.1
Rb	1	7	12	2
Ba	3	4	249	13
Th	0.05	3	1.9	0.1
U	0.03	4	0.71	0.06
Nb	0.7	5	28	2

[1]Detection Limit
[2]From Envelope

Table 9. Absolute and relative analytical uncertainty for each element analysed in this study (continued)

	Absolute Error[1]	Relative % Error[2]	Mean data value (wt% or ppm)	Net error at mean (wt% or ppm)
Ta	0.05	3	1.7	0.1
La	0.5	3	18	1
Ce	0.05	5	38	2
Pb	5	2	3	5
Pr	0.03	7	4.7	0.4
Sr	3	0.9	672	9
Nd	0.1	3	19.8	0.7
Zr	3	5.5	134	10
Hf	0.1	7	3.3	0.3
Sm	0.03	7	4.9	0.4
Eu	0.02	4	1.7	0.1
Gd	0.03	6	4.3	0.3
Tb	0.02	6	0.69	0.06
Dy	0.1	10	3.3	0.4
Y	1.5	5	15	2
Ho	0.02	6	0.56	0.05
Er	0.02	8	1.5	0.1
Tm	0.005	9	0.20	0.02
Yb	0.04	15	1.2	0.2
Lu	0.003	12	0.16	0.02
Zn	2	7	81	8
V	5	1	153	7
Sc	0.3	3.5	19	1
Co	1.3	7	43	4
Cu	1	5	46	3
Cr	0.7	10	244	25
Ni	2	2	133	5

[1]Detection Limit

[2]From Envelope

Appendix F: ^{40}Ar–^{39}Ar Geochronology

Methodology

The samples for ^{40}Ar–^{39}Ar analysis were crushed by hand into pieces between 0.45 and 1 mm in diameter. Microphenocrysts visible under low magnification were then hand-picked out of the samples, including the large augite phenocrysts from the Loon Lake sample, and any highly magnetic material was removed with a hand magnet (some samples were much more magnetic than others). All the samples were then washed in deionized water and then air-dried at room temperature.

The samples were then submitted to the Pacific Centre for Isotopic and Geochemical Research, where they were wrapped in aluminum foil and stacked in an irradiation capsule with similar-aged samples and neutron flux monitors (Fish Canyon Tuff sanidine, 28.02 Ma (Renne et al., 1998) and Alder Creek sanidine, 1.193 Ma (Nomade et al., 2005)). The samples were irradiated on September 8, 2005 at the McMaster Nuclear Reactor in Hamilton, Ontario, for 90 MWH, with a neutron flux of approximately $3x10^{16}$ neutrons/cm^2. Analyses (n=57) of 19 neutron flux monitor positions produced errors of <0.5% in the J value.

The samples were analyzed on December 14–15, 2005 and January 6–9, 2006, at the Pacific Centre for Isotopic and Geochemical Research, University of British Columbia, Vancouver, BC, Canada. The mineral separates were step-heated at incrementally higher powers in the defocused beam of a 10W CO_2 laser (New Wave Research MIR10) until fused. The gas evolved from each step was analyzed by a VG5400 mass spectrometer equipped with an ion-counting electron multiplier. All

measurements were corrected for total system blank, mass spectrometer sensitivity, mass discrimination, radioactive decay during and subsequent to irradiation, as well as interfering Ar from atmospheric contamination and the irradiation of Ca, Cl and K (Isotope production ratios: $(^{40}Ar/^{39}Ar)_K$=0.0302±0.00006, $(^{37}Ar/^{39}Ar)_{Ca}$=1416.4±0.5, $(^{36}Ar/^{39}Ar)_{Ca}$=0.3952±0.0004, Ca/K=1.83±0.01($^{37}Ar_{Ca}/^{39}Ar_K$)).

The analytical results are presented in Table 10, and plateau and inverse isochron plots for each sample are presented in Figure 33. The plateau and inverse isochron ages are discussed for each sample in the next section. The plateau and correlation ages were calculated using Isoplot version 3.09 (Ludwig, 2003). Errors are quoted at the 2-sigma (95% confidence) level and are propagated from all sources except mass spectrometer sensitivity and age of the flux monitor. The best statistically-justified plateau and plateau age were picked based on the following criteria:

1. Three or more contiguous steps comprising more than 50% of the ^{39}Ar;
2. Probability of fit of the weighted mean age greater than 5%;
3. Slope of the error-weighted line through the plateau ages equals zero at 5% confidence;
4. Ages of the two outermost steps on a plateau are not significantly different from the weighted-mean plateau age (at 1.8σ six or more steps only);
5. Outermost two steps on either side of a plateau must not have nonzero slopes with the same sign (at 1.8σ nine or more steps only).

Table 10. ^{40}Ar–^{39}Ar results for whole rock samples from six Quilchena lava samples and one Lambly Creek lava sample

CS-04-2-28-1

J = 0.000540±0.000006

Laser Power %	$\frac{^{40}Ar}{^{39}Ar}$	$\frac{^{38}Ar}{^{39}Ar}$	$\frac{^{37}Ar}{^{39}Ar}$	$\frac{^{36}Ar}{^{39}Ar}$	Ca/K	Cl/K	$\%^{40}Ar$ atm	$f\ ^{39}Ar$	$\frac{^{40}Ar^*}{^{39}Ar_K}$	Age (Ma)
2	20.611 ± 0.026	0.417 ± 0.067	0.373 ± 0.047	0.081 ± 0.068	2.265	0.087	92.88	0.32	1.201 ± 1.630	1.17 ± 1.59
2.4	7.325 ± 0.017	0.361 ± 0.018	0.075 ± 0.041	0.022 ± 0.027	1.152	0.079	83.13	4.55	1.165 ± 0.198	1.13 ± 0.19
2.8	2.454 ± 0.017	0.319 ± 0.020	0.062 ± 0.036	0.006 ± 0.065	1.112	0.070	67.64	11.47	0.732 ± 0.127	0.71 ± 0.12
3.2	1.597 ± 0.018	0.285 ± 0.020	0.076 ± 0.020	0.003 ± 0.083	1.447	0.062	51.52	16.78	0.711 ± 0.090	0.69 ± 0.09
3.6	1.023 ± 0.025	0.262 ± 0.022	0.094 ± 0.026	0.002 ± 0.111	1.824	0.057	27.08	16.72	0.666 ± 0.062	0.65 ± 0.06
4	1.567 ± 0.020	0.258 ± 0.020	0.099 ± 0.030	0.004 ± 0.065	1.909	0.056	53.46	14.74	0.663 ± 0.074	0.65 ± 0.07
4.4	1.055 ± 0.014	0.259 ± 0.018	0.096 ± 0.033	0.002 ± 0.164	1.798	0.056	32.88	10.06	0.601 ± 0.110	0.59 ± 0.11
5	1.333 ± 0.008	0.262 ± 0.016	0.109 ± 0.021	0.003 ± 0.125	2.072	0.057	45.82	11.46	0.638 ± 0.114	0.62 ± 0.11
5.5	1.441 ± 0.009	0.264 ± 0.022	0.145 ± 0.020	0.003 ± 0.136	2.742	0.057	38.40	7.96	0.768 ± 0.132	0.75 ± 0.13
6	1.388 ± 0.006	0.273 ± 0.016	0.201 ± 0.018	0.004 ± 0.143	3.828	0.059	37.00	5.94	0.722 ± 0.154	0.70 ± 0.15

CS-04-2-14-1

J = 0.000538±0.000006

Laser Power %	$\frac{^{40}Ar}{^{39}Ar}$	$\frac{^{38}Ar}{^{39}Ar}$	$\frac{^{37}Ar}{^{39}Ar}$	$\frac{^{36}Ar}{^{39}Ar}$	Ca/K	Cl/K	$\%^{40}Ar$ atm	$f\ ^{39}Ar$	$\frac{^{40}Ar^*}{^{39}Ar_K}$	Age (Ma)
2	66.016 ± 0.024	0.592 ± 0.087	0.285 ± 0.069	0.215 ± 0.057	1.937	0.122	92.00	0.92	4.827 ± 3.350	4.68 ± 3.24
2.4	22.906 ± 0.012	0.389 ± 0.023	0.101 ± 0.053	0.076 ± 0.027	1.584	0.083	95.31	7.71	1.014 ± 0.597	0.98 ± 0.58
2.85	12.514 ± 0.013	0.366 ± 0.030	0.163 ± 0.028	0.043 ± 0.035	2.947	0.079	97.68	10.52	0.250 ± 0.442	0.24 ± 0.43
3.2	8.900 ± 0.012	0.309 ± 0.017	0.230 ± 0.030	0.029 ± 0.022	4.510	0.067	92.84	29.28	0.597 ± 0.192	0.58 ± 0.19
3.6	6.236 ± 0.010	0.255 ± 0.023	0.359 ± 0.024	0.021 ± 0.035	7.059	0.054	93.55	22.03	0.358 ± 0.219	0.35 ± 0.21
4	5.268 ± 0.005	0.234 ± 0.019	0.468 ± 0.016	0.019 ± 0.044	9.221	0.05	94.22	17.83	0.259 ± 0.242	0.25 ± 0.23
4.5	5.609 ± 0.007	0.258 ± 0.024	0.540 ± 0.026	0.019 ± 0.048	10.589	0.055	86.11	11.72	0.692 ± 0.270	0.67 ± 0.26

Table 10. ^{40}Ar–^{39}Ar results for whole rock samples from six Quilchena lava samples and one Lambly Creek lava sample (continued)

CS-04-2-29-1

J = 0.000543±0.000006

Laser Power %	$\frac{^{40}Ar}{^{39}Ar}$	$\frac{^{38}Ar}{^{39}Ar}$	$\frac{^{37}Ar}{^{39}Ar}$	$\frac{^{36}Ar}{^{39}Ar}$	$\frac{Ca}{K}$	$\frac{Cl}{K}$	$\%^{40}Ar$ atm	$f\ ^{39}Ar$	$\frac{^{40}Ar^*}{^{39}Ar_K}$	Age (Ma)
2	50.787 ± 0.025	0.251 ± 0.204	0.156 ± 0.204	0.190 ± 0.096	2.978	0.047	118.22	0.27	-7.536 ± 5.161	-7.40 ± 5.08
2.4	24.051 ± 0.009	0.073 ± 0.071	0.153 ± 0.102	0.084 ± 0.070	3.164	0.010	103.43	1.88	-0.811 ± 1.727	-0.79 ± 1.69
3	4.042 ± 0.018	0.037 ± 0.064	0.194 ± 0.052	0.013 ± 0.056	4.044	0.005	90.37	8.08	0.331 ± 0.217	0.32 ± 0.21
3.5	4.069 ± 0.012	0.033 ± 0.043	0.173 ± 0.033	0.013 ± 0.052	3.618	0.004	92.75	13.89	0.253 ± 0.203	0.25 ± 0.20
4	2.836 ± 0.011	0.039 ± 0.061	0.145 ± 0.030	0.009 ± 0.049	3.032	0.005	83.72	21.57	0.415 ± 0.123	0.41 ± 0.12
4.5	1.608 ± 0.005	0.052 ± 0.036	0.137 ± 0.027	0.005 ± 0.054	2.862	0.009	86.63	16.14	0.165 ± 0.081	0.16 ± 0.08
5	2.351 ± 0.007	0.066 ± 0.029	0.157 ± 0.025	0.007 ± 0.061	3.272	0.012	86.20	12.71	0.269 ± 0.133	0.26 ± 0.13
5.5	2.528 ± 0.006	0.075 ± 0.042	0.188 ± 0.022	0.008 ± 0.086	3.930	0.014	89.25	9.98	0.216 ± 0.207	0.21 ± 0.20
6	2.745 ± 0.008	0.071 ± 0.047	0.213 ± 0.020	0.009 ± 0.092	4.443	0.013	91.80	6.87	0.167 ± 0.245	0.16 ± 0.24
7	2.383 ± 0.009	0.069 ± 0.066	0.222 ± 0.025	0.008 ± 0.048	4.630	0.012	91.84	8.62	0.142 ± 0.114	0.14 ± 0.11

CS-04-3-1-1

J = 0.000540±0.000006

Laser Power %	$\frac{^{40}Ar}{^{39}Ar}$	$\frac{^{38}Ar}{^{39}Ar}$	$\frac{^{37}Ar}{^{39}Ar}$	$\frac{^{36}Ar}{^{39}Ar}$	$\frac{Ca}{K}$	$\frac{Cl}{K}$	$\%^{40}Ar$ atm	$f\ ^{39}Ar$	$\frac{^{40}Ar^*}{^{39}Ar_K}$	Age (Ma)
2	72.536 ± 0.060	1.310 ± 0.096	0.787 ± 0.114	0.293 ± 0.189	1.883	0.288	62.78	0.24	16.377 ± 16.358	15.47 ± 15.39
2.3	5.660 ± 0.012	0.719 ± 0.028	0.473 ± 0.024	0.022 ± 0.193	1.405	0.161	40.47	2.91	1.831 ± 1.243	1.74 ± 1.18
2.6	2.103 ± 0.007	0.385 ± 0.020	0.385 ± 0.018	0.007 ± 0.126	1.167	0.085	43.09	9.98	0.746 ± 0.270	0.71 ± 0.26
2.9	1.402 ± 0.008	0.245 ± 0.018	0.299 ± 0.021	0.004 ± 0.174	0.910	0.053	21.48	17.54	0.741 ± 0.193	0.70 ± 0.18
3.2	1.337 ± 0.007	0.192 ± 0.022	0.285 ± 0.021	0.003 ± 0.225	0.865	0.041	5.87	16.41	0.805 ± 0.225	0.76 ± 0.21
3.5	1.467 ± 0.007	0.205 ± 0.022	0.309 ± 0.021	0.004 ± 0.158	0.946	0.044	11.81	14.83	0.825 ± 0.184	0.78 ± 0.17
3.8	1.573 ± 0.008	0.198 ± 0.028	0.379 ± 0.019	0.004 ± 0.185	1.162	0.042	19.96	14.62	0.825 ± 0.239	0.78 ± 0.23
4.3	1.779 ± 0.009	0.191 ± 0.028	0.519 ± 0.019	0.006 ± 0.203	1.593	0.040	31.33	11.52	0.752 ± 0.350	0.71 ± 0.33
4.8	4.031 ± 0.008	0.218 ± 0.027	1.014 ± 0.018	0.013 ± 0.140	3.122	0.046	51.07	7.32	1.454 ± 0.526	1.38 ± 0.50
5.5	3.331 ± 0.011	0.244 ± 0.034	1.618 ± 0.018	0.011 ± 0.248	4.993	0.052	-13.13	4.64	1.939 ± 0.781	1.84 ± 0.74

Table 10. ^{40}Ar–^{39}Ar results for whole rock samples from six Quilchena lava samples and one Lambly Creek lava sample (continued)

CS-04-10-2-2

J = 0.000535±0.000006

Laser Power %	$\frac{^{40}Ar}{^{39}Ar}$	$\frac{^{38}Ar}{^{39}Ar}$	$\frac{^{37}Ar}{^{39}Ar}$	$\frac{^{36}Ar}{^{39}Ar}$	$\frac{Ca}{K}$	$\frac{Cl}{K}$	$\%^{40}Ar$ atm	$f\ ^{39}Ar$	$\frac{^{40}Ar^*}{^{39}Ar_K}$	Age (Ma)
1.8	-1183.254 ± 1.979	0.008 ± 234.610	-29.891 ± 1.983	-3.850 ± 2.089	0.000	0.265	0.05	-0.01	-181.917 ± 1192.264	-184.73 ± 1274.83
2	141.279 ± 0.076	0.440 ± 0.242	0.743 ± 0.124	0.483 ± 0.129	1.677	0.073	94.95	0.19	6.186 ± 5.168	5.96 ± 14.59
2.3	86.637 ± 0.009	0.378 ± 0.050	0.138 ± 0.079	0.287 ± 0.024	1.367	0.071	96.10	1.84	3.277 ± 1.951	3.16 ± 1.88
2.6	34.294 ± 0.021	0.253 ± 0.035	0.084 ± 0.062	0.112 ± 0.035	1.248	0.050	94.40	5.97	1.859 ± 1.169	1.79 ± 1.13
3	6.477 ± 0.006	0.251 ± 0.024	0.114 ± 0.033	0.020 ± 0.021	2.156	0.054	88.08	27.63	0.727 ± 0.123	0.70 ± 0.12
3.4	4.927 ± 0.008	0.294 ± 0.013	0.205 ± 0.025	0.015 ± 0.030	3.938	0.064	83.83	24.57	0.744 ± 0.131	0.72 ± 0.13
3.8	3.222 ± 0.007	0.321 ± 0.018	0.316 ± 0.025	0.010 ± 0.032	6.098	0.070	77.68	19.88	0.649 ± 0.093	0.63 ± 0.09
4.2	5.579 ± 0.008	0.346 ± 0.023	0.447 ± 0.024	0.020 ± 0.047	8.610	0.075	96.07	11.83	0.178 ± 0.282	0.17 ± 0.27
4.6	7.098 ± 0.009	0.361 ± 0.029	0.579 ± 0.027	0.025 ± 0.066	11.123	0.079	91.29	8.09	0.551 ± 0.480	0.53 ± 0.46

CS-04-8-3-1

J = 0.000539±0.000006

Laser Power %	$\frac{^{40}Ar}{^{39}Ar}$	$\frac{^{38}Ar}{^{39}Ar}$	$\frac{^{37}Ar}{^{39}Ar}$	$\frac{^{36}Ar}{^{39}Ar}$	$\frac{Ca}{K}$	$\frac{Cl}{K}$	$\%^{40}Ar$ atm	$f\ ^{39}Ar$	$\frac{^{40}Ar^*}{^{39}Ar_K}$	Age (Ma)
2	138.865 ± 0.014	0.436 ± 0.108	0.655 ± 0.051	0.462 ± 0.036	2.666	0.073	90.81	0.74	12.527 ± 4.815	12.14 ± 4.65
2.4	21.284 ± 0.016	0.255 ± 0.051	0.133 ± 0.026	0.068 ± 0.031	1.541	0.052	88.50	6.93	2.339 ± 0.628	2.27 ± 0.61
2.8	5.770 ± 0.026	0.235 ± 0.032	0.117 ± 0.043	0.017 ± 0.049	1.885	0.050	74.70	16.21	1.348 ± 0.261	1.31 ± 0.25
3.2	2.762 ± 0.023	0.233 ± 0.020	0.169 ± 0.039	0.008 ± 0.116	3.060	0.050	61.31	20.22	0.936 ± 0.270	0.91 ± 0.26
3.6	2.504 ± 0.013	0.250 ± 0.029	0.256 ± 0.022	0.008 ± 0.099	4.811	0.054	60.41	18.74	0.848 ± 0.221	0.82 ± 0.21
4	2.753 ± 0.007	0.270 ± 0.028	0.431 ± 0.021	0.009 ± 0.077	8.469	0.058	60.81	17.80	0.933 ± 0.200	0.91 ± 0.19
4.4	2.892 ± 0.007	0.301 ± 0.029	0.685 ± 0.018	0.011 ± 0.079	13.474	0.065	60.77	10.60	0.908 ± 0.256	0.88 ± 0.25
5	5.639 ± 0.009	0.370 ± 0.035	1.003 ± 0.024	0.019 ± 0.136	19.995	0.081	63.15	8.77	1.838 ± 0.756	1.79 ± 0.73

Table 10. ^{40}Ar–^{39}Ar **results for whole rock samples from six Quilchena lava samples and one Lambly Creek lava sample (continued)**

CS-04-15-8-1

J = 0.000545±0.000008

Laser Power %	$\frac{^{40}Ar}{^{39}Ar}$	$\frac{^{38}Ar}{^{39}Ar}$	$\frac{^{37}Ar}{^{39}Ar}$	$\frac{^{36}Ar}{^{39}Ar}$	$\frac{Ca}{K}$	$\frac{Cl}{K}$	$\%^{40}Ar$ atm	$f\ ^{39}Ar$	$\frac{^{40}Ar^*}{^{39}Ar_K}$	Age (Ma)
2	43.607 ± 0.014	0.243 ± 0.082	0.262 ± 0.039	0.151 ± 0.040	2.726	0.045	95.99	1.23	1.667 ± 1.794	1.64 ± 1.76
2.4	151.840 ± 0.011	0.193 ± 0.054	0.302 ± 0.035	0.509 ± 0.020	4.899	0.019	97.44	2.50	3.864 ± 2.747	3.80 ± 2.70
2.8	65.942 ± 0.012	0.060 ± 0.059	0.242 ± 0.027	0.219 ± 0.020	4.594	0.001	96.32	8.91	2.397 ± 1.193	2.36 ± 1.17
3.2	19.581 ± 0.016	0.026 ± 0.058	0.204 ± 0.026	0.062 ± 0.022	3.971	0.000	91.29	16.38	1.669 ± 0.408	1.64 ± 0.40
3.6	11.479 ± 0.011	0.019 ± 0.040	0.171 ± 0.027	0.035 ± 0.027	3.330	0.000	86.43	18.65	1.516 ± 0.287	1.49 ± 0.28
4	11.832 ± 0.006	0.019 ± 0.041	0.150 ± 0.023	0.036 ± 0.024	2.905	0.000	87.36	19.80	1.455 ± 0.263	1.43 ± 0.26
4.35	9.987 ± 0.008	0.023 ± 0.081	0.156 ± 0.030	0.030 ± 0.026	2.948	0.001	84.59	13.60	1.488 ± 0.233	1.46 ± 0.23
5	7.415 ± 0.009	0.026 ± 0.071	0.201 ± 0.024	0.022 ± 0.029	3.766	0.002	80.08	9.06	1.404 ± 0.191	1.38 ± 0.19
5.5	6.232 ± 0.010	0.031 ± 0.038	0.276 ± 0.021	0.018 ± 0.034	5.116	0.003	71.55	6.01	1.647 ± 0.181	1.62 ± 0.18
6	6.173 ± 0.010	0.034 ± 0.106	0.345 ± 0.033	0.019 ± 0.095	6.239	0.003	69.97	3.84	1.661 ± 0.526	1.63 ± 0.52

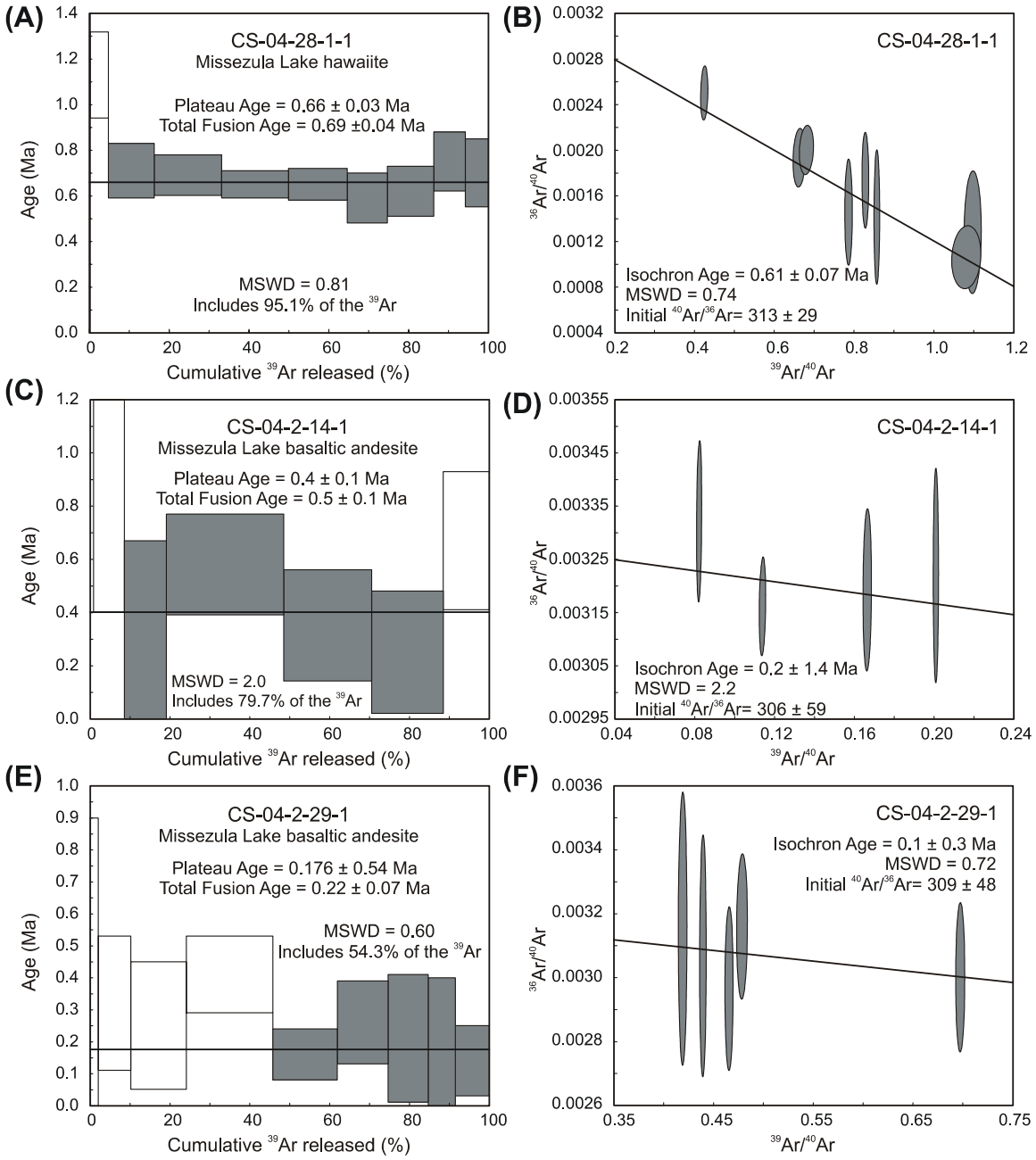

Figure 33. **^{40}Ar–^{39}Ar degassing spectra (plateau and inverse isochron graphs) of valley lava samples**

(A) and (B) Sample CS-04-2-28-1, base of Missezula Lake East section. (C) and (D) Sample CS-04-2-14-1, Missezula East section. (E) and (F) Sample CS-04-2-29-1, top of Missezula Lake East section.

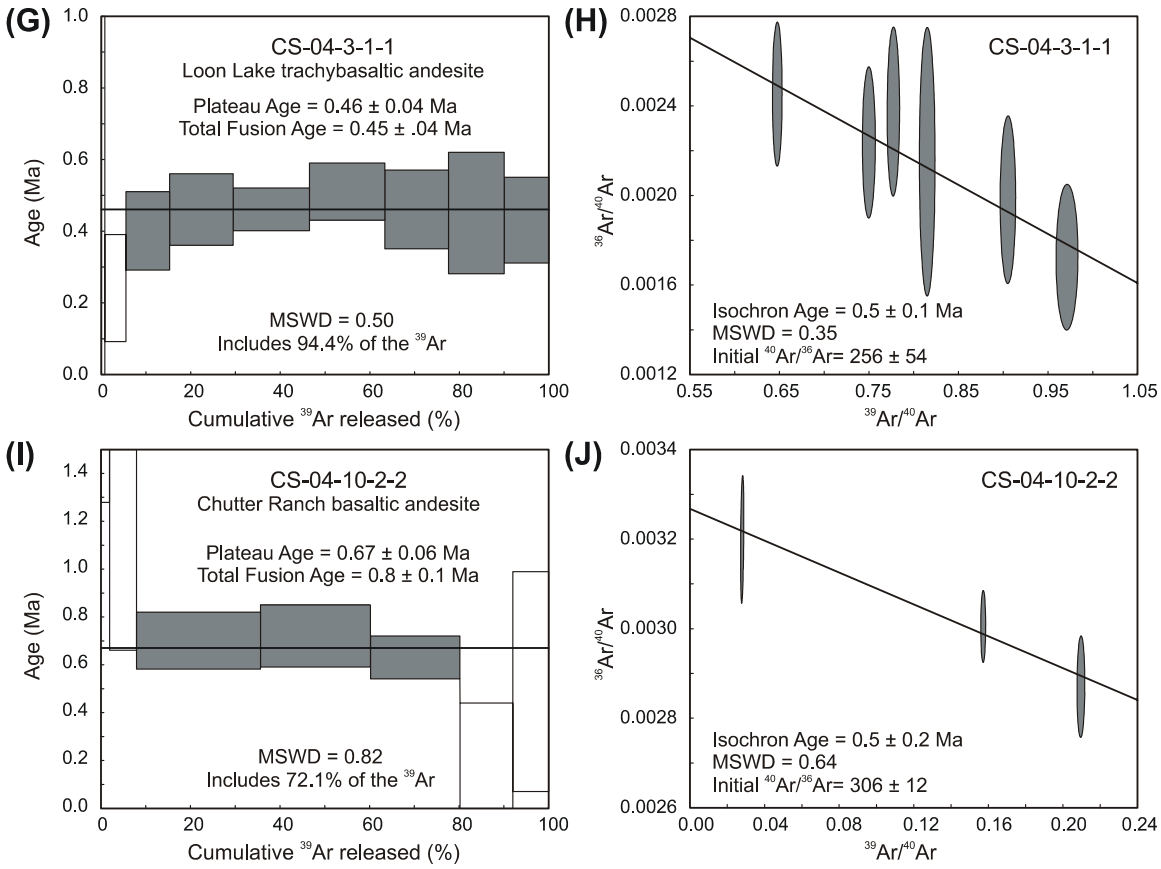

Figure 33. **^{40}Ar–^{39}Ar degassing spectra (plateau and inverse isochron graphs) of valley lava samples (continued)**

(G) and (H) Sample CS-04-3-1-1, Loon Lake section. (I) and (J) Sample CS-04-10-2-2, Chutter Ranch section.

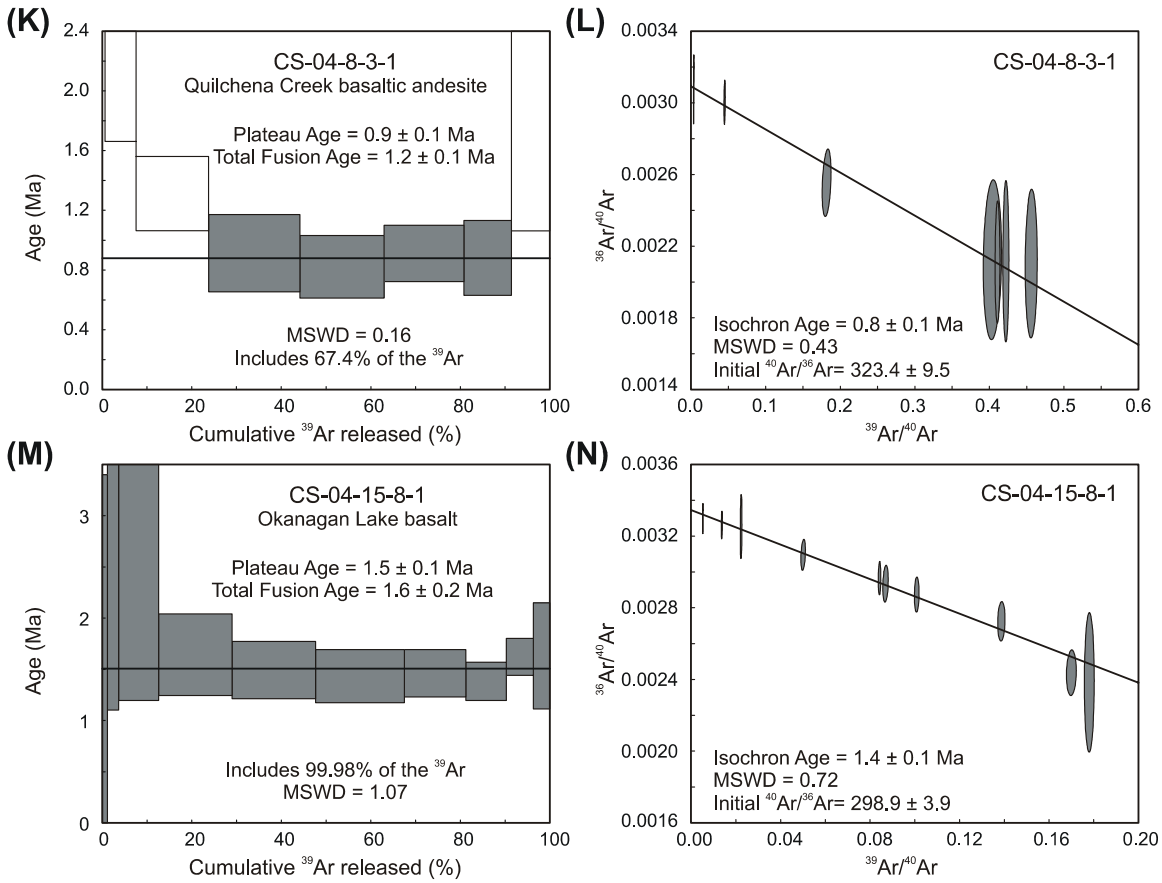

Figure 33. **^{40}Ar–^{39}Ar degassing spectra (plateau and inverse isochron graphs) of valley lava samples (continued)**

(K) and (L) Sample CS-04-8-3-1, Quilchena Creek section. (M) and (N) Sample CS-04-15-8-1, Okanagan Lake section.

Sample Descriptions

Missezula Lake Hawaiite (CS-04-2-28-1-1)

Sample CS-04-2-28-1 contains microphenocrysts of plagioclase, olivine and rare augite, in a groundmass of plagioclase + augite with minor olivine, magnetite/ilmenite and glass. Alteration of the sample is limited to iddingsite rims on olivine microphenocrysts. The sample belongs to the alkaline type of lavas at the base of the Missezula section (Quilchena lava), and was taken from one of the lowest flows exposed in that section, directly above the exposed unconformity with the Nicola Group. The whole rock analysis yielded a plateau age of 660 ± 30 ka based on eight contiguous steps using 95.1% of the ^{39}Ar (Figure 33a). The inverse isochron age of 610 ± 70 ka (based on the same steps) is in good agreement with the plateau age (Figure 33b). The plateau age is interpreted as the igneous crystallization age, and the minimum age of the onset of volcanism of the Quilchena lavas near Missezula Lake.

Missezula Lake Basaltic Andesite (CS-04-2-14-1)

Sample CS-04-2-14-1 is unaltered and aphyric, and is dominantly composed of a groundmass of unaltered augite + plagioclase with minor magnetite/ilmenite. The sample is from mid-way up the Missezula Lake section (Quilchena lava), at the transition from the alkaline type to the calc-alkaline type of lavas. The whole rock analysis yielded a plateau age of 400 ± 100 ka, and an imprecise inverse isochron age of 200 ± 1400 ka (Figure 33c and d). Although the results are poor, the plateau age lies between the ages stratigraphically below (CS-04-2-28-1) and above it (CS-04-2-29-1), suggesting it is

reasonable. The plateau age, using four contiguous steps with 79.7% of the ^{39}Ar is interpreted to be the igneous crystallization age.

Missezula Lake Basaltic Andesite (CS-04-2-29-1)

Sample CS-04-2-29-1 has microphenocrysts of olivine, plagioclase and augite, set in a groundmass of plagioclase + augite with minor olivine and magnetite/ilmenite. Alteration of the sample is limited to iddingsite rims on the olivine microphenocrysts. The sample was taken from the top of the Missezula Lake section (Quilchena lava), and belongs to the calc-alkaline type of samples. The whole rock analysis yielded a plateau age of 180 ± 50 ka, based on five contiguous steps with 54.3% of the ^{39}Ar (Figure 33e). However, there also appears to be a plateau at the low-temperature end of the run, with an age of 360 ± 90 ka (based on four contiguous steps containing 45.4% of the ^{39}Ar), possibly a result of excess Ar. The inverse isochron plot based on the same steps gives an age of 100 ± 300 ka, and does not show a great amount of excess Ar, although the error on the initial Ar is large (Figure 33f). The high-temperature plateau age of 180 ± 50 ka is interpreted to be the igneous crystallization age (as it is based on more ^{39}Ar than the low temperature plateau), and is the minimum age of volcanic activity near Missezula Lake. An unpublished K–Ar analysis by W.H Mathews (as reported in Breitsprecher and Mortensen, 2004) from the Missezula Lake East section (specific flow not known) gives an age of 310 ± 80 ka, which is in between the two plateaus.

Loon Lake Trachybasaltic Andesite (CS-04-3-1-1)

Sample CS-04-3-1-1 is the possible intrusive equivalent of the Quilchena lavas, collected from a hilltop south of Loon Lake. Glomerocrysts of augite ± olivine are

surrounded by plagioclase, all of which is almost completely unaltered. Chemically, the sample is most similar to the alkaline type of samples at Missezula Lake 7 km to the south. The whole rock analysis of the sample produced a plateau age of 460 ± 40 ka, based on 7 contiguous steps containing 94.4% of ^{39}Ar (Figure 33g). The inverse isochron age is 500 ± 100 ka, based on the same steps (Figure 33h). The plateau age is interpreted to be the igneous crystallization age.

Chutter Ranch Basaltic Andesite (CS-04-10-2-2)

Sample CS-04-10-2-2 is aphyric, with an unaltered groundmass of plagioclase + olivine + augite with minor magnetite/ilmenite. The sample comes from a Quilchena lava exposure on the Chutter Ranch, 2 km east of Merritt, from the lowest exposed flow in the section, which unconformably overlies a channel deposit. The whole rock analysis of this sample produced a plateau age of 670 ± 60 ka, based on three contiguous steps containing 72.1% of the ^{39}Ar (Figure 33i). The inverse isochron age is imprecise at 500 ± 200 ka, although excess Ar does not appear to be a problem (Figure 33j). Therefore, the plateau age is interpreted to be the igneous crystallization age of this sample. This age is in agreement with a poorly constrained K–Ar age of 600 ± 400 ka (Church, 1980). It is also in good agreement with previous paleomagnetic determinations at the site, which indicated that the normally magnetized basalts are younger than the 780 ka Brunhes–Matuyama magnetic boundary (Fulton et al., 1992; Cande and Kent, 1995).

Quilchena Creek Basaltic Andesite (CS-04-8-3-1)

Sample CS-04-8-3-1 is taken from west of Quilchena creek, 5 km south of the community of Quilchena, and is part of the Quilchena lavas. The sample contains a

minor proportion of olivine microphenocrysts, set in a groundmass of plagioclase + olivine + augite. Alteration is limited to olivine rims partially altered to iddingsite. The whole rock analysis produced a plateau age of 900 ± 100 ka, based on four contiguous steps containing 67.4% of the ^{39}Ar (Figure 33k). The plateau is saddle-shaped, suggesting excess Ar, which is confirmed by the initial $^{40}Ar/^{36}Ar$ ratio (= 323.4 ± 9.5) determined in the inverse isochron plot (Figure 33l). Therefore, the inverse isochron age of 800 ± 100 ka (based on the same steps as the plateau age) is interpreted as the igneous crystallization age. Previously published paleomagnetic analyses show basalts in the Quilchena section are normally magnetized (as does the paleomagnetic analysis of this sample in Appendix D), suggesting that the age of this sample can be further confined to less that 780 ka. The combination of the inverse isochron age and the paleomagnetic information suggest that the age of this sample is between 700 ka and 780 ka (Fulton et al., 1992). A unpublished age of 400 ± 800 ka by Mathews (as reported in Breitsprecher and Mortensen, 2004) exists, but is disregarded due to the large associated error.

Okanagan Lake Basalt (CS-04-15-8-1)

Sample CS-04-15-8-1 is from a section of Lambly Creek basalt exposed on the west bank of Okanagan Lake, due west of the city of Kelowna. The sample was taken at the base of the exposed section. The sample contains microphenocrysts of olivine set in a groundmass of plagioclase + augite + olivine, all of which are unaltered. The whole rock analysis yielded a plateau age of 1.5 ± 0.1 Ma, based on 10 steps containing 99.98% of the ^{39}Ar (Figure 33m). The inverse isochron plot shows no excess Ar, and gives a comparable age of 1.4 ± 0.1 Ma based on the same steps (Figure 33n). Previously published K–Ar ages for the Lambly Creek basalt further north in this section (810 ± 140

Ma) and along Lambly Creek (760 ± 240 Ma) suggest that the Lambly Creek basalt is younger that the ^{40}Ar–^{39}Ar age, although these may be on flows stratigraphically higher than the flow sampled for this analysis (exact flow in section not known) (Church, 1980; Mathews, 1988).

Paleomagnetic analyses of other flows, as well as our analysis of this flow, show that the Lambly Creek basalt is normally magnetized, which does not correlate with our determined ages (Church, 1980; Mathews, 1988; Mejia et al., 2002). The errors on both the plateau age and inverse isochron age do not overlap known normal polarity magnetic boundaries, although the total fusion age (1.6 ± 0.2 Ma) overlaps the brief Gilså normal polarity cryptochron (1.68 Ma) and the upper end of Olduvai normal polarity interval at 1.77 Ma (Cande and Kent, 1995, Gibbard and Kolfschoten, 2004). However, this would indicate that this sample is 1 Ma older than a flow less than 1 km further north (and not much up section, if at all), which seems unlikely. As it is difficult to reconcile the ^{40}Ar–^{39}Ar results with the paleomagnetic results, the plateau age of 1.5 ± 0.1 Ma is reported as the igneous crystallization age, but the error on this analysis is likely greater than the reported analytical error based on paleomagnetic evidence.

Appendix G: Detailed Geochemical Modelling Procedure and Results

Geochemical modelling was performed using a series of Microsoft Excel spreadsheets. The modelling was first completed using samples from the Missezula Lake section only, and was then expanded to incorporate all Quilchena lava samples. Samples of the Lambly Creek lavas were excluded because of a low sample number and distant location from the Quilchena lavas.

Importance of Fractional Crystallization to Quilchena Lava Types

First, fractional crystallization models were employed to identify relationships between the Quilchena lava samples. Samples were first plotted on compatible vs. incompatible element bivariate diagrams, for example, Ni vs. La or Sc vs. Nb. The samples clustered into four groups, three of which had calc-alkaline compositions (termed calc-alkaline types 1, 2 and 3), and one with an alkaline composition. The distinctiveness of the four groups suggested that they were not derived from a single parental magma composition, and this idea was then tested using FRAVECT version 1.2, a Microsoft Excel program developed by Dr. Derek Thorkelson. The program allows the user to model the fractional crystallization of multiple minerals from a given melt composition, and to adjust proportions of the fractionating minerals to match sample compositions by comparing the two in graphical and numerical formats. The program is based on the Rayleigh fractionation equation:

$$\frac{C_i^l}{C_i^O} = (1 - X)^{(D-1)}$$

where C_i^l is the concentration of element *i* in the melt, C_i^O is the initial concentration of element *i* in the melt, X is the fraction of material crystallized and D is the partition coefficient of the element of interest in the fractionating phenocryst.

To begin the fractional crystallization modelling, melt compositions that may have been parental to the sample compositions were identified. For each group, the most "primitive" samples (highest Mg#, highest Ni concentrations) were used as starting (parental) melt compositions. From these compositions, various minerals (olivine, clinopyroxene, orthopyroxene, plagioclase and magnetite), alone and in combination, were modelled to fractionally crystallize. The results showed that the four sub-types of Quilchena lavas could not be related to each other by fractional crystallization, although that the fractional crystallization of primarily olivine ± clinopyroxene could relate primitive samples to more evolved samples within the individual subtypes.

Calculation of Primary Magmas

The process of variable partial melting of a mantle source (peridotite) was then explored because fractional crystallization alone could not account for the chemical diversity of the Quilchena lavas. To begin, the compositions of two primary, mantle-equilibrated magmas were calculated – one for the Quilchena lava alkaline type and one for the Quilchena lava type 1 calc-alkaline type. A sample from calc-alkaline type 1 was used to represent all the calc-alkaline subtypes, as it had the highest Ni and Mg#, and calc-alkaline type 1 was the calc-alkaline sub-type most different from the alkaline type. Calculation of primary magma compositions was accomplished by (1) selecting the most "primitive" compositions (highest Mg# and Ni abundance) for the alkaline and calc-

alkaline geochemical types, and (2) incrementally adding the composition of olivine to the primitive magma compositions. Olivine was used because it is the most abundant or sole mineral phase in the Quilchena lavas, and the addition of olivine to a primitive magma is a recognized way to generate a mantle-equilibrated primary magma (Albarede, 1992; Asimow and Longhi, 2004). Essentially, this method reverses the chemical effect that olivine fractionation had in the generation of primitive Quilchena lavas from their parental, primary magmas.

The composition of the olivine that was added to the primitive Quilchena compositions was based on the mineral–melt exchange coefficients for FeO and MgO and the methods described in Roeder and Emslie (1970) with an assumed Fe_2O_3/FeO weight ratio of 0.2. The procedure works by (1) calculating the composition of olivine that would be in equilibrium with the primitive magmas, (2) adding 1% by weight of that olivine to the primitive magma to form a new (more primitive) composition, (3) calculating the composition of olivine that would be in equilibrium with the new magma composition, and (4) repeating the procedure iteratively until the calculated olivine composition is equivalent to that of mantle olivine (generally $Fo_{90–92}$; Albarede, 1992; Grove, 2000) and the Mg# of the sample was 73 (Grove, 2000), thereby yielding a primary major element melt composition for each of the geochemical types.

The alkaline type was calculated to be derived from a primary magma (PL-A) that had undergone 11% fractional crystallization of olivine, and the calc-alkaline (type 1) was calculated to be derived from a primary magma (PL-C1) that had undergone 6% fractional crystallization of olivine. These estimates of the degree of fractional crystallization of olivine from the primary magma were then used to calculate the trace

element concentrations in the two primary magmas, using the Rayleigh fractional crystallization equation (above), and the partition coefficients in Table 11.

Calculation of Mantle Source

Initial Steps and Considerations

The calculated primary magma compositions were then compared to calculated partial melts of peridotite. The calculation of the peridotite melts was carried out using two formulas, one for fractional melting and the other for equilibrium melting (as reported in Rollinson, 1993):

Equilibrium Melting: $$\frac{C_i^l}{C_i^O} = \frac{1}{(\overline{D}_i(1-F)) + F}$$

Fractional Melting: $$\frac{\overline{C_i^l}}{C_i^O} = \frac{1-(1-F)^{\frac{1}{\overline{D}_i}}}{F}$$

where F is the melt fraction and $\overline{C_i^l}$ is the composition of the aggregate liquid (the combined composition of the melt fractions), and $\overline{D_i}$ is the bulk distribution coefficient, given as:

$$\overline{D_i} = \sum W_A D_i^A$$

where W_A is the weight fraction of mineral A in the starting rock, and D_i^A is the partition coefficient for the element *i* in mineral A. In both cases the melting is assumed to be modal (the minerals melt out in the same proportion with which they are contained within the starting rock).

Table 11. Partition coefficients used in geochemical modelling

	Olivine		Opx		Cpx		Garnet	
D^{Rb}	0.0003	*S04*	0.0002	*S04*	0.0004	*S04*	0.0002	*S04*
D^{Ba}	0.000005	*S04*	0.000006	*S04*	0.0004	*S04*	0.00007	*S04*
D^{Th}	0.00005	*S04*	0.002	*S04*	0.00566	*S04*	0.009	*S04*
D^{U}	0.00038	*S04*	0.002	*S04*	0.0113	*S04*	0.028	*S04*
D^{Nb}	0.0005	*S04*	0.004	*S04*	0.01	*S04*	0.015	*S04*
D^{Ta}	0.0005	*S04*	0.004	*S04*	0.01	*S04*	0.015	*S04*
D^{La}	0.0004	*M91*	0.002	*M91*	0.054	*M91*	0.01	*M91*
D^{Ce}	0.0005	*M91*	0.003	*M91*	0.098	*M91*	0.021	*M91*
D^{Pr}	0.008	*M91*	0.0048	*M91*	0.15	*M91*	0.054	*M91*
D^{Sr}	0.00019	*M91*	0.007	*M91*	0.067	*M91*	0.0011	*M91*
D^{Nd}	0.0013	*M91*	0.0068	*M91*	0.21	*M91*	0.087	*M91*
D^{Zr}	0.011	*F84*	0.0465	*F84*	0.131	*F84*	0.281	*F84*
D^{Hf}	0.01	*M91*	0.01	*M91*	0.233	*M91*	0.23	*M91*
D^{Sm}	0.0013	*M91*	0.01	*M91*	0.26	*M91*	0.217	*M91*
D^{Eu}	0.0016	*M91*	0.013	*M91*	0.31	*M91*	0.32	*M91*
D^{Gd}	0.0015	*M91*	0.016	*M91*	0.3	*M91*	0.498	*M91*
D^{Tb}	0.0015	*M91*	0.019	*M91*	0.31	*M91*	0.75	*M91*
D^{Dy}	0.0017	*M91*	0.022	*M91*	0.33	*M91*	1.06	*M91*
D^{Y}	0.0036	*N92*	0.19	*D94*	0.245	*S96*	4.2	*J93*
D^{Ho}	0.0016	*M91*	0.026	*M91*	0.31	*M91*	1.53	*M91*
D^{Er}	0.0015	*M91*	0.03	*M91*	0.3	*M91*	2	*M91*
D^{Yb}	0.0015	*M91*	0.049	*M91*	0.28	*M91*	4.03	*M91*
D^{Lu}	0.0015	*M91*	0.06	*M91*	0.28	*M91*	5.5	*M91*
D^{V}	0.06	*GERM*	0.9	*GERM*	1.81	*GERM*	1.48	*H94*
D^{Sc}	0.16	*GERM*	0.33	*GERM*	0.808	*GERM*	2.62	*H94*
D^{Co}	6.6	*R93*	3	*R93*	1	*R93*	1	*R93*
D^{Cr}	0.7	*R93*	10	*R93*	34	*R93*	2.01	*H94*
D^{Ni}	15.5	*M78*	1.1	*M78*	2.6	*M78*	5.1	*M78*

***Reference Abbreviations: S04**, Salters and Stracke (2004); **M91**, McKenzie and O'Nions (1991); **F84**, Fujimaki et al. (1984); **N92,** Neilson et al. (1992)**; D94,** Dunn and Sen (1994); **S96**, Sobolev et al. (1996); **J93**, Jenner et al. (1993); **R93**, Rollison (1993); **H94**, Hauri et al. (1994); **M78**, Mysen (1978); **GERM**, estimated from Geochemcial Earth Reference Model (http://www.earthref.org)*

Initially, the chemical composition and modal mineralogy of a spinel lherzolite xenolith from the Chilcotin Group (Peslier et al., 2002) was used as the peridotite (mantle source) composition. Model curves for partial melting of that source were plotted on compatible–incompatible element diagrams (e.g., Ni vs. La) along with the Quilchena lava compositions and the calculated primary magmas. The purpose of the graphical display was to determine if either of the calculated primary magmas could have been generated by melting of the selected peridotite. If, for example, the primary magmas plotted on one of the melting curves (equilibrium or fractional), at reasonable degrees of partial melting (e.g., 2–20%), then the Quilchena lava compositions could be explained in a two-stage model beginning with various degrees of melting of the selected mantle composition and followed by fractionation of olivine. However, the results indicate that the selected peridotite xenolith cannot represent the mantle source area because, for a given pair of elements, the four calculated primary magma compositions generally do not lie on a single melting curve, and, if they do, not within reasonable degrees of partial melting. Modelling using other spinel lherzolite compositions (Peslier et al., 2002) was also attempted, with similar results.

The model was next expanded to account for 31 elements at a time, instead of just two, therefore allowing a given xenolith composition to be melted and easily compared to Quilchena lava composition across a wide range of elements for a given degree of partial melting. The graphic representation of model curves was changed from a bivariate plot to a primitive mantle-normalized extended trace element diagram, which although it only showed the melt composition for a user-specified degree of partial melting (e.g. 5%), the graph illustrated the results of partial melting for all 31 elements. The model was also

adapted to include (if desired) a user-specified degree fractional crystallization of olivine, clinopyroxene and orthopyroxene from the melt (alone or in combination), to produce a combined partial melting–fractional crystallization curve that could be graphically compared to the Quilchena lavas.

Determination of Garnet Lherzolite Characteristics

As the valley lavas were derived from a garnet-bearing source, the modelling procedure was then corrected to use a garnet lherzolite source. No garnet-bearing xenoliths have been collected within the plateau basalts. While garnet-bearing mantle xenoliths are common within cratonic environments (e.g. kimberlites), they are not found within the continental intraplate tectonic environment of southern British Columbia (Pearson et al., 2003). Therefore, the modal mineralogy of a source garnet lherzolite beneath British Columbia was estimated (58% olivine, 19% orthopyroxene, 14% clinopyroxene and 9% garnet) using modal data from continental lithospheric settings (e.g. McDonough, 1990; Ionov, 1993; McDonough and Rudnick, 1998; Pearson et al., 2003; Walter, 2003). Partition coefficients for all modelled elements for olivine, orthopyroxene, clinopyroxene and garnet were estimated using the GERM database (Geochemical Earth Reference Model; http://www.earthref.org) and are presented in Table 11.

Non-modal Melting Model

To further refine the melting model, the concept of non-modal melting was introduced to the procedure. In general, melting in the mantle is not a modal process – some minerals contained within the parental lherzolite will melt out sooner than others

(Walter, 2003). In a garnet lherzolite at 3.0 GPa (close to the garnet–spinel transition), garnet is consumed in greater proportion relative to olivine and clinopyroxene, and will generally melt out entirely after 10–15% melting, while orthopyroxene will crystallize (Walter, 1998; Walter, 2003). In this study, the garnet lherzolite melting model of Walter (1998) at 3.0 GPa was used (4 Ol + 84 Cpx +12 Gt = 87 Liq + 13 Opx), using the following equations:

Non-modal equilibrium melting: $$\frac{C_i^l}{C_i^O} = \frac{1}{F(1-P_i) + \overline{\overline{D_i}}}$$

Non-modal fractional melting: $$\frac{\overline{C_i^l}}{C_i^O} = \frac{1}{F}\left(1-\left(1-\frac{P_i F}{\overline{\overline{D_i}}}\right)^{\frac{1}{P_i}}\right)$$

Where P_i is the average individual partition coefficients weighted according to how the proportions in which minerals enter the melt (p is the proportion in which phase ϕ enters the melt), given as:

$$P_i = \sum_{\phi} p_{\phi} D_i$$

All equations are referenced from Rollinson (1993).

Final Melting Model

As all Cordilleran xenoliths are spinel-bearing (Shi et al, 1998), no Cordilleran garnet lherzolite trace element concentrations were available to use in this model. Therefore, the final fractional melting model was configured to assume 5% partial melting of a mantle source was needed to produce the two primary magmas calculated for the Quilchena lavas (PL-A and PL-C1), using the partition coefficients, garnet lherzolite mode and non-modal fractional melting model detailed above. These two calculated

mantle sources were named MS-A (melts to produce the alkaline primary magma PL-A) and MS-C1 (produces primary magma PL-C1); compositions are reported in Table 4.

The modelled garnet lherzolite source MS-A was then used to test if greater degrees of partial melting would produce the calc-alkaline subtypes of the Quilchena lavas (as attempted in the spinel lherzolite models). However, although increased (between 8–15%) partial melting of this garnet lherzolite source could replicate the Ba, Sr and HREE found in the calc-alkaline Quilchena lavas, Nb, Ta and the light to middle REE concentrations in the calculated melt were 1.5–2 times higher than PL-C1. The garnet lherzolite source MS-C1 could not replicate the alkaline Quilchena lavas, nor the other (less depleted) calc-alkaline lavas. Therefore, based on the trace element patterns and modelling described previously, it was concluded that the alkaline and calc-alkaline lavas were derived from two mantle sources.

Based on the above methods, two separate garnet lherzolite sources are reported in this thesis: MS-A for the Quilchena lava alkaline samples and MS-C1 for the most depleted Quilchena lava calc-alkaline samples (type 1). Both have the same modal mineralogy (as described above) are based on the same melting model, and were created using 5% partial melting, so that the two source compositions could be more easily compared. The composition of MS-A is based on PL-A (alkaline primary magma, which assumed the alkaline suite of Quilchena lavas underwent 11% fractional crystallization), while MS-C1 is based on PL-C1 (type 1 calc-alkaline primary magma, which assumed that the type 1 calc-alkaline Quilchena lavas underwent 6% fractional crystallization.